TRANSIENTS IN A SMALL LEAD COOLED REACTOR

DEVELOPMENT OF A MULTISCALE ANALYSIS METHODOLOGY FOR ANALYSIS OF TRANSIENTS IN A SMALL LEAD COOLED ADVANCED REACTOR

By CUAUHTEMOC REALE HERNANDEZ, B.ENG., M.SC.

A Thesis Submitted to the School of Graduate Studies in Partial Fulfilment of the Requirements for the Degree Doctor of Philosophy

McMaster University DOCTOR OF PHILOSOPHY (2022) Hamilton, Ontario (Engineering Physics)

TITLE: Development of a Multiscale Analysis Methodology for Analysis of Transients in a Small Lead Cooled Advanced Reactor

AUTHOR: Cuauhtemoc Reale Hernandez, B.Eng (Ecole Polytechnique de Montreal), M.Sc. (Institut National de la Recherche Scientifique, Varennes)

SUPERVISOR: Professor John Luxat

NUMBER OF PAGES: xvii, 153

Lay Abstract

In the recent years, new types of small nuclear reactors for producing electricity are being developed. The motivation of this thesis is to investigate a particular safety aspect of one of those reactors. One of the main tasks of a nuclear reactor is to transport heat from the core, where the nuclear reaction produces heat, to the component that produces steam which will then activate a turbine to generate electricity. This is achieved by circulating a fluid between those two parts of the reactor with the help of pumps. Any new reactor needs to be designed in a way that if the pumps stop working, no component will overheat and the reactor will shut down safely. This thesis investigates this safety aspect by developing a computer model that can simulate the behavior of the reactor in the case of a loss of pump power. The main takeaway is that the computer model works well and the results from the simulations show that the reactor remains safe in such an accident scenario.

Abstract

In the recent years there has been growing interest in small modular reactors (SMRs). Before this type of reactors are deployed it is necessary to assess their safety with the newest available tools. This thesis focuses on one SMR, the SEALER reactor, which is a 3 to 10 MWe lead cooled reactor intended for remote communities or mines. The designer of the SEALER reactor has previously identified a possible issue during a loss of flow transient. At the beginning of the transient, the mass flow at the pumps undergoes a fluctuation that could lead to reverse flow if amplified. The first part of the thesis was to perform an uncertainty and sensitivity analysis using an existing lumped-parameter model. Two types of transients were studied: unprotected loss of flow and unprotected overpower. Results show that, for both transients, temperatures remain well below safety limits for the entire parameters space. However, it is also found that reverse flow at the pumps is possible by changing some parameters in a realistic way. It was therefore decided to develop a more realistic model to study the same transients, which constitutes the second and main part of the thesis. The new model uses CFD for simulating the flow of coolant in the entire primary circuit. The complex components (fuel channels, pumps and steam generators) are replaced with a simple geometry and appropriate heat and momentum sources/sinks. The CFD simulation is coupled with a custom-made code for solving heat transfer in the fuel pins and to point kinetics for neutronics. To demonstrate the viability of the model, a validation exercise was performed to ensure that the CFD part is able to reproduce experimental data with important features, like temperature stratification and a jet into a plenum. Results from the new model confirm the mass flow fluctuation if a small pump flywheel is used. For a flywheel of reasonable size, transients are slow without any mass flow fluctuation, and temperature variations are small.

Acknowledgements

I wish to express my deep gratitude and thanks to my supervisor, Prof. John Luxat, for his continuous support and guidance throughout the long process of my doctoral studies. On top of his technical advice, he also encouraged me to have a good balance between studies and life, for which I'm very grateful. I would also like to thank my committee, Prof. Adriaan Buijs and Prof. David Novog, for the very useful and insightful feedback that I received from them. I can't forget to offer my sincere thanks to Prof. Janne Wallenius, the designer of the SEALER reactor, who accepted to collaborate with us, and to provide all the necessary data and information. The feedback that I received from him is also very appreciated. Finally, PhD student Christopher Hollingshead provided invaluable help in setting up and fixing the computing cluster which I used for my simulations.

Table of Contents

List of Figures

List of Tables

List of All Abbreviations and Symbols

ADS	: Accelerator Driven System
BELLA	: Lumped parameter code for simulating transients in lead cooled reactors
CFD	: Computational Fluid Dynamics
EPR	: European Pressure Reactor
LBE	: Lead Bismuth Eutectic
PK	: Point Kinetics
QOI	: Quantity Of Interest
SEALER	: SwEdish Advanced LEad cooled Reactor
SG:	: Steam Generator
SMR	: Small Modular Reactor
SRC	: Standardised Regression Coefficient
STH	: System Thermal Hydraulics
TALL-3D	: experimental facility (lead loop) located in KTH, Sweden
TC	: Thermocouple
UCTD	: Updated Cheng and Todreas Detailed correlation
ULOF	: Unprotected Loss Of Flow accident
UTOP	: Unprotected Transient OverPower accident
VOF	: Volume Of Fluid

List of All Variables

c_P	Heat capacity
D_e	Equivalent hydraulic diameter
D_h	Hydraulic diameter
K_D	Doppler constant
Λ_{eff}	Effective neutron reproduction time
σ_x	Standard deviation
A	Surface area
C	Concentration of delayed neutron precursor
f	Friction factor
h	Heat transfer coefficient
k	Thermal conductivity
L	Length
Nu	Nusselt number
Pe	Peclet number
Q	Heat flow / power
Re	Reynolds number
T	Temperature
v	Velocity
V	Volume
α	Reactivity coefficient
β	Delayed neutron fraction
λ	Decay rate
ρ	Density
$\rho(t)$	Time dependent reactivity

Declaration of Academic Achievement

All the work presented in this thesis is the original work of the author, under the supervision of Dr. John Luxat. This includes the conceptual design of the studies and methodologies, the Matlab scripts used to perform calculations and to automate the analysis of the results, the preparation of the simulations cases, the writing of the article manuscripts and the production of the figures. My committee meeting, Dr. David Novog and Dr. Adriaan Buijs, also provided instrumental guidance during the different stages of the thesis. The author of the SEALER reactor design, Dr. Janne Wallenius, provided all the necessary data and information about the reactor, and he also helped in the analysis of the first article. That reactor is used as a reference in all the parts of the thesis.

The first part of the thesis is an uncertainty and sensitivity analysis in order to understand a particular engineering issue of the SEALER reactor. That study was able to determine the causes and limitations of that issue. The second part is the development of a CFD-based model for simulating transients in the SEALER reactor. The model contains four components: a CFD model, a fuel pin heat transfer model, neutronics and a pump model. The author of this thesis built everything from zero. The CFD model was set up for modelling a heavy metal fluid with free surfaces. A validation exercise was carried out with experimental data in order to ensure the CFD configuration can correctly simulate a jet into a plenum and temperature stratification. The geometry used in CFD was built based on available drawings and dimensions of the SEALER reactor. The fuel pin heat transfer model was written in Matlab and uses a control volume approach. It simulates transients and takes into account temperature dependency of material properties. Neutronics is modelled with point kinetics and the pump uses a flywheel energy coupling for loss of flow simulations. All the solvers (except CFD which uses STAR-CCM+), the main script which connects them together and the tools for analysing the results are all written in Matlab scripts by the author.

Chapter 1 - Introduction

1.1 Background

Canada is a unique place for the development of small modular reactors (SMRs). This stems from the fact that different types of reactors with different applications have the potential to be deployed in this country. Additionally, there is a good regulatory environment and a nuclear expertise that has been developed for decades. Three different markets, with different types of reactors, are considering the adoption of SMRs. One of them is to provide electricity to the grid with "large" SMRs of about 300 MWe. Another would employ fourth-generation advanced reactors to provide electricity and process heat to large industrial facilities. The last one consists in providing electricity (and potentially heat) to remote communities that are not connected to the grid and depend on diesel generators. That would require micro SMRs of less than 10 MWe. Many vendors are seriously developing their SMR and have initiated the licensing process. It is very likely to see the deployment of such reactors within the next 10 years.

In this context, it is very important to assess the safety of these new types of reactors. For this purpose, one of the micro SMRs was selected for further investigation in this thesis. The SEALER reactor (for SwEdish Advanced LEad Reactor) is a 3-10 MWe SMR intended for the Canadian arctic (Wallenius et al., 2018). It is a lead-cooled fast-spectrum reactor that can be operated for 10 to 30 years without refueling. Details of the reactor are provided in Chapter 2. Prof. Janne Wallenius, from KTH in Stockholm, is the person behind the design of this reactor. A collaboration has been established with him to obtain details of the design and other useful data.

Lead cooled reactors are a promising technology for advanced reactors in general. The liquid phase of lead has a really wide temperature range, from 327 to 1749 °C at atmospheric pressure. For comparison, sodium boils at 883 °C. This allows lead cooled reactors to operate at higher temperature, increasing the efficiency of the plant, and/or to

have higher safety margins to boiling. Lead does not react violently with air or water and can be operated at atmospheric pressure, thus making the reactor simpler and safer. Being a metal, lead exhibits high thermal conductivity, making it an excellent coolant. The fast spectrum of lead cooled reactors enables the possibility of making breeder reactors, thus paving the way for closing the fuel cycle and eliminating most of the waste. Because of its small size, SEALER is not a breeder, but its breeding ratio is high. The only significant issue with lead is that it's highly corrosive. Special steels are being developed for that purpose and have already shown promising results (Ejenstam et al., 2013).

The safety aspect that is considered in this thesis is the behaviour of the reactor during transients that could occur in an accident scenario, like a loss of flow or overpower. Therefore, most of the work is directed at using and developing models that can simulate that kind of transients. It should be noted that progress in computing technology offers the possibility to develop modelling methods that are much more computing intensive. Indeed, many of the established codes for modelling the existing reactors were developed many years ago when computing resources were limited. It is therefore relevant to develop new modelling methods that can take advantage of modern computing resources.

1.2 Objective

Transients of the SEALER reactor have been modelled with a code named BELLA (Bortot et al., 2015). It is a lumped parameter model coupled with point kinetics. The coolant temperature is divided into 4 sections (lumps): reactor core, hot leg, steam generator, cold leg and cold pool. For the entire reactor core, the fuel pin temperature is described with five temperatures: fuel center, fuel middle, fuel surface, clad inner and clad surface. The model calculates free surface levels and can take into account buoyancy and natural convection.

The transients obtained with this model generally exhibit the expected results from an advanced reactor. Namely, that reactivity feedback limits temperature excursions and that in the case of a loss of pumps, natural convection will take place and keep temperatures

below safety limits. However, between the forced flow and the natural convection during a loss of flow transient, the mass flow going through the pumps will undergo a disturbance or oscillation that could result in having reverse flow, see "disturbance amplitude" on Figure 1. This was identified as a potential safety issue by the authors of the SEALER design.

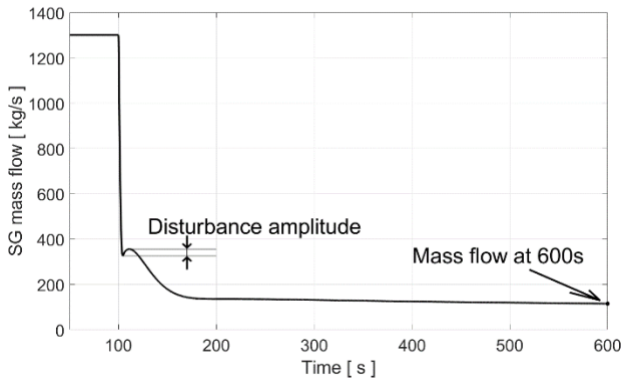

Figure 1 Mass flow disturbance at the beginning of a ULOF transient

The general objective of this thesis is to assess the safety of this type of reactors. In order to select a more specific objective, it was decided to study the issue described above. The result of that study should be able to establish the mechanism of that phenomenon and provide design recommendations. In the process of this study, a second objective emerged: to develop a more precise model for transient simulations. Instead of a lumped-parameter model, which has limited capabilities, a CFD-based model is to be developed. On top of coolant flow, it should also be able to model the free surfaces, neutronics feedback and accurate heat transfer inside fuel pins. In the context of this thesis, the new model will be used to study SEALER and the mass flow disturbance issue. However, that model could easily be adapted for any pool-type small reactor.

1.3 Outline of the thesis

This thesis is composed of three published (or publishable) articles, commonly called a "sandwich" thesis. Before the presentation of the actual articles, chapter 2 presents a literature review of works that were either used during the thesis or contain information

that was necessary to understand key concepts. That chapter also present a detailed description of the SEALER reactor.

Chapter 3 contains the methodology. Since the articles themselves already have a section on methodology, and in order to avoid repetition, this chapter aims to provide additional details that were out of scope for the articles. For example, details on the scripts used in the different studies are given in this chapter.

Chapter 4 to 6 contain the actual articles. The first part in the investigation of the issue described in the last section was to perform an uncertainty and sensitivity analysis using the already existing code BELLA. This study was able to determine which parameters have a strong impact on the "fluctuation" and to what extent. It was discovered that varying some parameters by realistic amounts could cause reverse flow. For example, reducing the pump coastdown time constant from 10s to 7s, or increasing the core friction factor by 30%. This study also investigated the cause of the fluctuation itself. All the work related to this study is presented in the first article, chapter 4.

The second part was to develop a model based on CFD that would be more precise than the lumped parameter model used in the sensitivity analysis study. That would allow to confirm the behaviour observed with the lumped parameter model and to explore the effect of selected parameters.

The new model encompasses the entire primary circuit with a simplification of the fuel channels, pumps and steam generators. Those parts are modelled through heat and momentum sources (or sinks), similar to the porous medium used in other studies. The CFD solver is coupled with a finite volume solver for fuel pin temperature and a point kinetics solver for neutronics. Free surface is modelled in CFD with multiphase volume of fluid method.

As part of the development of this model, a validation exercise was performed where CFD is used to simulate a flow of lead and compared against experimental data. TALL-3D is the name of the LBE loop (lead bismuth eutectic) that provided the experimental data and is located at KTH (Stockholm). The loop is a simple pipe network which contains a vessel

that was specifically designed for CFD validation. The CFD software (STAR-CCM+) was set in the exact same configuration that is needed for calculating reactor transients. The purpose was to ensure that the CFD software (as used in the reactor model) can properly predict important features in a flow of heavy metal, like temperature stratification and a jet into a plenum.

The second part of the thesis was divided into two articles. One of them, presents all the details of the methods used in the new CFD based model as well as the validation work with the LBE loop. The purpose of this article is to present all the background information necessary to understand how the model works and why it is viable, it's the second article of the thesis, presented in chapter 5. The other one, which is the third and last article of the thesis, in chapter 6, presents simulation results of a loss of flow transient, a comparison with the lumped parameter model and the effect of the pump flywheel.

The following diagram shows the different parts of the thesis, how they fit into three articles and the connection between all of them.

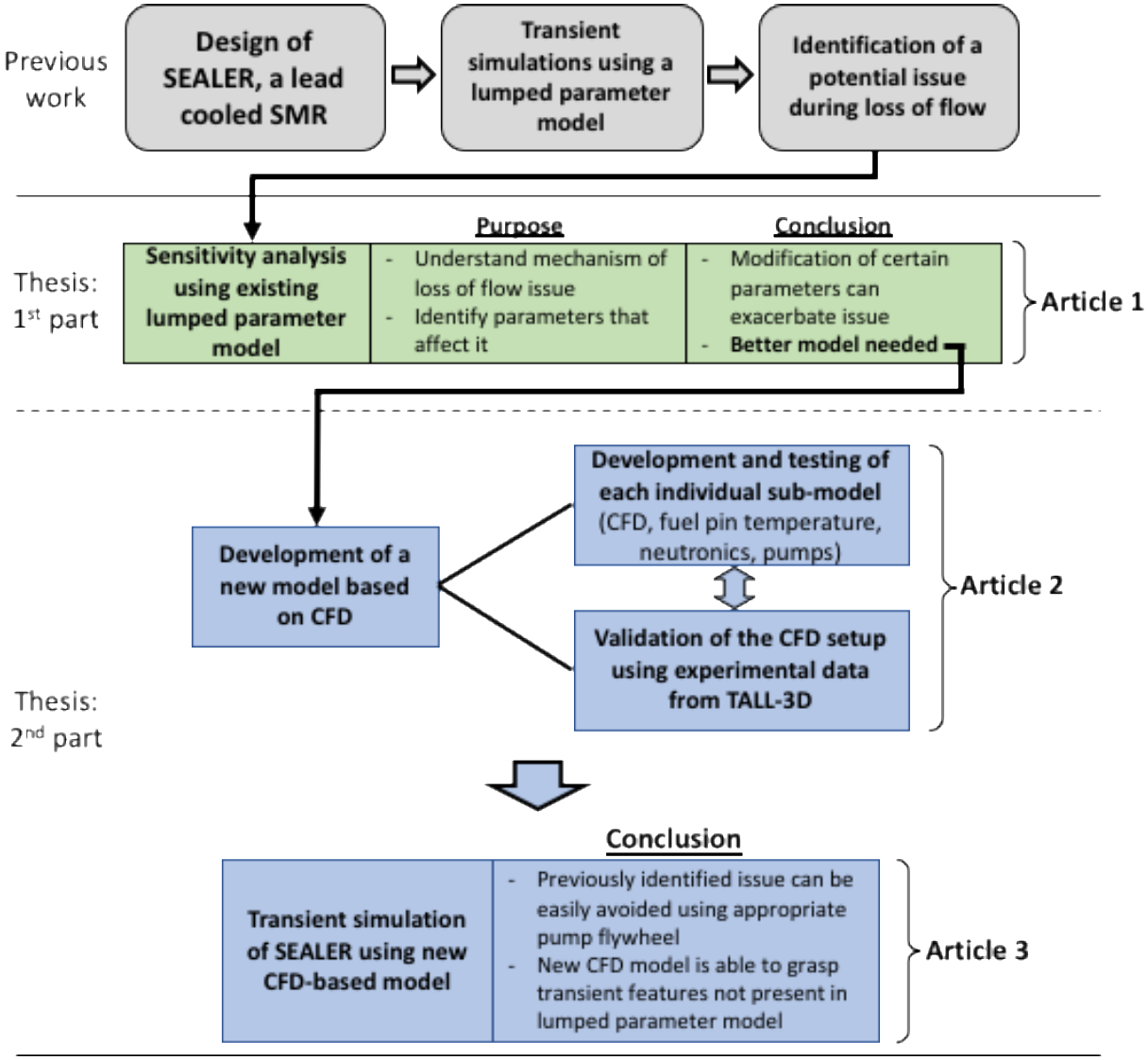

Figure 2 Diagram showing the different components of the thesis and the connection between them

Chapter 2 – Technical background

2.1 Design of the SEALER reactor

This section provides some details about the design of the SEALER reactor, which is used in all the sections of the thesis. This design was developed by Janne Wallenius, from KTH in Stockholm. A collaboration was set up with him in which he would provide all reactor parameters and details.

The target market for this reactor are remote communities and mines in the Canadian arctic. For this purpose, the reactor should be maintenance free, small enough for easy transportation, shouldn't require refueling and be walk away safe. The designer of SEALER concluded that the technology which best fits those requirements is a small lead cooled reactor. Its fast spectrum allows it to have a high conversion ratio which yields a long life without refueling. A thermal spectrum reactor of this size would not be able have such a long life without refueling. Among the coolants that are compatible with a fast reactor are lead, lead-bismuth eutectic (LBE) and sodium. A sodium cooled reactor requires a really high elevation between core and steam generator in order to achieve natural circulation, which doesn't fit the size requirement. LBE has similar properties to lead, but is more toxic and would require a larger evacuation area in case of coolant release. Therefore, lead was the preferred coolant.

The primary circuit of the reactor is contained in a vessel that is 2.75 m in diameter and 6 m high. A barrel divides the reactor vessel in two concentric regions, the middle one contains the cold pool, reactor core and hot leg (or upper plenum), and the outer region contains the pumps, steam generators and cold leg, see Figure 3. During normal operation, the coolant will move from the cold pool upwards into the fuel channels, where it is heated and then discharged into the upper plenum. From there, the coolant is moved to the outer region through 8 holes on the barrel, each connected to a pump. On the outer region, lead moves downwards through the steam generators and then to the cold leg. Finally, the cold

leg connects to the cold pool through holes on the barrel. The free surface is higher on the outer region because of the pressure generated by the pumps.

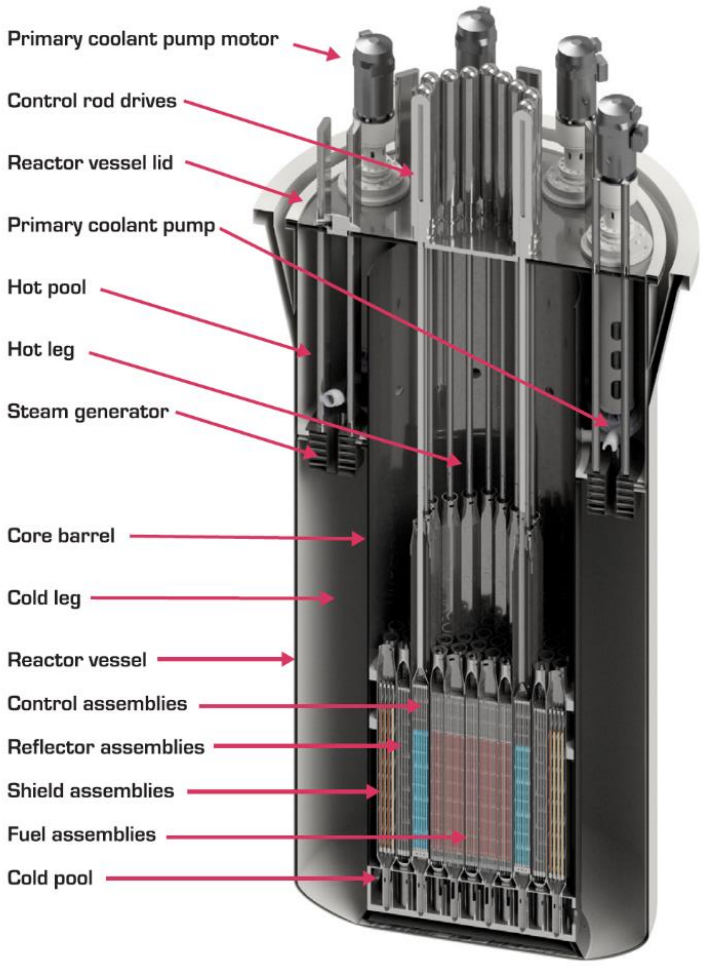

Figure 3 CAD rendering of the SEALER reactor

The reactor core has an hexagonal geometry, see Figure 4. In the center, there are 19 fuel assemblies, each containing 91 pins. The fuel material is ceramic UO_2 enriched at 19.75%. The fuel assemblies are surrounded by 12 burn-up control assemblies made of B_4C and 6

shut-down assemblies made of $(W_{0.48},Re_{0.52})B_2$. Since the reactor core is small, control and shut-down assemblies are not required in between the fuel. The burn-up control pellets use natural boron and shut-down pellets use boron enriched with ^{10}B at 96%. Those assemblies are themselves surrounded by reflector assemblies which contain pellets made of YSZ (yttria-stabilized zirconia). The last layer of assemblies are for shielding and contain pellets made of B_4C (^{10}B enriched at 96%). All assemblies are filled with coolant (lead) but only the fuel assemblies have a significant flow.

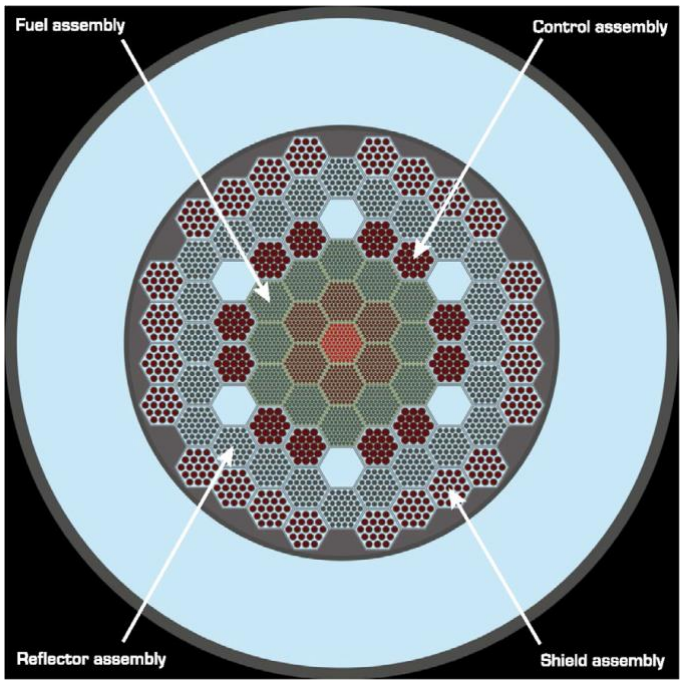

Figure 4 Map of the reactor core of SEALER

The reactor produces 8 MW thermal, which translate into 3 MW electric. It can operate 9900 full power days without refueling, or 30 years if assuming an availability of 90%. The average burnup of the fuel is 33 GWd/ton. The reactor has a negative temperature reactivity feedback coefficient. When the coolant temperature in the fuel, control and shut-down assemblies increases, its large reduction in density results in more neutron leakage. When the fuel temperature increase, the axial expansion of the fuel pins also decreases the reactivity.

During normal operation, coolant enters the reactor core at 663 K and undergoes a temperature increase of 42 K. One of the main considerations for choosing the operating temperatures is to avoid corrosion in the components of the primary circuit. The total mass flow of 1300 kg/s is achieved by eight pumps of radial impellers type. The head and mass flow of each pump is comparable to existing pumps used in the lead refining industry. Since this is the component which undergoes the highest level of corrosion, the design of the reactor is made to facilitate its replacement on a yearly basis if necessary. The steam generators located under the pumps require a very compact design. To this end, each steam generator consist in ten tubes staggered vertically where each tube is a spiral of four turns. The result is a bean shaped steam generator which fits precisely in the outer region of the reactor.

2.2 Literature review

This section presents selected publications that were either directly used in this thesis as a source of information, methods or data, or that were relevant in the understanding of certain concepts. The publications are organized by category and many of them are also mentioned in the three articles that make up the body of the thesis.

2.2.1 Publications relevant for reactor modeling

This section will briefly present relevant publications for modelling reactors. Special attention is given to recent methods and those that are designed for heavy metal reactors.

Jincheng Wang et al. wrote an extensive review of the existing neutronics/thermal hydraulics coupling methods (Wang et al., 2020). It lists and categorizes the different methods for solving thermal hydraulics, neutronics and the possible and most common combination of both. Thermal hydraulics contains three categories: 1D (system codes), 2D (sub-channel codes) and 3D (CFD). Neutronics is divided into two broad categories, stochastic (Monte Carlo) and deterministic. Where the latter is divided again in three categories: point kinetics, neutron diffusion and neutron transport models. The article offers

many tables listing different coupling methods, the commercial codes that are employed and the research team that developed it.

When it comes to performing simulations of the entire primary circuit, the most mature methods currently consist in coupling a system thermal hydraulics (STH) code with a deterministic neutronics code. An example of this would be to couple TRACE with PARCS (Krepel et al., 2010). Those codes are fast to compute and have been extensively validated. However, they are limited in the amount of details they can deliver and the geometry of the reactor.

Bonifetto et al. developed a model for large lead-cooled reactors called FRENETIC (Bonifetto et al., 2013). It couples thermal hydraulics with neutronics and models only the core of the reactor. The thermal-hydraulics module is based on modelling each fuel channel with a 1D model and coupling adjacent channels with heat conduction. The neutronics module is based on a multi-group diffusion model. This article contains all the equations and useful information for developing a 1D thermal hydraulics model for liquid metal.

Carlo Fiorina et al. developed a model based on the open-source software OpenFOAM(Fiorina et al., 2015). It is aimed at simulating transients in different types of reactors, both for core analysis and full primary circuit. Thermal hydraulics are solved with CFD, where the fuel channels are replaced by a porous medium. Pin temperature field is solved with a finite-difference method and a diffusion model for neutronics. Their model even incorporates a thermal-mechanics model. Although OpenFOAM is mainly a CFD software, it can be customized to solve many types of equations on a scalar or vector field. For instance, the authors of this model implemented a neutron diffusion model in OpenFOAM. All the different sub-solvers are coupled within OpenFOAM.

Moreau et al. elaborated a CFD model for the MYRRHA reactor, which is an accelerator driven system (ADS) cooled by lead-bismuth eutectic (LBE) (Moreau et al., 2019). Many components, including the fuel assemblies, are replaced by a porous medium. The coolant in the fuel channels is thermally coupled with the fuel which occupies the same volume but

whose physical properties were modified to take into account the real mass. That coupling incorporates a characteristic time to produce the right heat transfer delay during transients.

P. Martinez et al. use CFD for modelling the EPR primary circuit (Martinez and Galpin, 2014). Only steady-state calculations are performed by using volumetric heat source in the core and fixed mass flow boundary conditions at the pumps. Neutronics and fuel temperature are part of the model. For the fuel assemblies, instead of using a porous medium, the CFD geometry uses a 7x7 bundle instead of the 17x17 of the real design. The 7x7 bundle has the same flow area so that the right coolant velocity is obtained. The CFD software used in this work is STAR-CD.

The OECD has produced a report titled “Best Practice Guidelines for the Use of CFD in Nuclear Reactor Safety Application” (OECD, Revision 2014). This extensive report addresses a wide range of topics related to CFD for nuclear applications. Guidance is provided on determining if CFD is the appropriate tool, on the verification and validation process, the selection of physical and numerical models, consideration for special phenomena, and other topics. A large portion of the CFD applications for nuclear are not for modelling the entire reactor but rather smaller areas inside the reactor with a complex geometry. Accordingly, the guide mostly focuses on this type of problems. In this thesis, CFD is not used for a detailed description of a smaller and complex structure, but rather to integrate all the reactor components into one simulation. There are still some sections that are relevant. There is a section that discusses at length the different types of turbulence models, their range of application and limitations. Other sections elaborate on the physical and numerical models for free surfaces.

Another useful source of information is the SESAME project (thermal-hydraulics Simulations and Experiments for the Safety Assessment of Metal cooled rEactors). This European project, which ended in 2019, grouped an array of research teams, both experimental and numerical. Their purpose was to establish experimental databases for code validation and to create guidelines for modelling metal cooled reactors. One of their major publications is a book titled “Thermal Hydraulics Aspects of Liquid Metal Cooled

Nuclear Reactors" (Roelofs, 2019). The book covers many topics including thermal-hydraulic experiments with liquid metals, system codes, CFD modeling, multi-physics modeling and verification, validation and uncertainty quantification. The SESAME project also issued a report on "Best practice guidelines for liquid metal CFD" (Roelofs et al., 2018). Aside from providing general CFD guidelines, it also contains specific recommendations for liquid metals. For instance, turbulence models are discussed at length since the low Prandtl number of liquid metals makes the Reynolds analogy invalid. Indeed, the latter holds that the velocity and temperature boundary layers have the same shape, which is the case for water and air. However, for liquid metals, because of their high conductivity, the temperature boundary layer extends well beyond the velocity boundary layer. This is most important when modeling conjugate heat transfer. The report suggests a list of turbulent models well suited for liquid metals for different flow regimes.

2.2.2 Previous publications on modelling the SEALER reactor

Bortot et al. developed a code called BELLA for modelling different types of transients in a pool-type lead cooled reactor (Bortot et al., 2015). It is a lumped parameter model coupled with point kinetics. The coolant temperature is divided into 4 sections (lumps): reactor core, hot leg, steam generator, cold leg and cold pool. For the entire reactor core, the fuel pin temperature is described with five temperatures: fuel center, fuel middle, fuel surface, clad inner and clad surface. The model calculates free surface levels and can take into account buoyancy and natural convection.

Kevin Zwijsen et al. produced a CFD model specifically for the SEALER UK DEMO reactor (Zwijsen et al., 2020). The latter is a demo version of the SEALER UK, which itself is a bigger variation of the SEALER-arctic, the reference reactor of this thesis. For comparison, SEALER-arctic is about 8MWth, SEALER UK DEMO is 52 MWth and SEALER UK is 140 MWth. The CFD model contains the entire primary circuit and simplifies some of the components with porous media and specified momentum and heat sources. That CFD model is for calculating steady-states, so neither the free surface, the fuel pin temperature nor the neutronics are modelled.

2.2.3 Experimental facilities for heavy metal thermal hydraulics

KTH, in Stockholm, houses an lead-bismuth eutectic (LBE) loop called TALL-3D (Grishchenko et al., 2015). In the recent years, a battery of tests has been performed and used in benchmarks to validate system codes, CFD (Jeltsov et al., 2019) and the coupling of both (Grishchenko et al., 2020). This was done as part of the European SESAME project. The loop consists of three vertical legs of about 6m in height. At the top and at the bottom, the legs are connected to each other by horizontal pipes. In the right ("cold") leg, which contains a heat exchanger and a pump, the coolant typically flows downwards. In the left ("hot") leg, which contains a rod heater, the flow is usually upwards. The middle leg contains a 3D test section which was designed to compare with CFD codes. Thermocouples, pressure sensors and flow meters are placed at all the relevant locations in order to obtain a complete characterization of the thermal-hydraulics in the loop. TALL-3D is best suited to validate the codes' capabilities to model heavy metal flow and heat transfer in different flow regimes.

Also part of the SESAME project, the CIRCE (CIRColazione Eutettico) facility is located at the ENEA Research Centre of Brasimone (Italy) (Zwijsen et al., 2019). This is a large pool-type facility which also uses LBE as working fluid. The vessel is 10 m high and has a diameter of 1.2 m. It contains an electrically heated fuel pin bundle of 37 pins capable of generating 1 MW of heat. Instead of a pump, it has a "riser", which is a cylinder equipped with a nozzle at the bottom that injects argon and forces the LBE coolant to move upwards. It also has a heat exchanger for heat removal. The pool-type nature of this facility, the components it has, and its size and power make it very suitable for validating codes that simulate entire reactors.

At the Karlsruhe Institute of Technology (KIT), there is a facility dedicated to studying various aspects of heavy metal liquids called KALLA (KArlsruhe Liquid metal Laboratory). The facility performs experiments in four different categories: stagnant experiments, loop experiments, oxygen control and thermo-physical properties experiments, and water facilities. For example, in this thesis, results from a loop experiment called THEADES is used select the appropriate Nusselt correlation (Pacio et al., 2018).

2.2.4 Material properties

For lead, bismuth and LBE properties, the OECD produced a report titled "Handbook on Lead-bismuth Eutectic Alloy and Lead Properties, Materials Compatibility, Thermal-hydraulics and Technologies" (OECD, 2015). The first publication was in 2007 and an updated version was issued in 2015. It contains all necessary properties as functions of temperature. Uncertainty data is also included.

Carbajo et al. published a review which contains all relevant properties for MOX an UO2 fuels (Carbajo et al., 2001). Most of the properties are functions of temperature and porosity.

The specific type of stainless steel used for lead cooled reactors is still being developed and optimized. Indeed, corrosion is one of the main issues with this type of reactors, and therefore special stainless steel which can resist corrosion from lead are required. However, for material properties purposes, it is sufficient to use the ones for alloy D9, which can be found in Leibowitz et al. (Leibowitz and Blomquist, 1988) and Banerjee et al. (Banerjee et al., 2005).

2.2.5 Correlations

Correlations for pressure drop and heat transfer in the fuel assemblies are needed for the model that is developed in this project. The type of assembly in consideration is a hexagonal geometry, wire wrapped, and cooled with liquid metal. E. Bubelis et al. wrote a review comparing different correlations for friction factor and pressure drop in wire-wrapped fuel bundles (Bubelis and Schikorr, 2008). The following correlations were part of the study: Novendstern model, Rehme model, Engel Markley and Bishop model, Cheng and Todreas model, Baxi and Dalle-Donne model and Sobolev model. That study identifies the Rehme model as being the most accurate with most type of coolants. G. Kennedy et al. published results from the COMPLOT LBE facility which replicates a fuel bundle from the MYRRHA reactor, an LBE-cooled research reactor (Kennedy et al., 2015). A comparison with some of the models listed above also shows the Rehme model as the most accurate. In 2018, Chen et al. published an upgraded version of the Cheng and Todreas model (UCTD)

(Chen et al., 2018), which was compared against many experimental data sets, including COMPLOT. This is currently the most accurate model for wire-wrapped fuel bundles.

The heat transfer between fuel pin surface and coolant is dictated by the Nusselt number. Pacio et al. published experimental results on Nusselt numbers in LBE-cooled fuel bundles (Pacio et al., 2018). The experiments were conducted at ENEA (Italy) and KIT (Germany). The results were compared against correlations. For wire-wrapped bundles, they recommend the Kazimi and Carelli correlation.

2.2.6 Pump

The relation between the pump head, torque and the volumetric flow can be modelled with the pump characteristic curves. There are two curves, one for the pump head and the other for the torque. Both are polynomials that are function of coolant volumetric flow and rotor angular speed. The coefficients of the polynomials are determined experimentally for a specific pump, or family of pump. In SEALER, the reference reactor used in this study, the pump has not been selected. Therefore, it was decided to use the coefficients of the pumps of another nuclear power plant, the Maine Yankee, which are provided in Todreas and Kazimi (Todreas and Kazimi, 1990). Note that the functions use dimensionless variables (head, torque, volumetric flow rate and rotor angular speed), so the same coefficients can be used for large and small pumps.

2.2.7 Sensitivity analysis

Sensitivity analysis is a wide field that has applications in many areas. Borgonovo published a book on this subject that explains in mathematical details many of the different methods and tools that exist (Borgonovo, 2017). One way of dividing the sensitivity analysis methods is into analytical and numerical. Analytical methods can only be used in models where it is possible to map inputs to outputs analytically. This usually involves partial derivatives. If the model needs to be solved numerically, as is the case with CFD and most cases related to reactor modelling, numerical methods have to be used. This is usually done by running the model at different input values and analyzing its effect on a

certain output. Saltelli et al., on a book that he published on sensitivity analysis, explains the concept of global sensitivity analysis (Saltelli et al., 2004). That is opposed to local sensitivity analysis, where only the effect of one input parameter is considered at a time. In a global sensitivity analysis, the effect of a certain input parameter is analyzed while varying all the other parameters at the same time. This is a more comprehensive approach that can take into account any kind of non-linear interaction between inputs. An easy implementation of this is with a Monte-Carle based method. Here, every input is defined as a distribution according to its uncertainty. The model is solved a large number of times. For every time, the value of each input is randomly selected according to its distribution. A linear regression is then obtained between the output and every input. The slope of that regression is the value of the sensitivity of that input. That method requires a large number of runs. Other methods, like the Morris method, employ a statistical analysis that can retrieve enough information with a limited number of runs.

As an example, Gajev et al. performed a sensitivity analysis on the modelling of a transient that occurred in the Oskarshamn-2 BWR (Gajev et al., 2014). The model is performed with the codes TRACE/PARCS. The transient, which was caused by a loss of feedwater preheaters and control system failure, consists in diverging power oscillations followed by a SCRAM. The sensitivity analysis performed in this study is similar to the Monte Carle method described above. However, a limited number of simulation runs is performed (93), and a Spearman rank correlation coefficient is used to determine the most sensitive input parameters.

Chapter 3 - Methodology

This chapter provides details about the methods used in the different studies of this thesis. In order to avoid repetition, it is intended to be complementary to the information already provided in the articles themselves. For instance, a description of the scripts used in the different studies is out of the scope for the articles, but is provided here. For a more coherent order, the reader may want to read the articles first, which are presented in the subsequent chapters.

3.1 Uncertainty and sensitivity analysis

This study employs a lumped-parameter model, called BELLA, to perform an uncertainty and sensitivity analysis of two types of transients of the SEALER reactor. It is presented entirely in the first article. This section is divided in two parts, the first one describes in details the lumped-parameter model, and the second one provides details on the methods to perform the uncertainty and sensitivity analysis.

3.1.1 Implementation of the lumped-parameter model BELLA

This model was developed by Bortot et al., from KTH, and is intended specifically for pool-type lead-cooled reactors (Bortot et al., 2015). The model was provided to the author of this thesis by Janne Wallenius, from KTH, in the form of a Mathematica script. The latter was then translated into Matlab in order to facilitate the integration with the rest of the analysis.

The model divides the reactor into a total of 9 regions:

- Center, middle and surface fuel
- Inner and surface clad
- Coolant in reactor core
- Hot leg

- Cold leg
- Cold pool

Then, 22 differential equations are used to obtain the evolution of the power, temperature, mass flow and free surface levels in the corresponding regions:

- 9 equations for heat transfer between all regions
- 2 equations for mass flow at the core and steam generator
- 2 equations for the free surface levels of the hot and cold legs
- 9 equations for point kinetics (8 precursor groups are used)

The following diagram illustrates, in a simplified manner, all the regions and equations mentioned above. The regions are the rectangular areas and the equations are the circles or rounded rectangles. Note that it is a simplified diagram which doesn't show all the inputs of every equation. For instance, point kinetics is influenced by coolant temperature and heat transfer inside fuel is affected by fission power, both not shown on this diagram for simplification purposes.

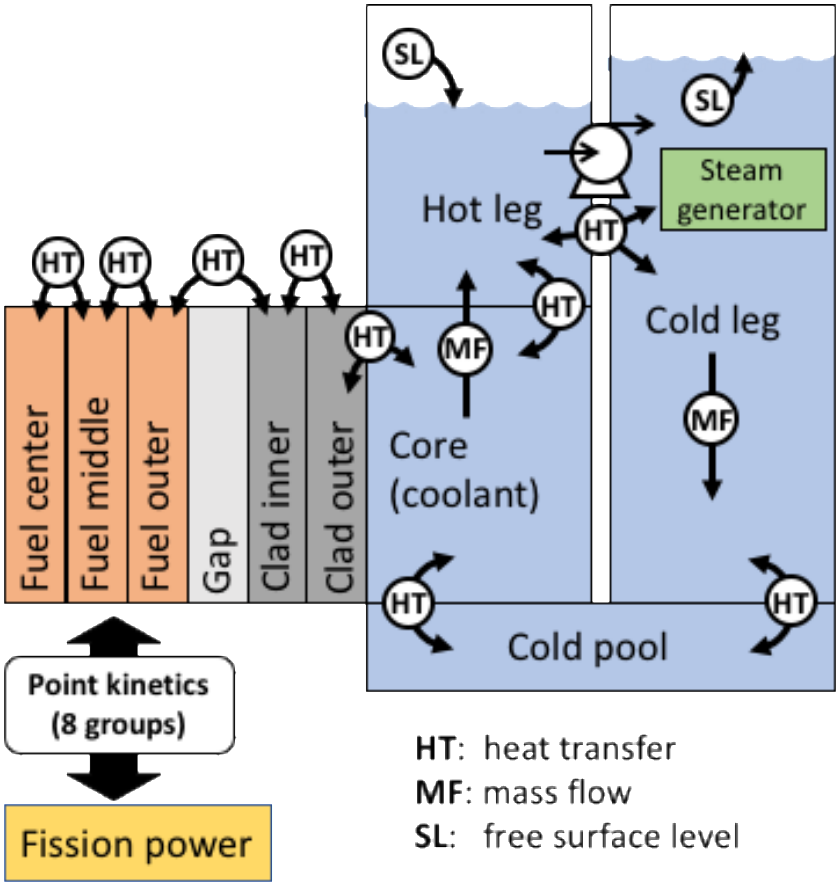

Figure 5 Structure of BELLA model showing how the reactor is divided into 9 regions (rectangles) and transients solved with 22 equations (circles and rounded rectangle)

The Matlab implementation of the model is divided in three scripts. The first one is a list of input parameters. This includes the geometry of the reactor, material properties, neutronics properties and thermal-hydraulic correlations. In Matlab terminology, this script is a function with no inputs and whose output is a structure array containing the inputs. The second one is also a function whose input is the structure array containing the input parameters, and the output is a structure array containing both input and derived parameters. The last one is also a function, its input is the structure array containing all parameters and its output is a structure array containing the evolution in time of every state variable. This last script contains the system of 22 differential equations and solves it using the Matlab function ode15s, with a relative tolerance of 1e-6. Material properties, thermal-hydraulic correlations and reactivity feedback are implemented as local functions that depend on

temperature (and flow velocity in some cases). Running the simulation takes less than a second on one processor.

3.1.2 Methods of the uncertainty and sensitivity analysis

The uncertainty and sensitivity analysis is performed using a Monte Carlo approach. Every input parameter is assigned an uncertainty as described in the article. It is then assumed that every input parameter is a uniform distribution ranging from the mean value minus to plus its uncertainty. A normal distribution would in principle be more accurate, but a uniform distribution was preferred for simplicity and is sufficient for this exercise. A large number of simulations runs is performed, in this case 5000 runs were used. In each run, each input parameter is randomly selected inside its uncertainty range. After running all the simulations, every output or quantity of interest (QOI) will result in a distribution that closely resembles a normal distribution. The mean value and standard deviation can be obtained from that distribution, which is the essence of the uncertainty analysis. It is not necessary to use such a large number of runs. However since one run takes a few seconds of computing time, a deliberate large number of runs was easy to perform and ensured a good accuracy. An alternative method could've been to set an accuracy threshold and stop running more simulations when reached.

The sensitivity analysis is performed by assuming that the QOI deviation from its mean value is a linear combination of all the parameters deviation from their mean value.

$$\Delta y = b_1 \Delta p_1 + b_2 \Delta p_2 + \cdots + b_n \Delta p_n$$

Equation 1

Where $\Delta y = y - \bar{y}$ is the QOI deviation from its mean value, $\Delta p_x = p_x - \overline{p_x}$ are the parameter deviations from their mean value and b_x are the coefficients.

The sensitivity of every parameter is derived from its coefficient b_x which itself is obtained by a linear regression using all the simulation runs. Figure 6 shows an example of that

regression with the parameter fuel conductivity and maximum fuel temperature as QOI. The plot displays the maximum fuel temperature of all 5000 runs, organised in the x-axis with the value of fuel conductivity.

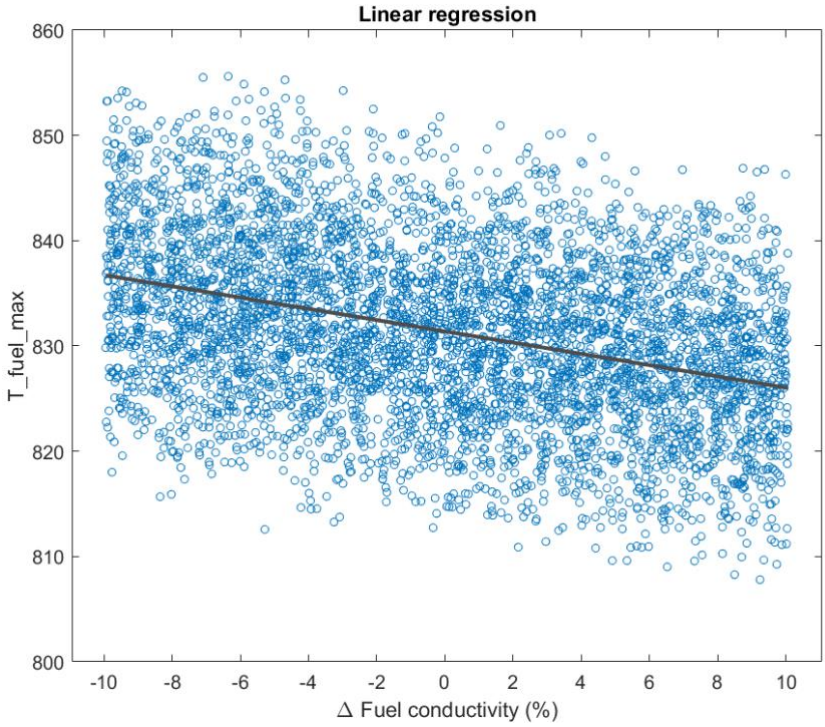

Figure 6 Example of linear regression to obtain the sensitivity of a parameter

Performing a linear regression on that data set yields the value of b for that parameter. The notion of sensitivity used in this study is the following: how much does the QOI varies if the parameter is changed by one standard deviation. To obtain a numerical value for that, it is necessary to multiply b by the standard deviation σ_x of that parameter. It is also convenient to divide by the standard deviation of the QOI σ_y to obtain a normalized value. The result is called standardised regression coefficient (SRC):

$$SRC_x = b_x \sigma_x / \sigma_y$$

Equation 2

Using Matlab functions to perform the simulations allows for an easy automation of the process to obtain the uncertainty and sensitivity. An Excel file contains a list of every input

parameter and its uncertainty. The procedure to perform the 5000 simulation runs is contained in one script that loops through the following steps:

1. A set of input parameters with the mean value is generated as explained previously.
2. The input parameters are modified randomly inside their uncertainty range, which is read from the Excel file.
3. The derived parameters are generated using the modified input parameters.
4. The modified parameters will affect the pressure drop, which will affect the mass flow and the reactor power. To maintain the nominal power, the pump head needs to be adjusted to the new parameters. This is done by iteratively running steady state calculations, looking at the difference between "measured" power and nominal power, and adjusting the pump head accordingly. It will also modify the initial conditions of the free surface levels and the cold and hot leg temperatures.
5. Having all the modified parameters and appropriate initial conditions, the actual simulation is performed by using the function that solves the 22 differential equations.
6. All the simulation results and parameters are stored.

These steps are repeated 5000 times. Since every simulation is very fast, the whole process could be achieved in one day on a desktop computer. Having all the necessary data, a different script is then used to calculate the uncertainty and sensitivities. The appropriate QOIs are extracted from each simulation. For each QOI, the 5000 points are used to plot the distribution and calculate the standard deviation and mean value. Also for each QOI, and each input parameter, a data set of 5000 points linking parameter with QOI is used to obtain the linear regression, see Figure 6. Finally, the SRC can be calculated as was described previously.

3.2 CFD-based model

The second article of this thesis is a methods paper about the CFD model. Therefore, most of the details are provided in that article. This section provides additional information that

is too detailed for the article. As was mentioned earlier, it makes more sense to read the article first.

The CFD model couples three different physics, each with its own solver:

- Thermal-hydraulics of the coolant in the entire primary circuit, solved by CFD
- Heat transfer in the fuel pins, solved by a custom code in Matlab
- Neutronics, solved by point kinetics (also custom code in Matlab)

The most accurate model for neutronics would be a transport or Monte Carlo code, however these are computing intensive and more complicated to integrate. For the purpose of this study, a point kinetics method was deemed sufficient. The distribution of fission power and reactivity feedback coefficients were all calculated in Serpent (a Monte Carlo code for neutronics). The transient of interest in this study is a loss of flow (ULOF), where the temperature change is quite uniform in the reactor core. Given this, it is reasonable to assume that the fission power will maintain the same distribution, only its amplitude will change. Reactivity feedback coefficients will also be used in accordance with the way they were originally calculated, i.e. uniform temperature change. Therefore, in this case, point kinetics can be used while maintaining a very good approximation of the fission power distribution inside the fuel pins throughout the transient.

The CFD software used for this work is STAR-CCM+. The geometry corresponds to the volume occupied by the coolant in the primary circuit. The solid parts are not modelled. A relatively coarse mesh is used and some components are simplified by using momentum and heat sources and sinks (similar to a porous medium). Those components are the fuel channels, the pumps and the steam generators. Figure 7 illustrates the geometry of every fuel channel used in this model. The coolant flows through the highlighted yellow area. The purpose of this shape is to maintain the same flow area to obtain the right coolant velocity, which is required for the heat transfer and friction correlations. The heat transfer in the fuel pins, neutronics and the coupling are all programmed in Matlab. Text and CSV files are used to interface between Matlab and STAR-CCM+.

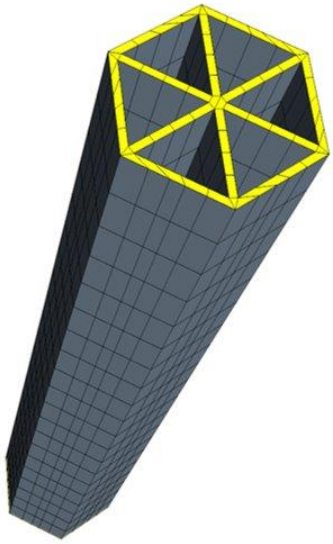

Figure 7 Fuel channel geometry in CFD model

The heat transfer and pressure drop correlations are calibrated for a developed flow. In reality, there is a short distance at the entrance of the channel where the flow is not developed yet. It should be noted that this introduces a small source of error since the correlations not fully apply in that short distance.

The following sections provide extensive details about the fuel channels (pressure drop and heat transfer) and the coupling algorithm. Other aspects are well covered in the second article.

3.2.1 Pressure drop in the fuel channels

Pressure drop is taken into account by introducing a customized momentum source in STAR-CCM+. That is done for each fuel channel independently. The source is calculated from the following relation:

$$\frac{\Delta P}{L} = f(Re)\frac{\rho \cdot v|v|}{2 \cdot D_e} \quad \left[\frac{kg}{m^2 s^2}\right]$$

Equation 3

Where:

$\frac{\Delta P}{L}$ is the momentum source (pressure drop per unit length),

$f(Re)$ is the friction factor, which is a function of Reynolds number,

ρ is the coolant density,

v is the coolant velocity, and

D_e is the equivalent hydraulic diameter of the fuel assembly

The main task is to obtain the right value for the friction factor. Many empirical correlations exist to calculate the friction factor as a function of the Reynolds number and the dimensions of the fuel bundle (Bubelis and Schikorr, 2008). The one used in this work is the Updated Cheng and Todreas Detailed (UCTD) correlation (Chen et al., 2018). This correlation was developed for wire wrapped bundles and has been tested against many experimental data sets.

The procedure to obtain the friction factor is not a simple equation, but rather a series of steps that would be too complicated to implement in STAR-CCM+. Therefore, the strategy adopted here is to calculate the friction factor using UCTD for a range of relevant Reynolds number and for one specific set of bundle dimensions. That data is then fitted with a function of the following form:

$$f(Re) = \frac{A}{\log Re} + B + C(\log Re) + D(\log Re)^2$$

Equation 4

Where A, B, C and D are the fitted parameters. That simple equation only depends on the Reynolds number and can be easily implemented in STAR-CCM+.

To validate and verify our model, it was compared against data from the COMPLOT experimental facility where thermal hydraulic tests are being performed for the MYRRHA reactor (Kennedy et al., 2020). That bundle has 127 pins and uses LBE as a coolant. The following figure shows the geometry used in STAR-CCM+ to model the COMPLOT

bundle. The green area in the middle is the fuel bundle, which consists of a simplified geometry as shown on Figure 7. The gray pieces on each side are normal (full) domains. Only the diameter of the hexagonal duct, the length of the bundle and the flow area are used directly in the STAR-CCM+ geometry. The other dimensions (pin diameters, pitch, etc.) are used to calculate the friction factor with UCTD and to derive the parameters of Equation 4. These parameters are used in STAR-CCM+ to calculate the momentum source.

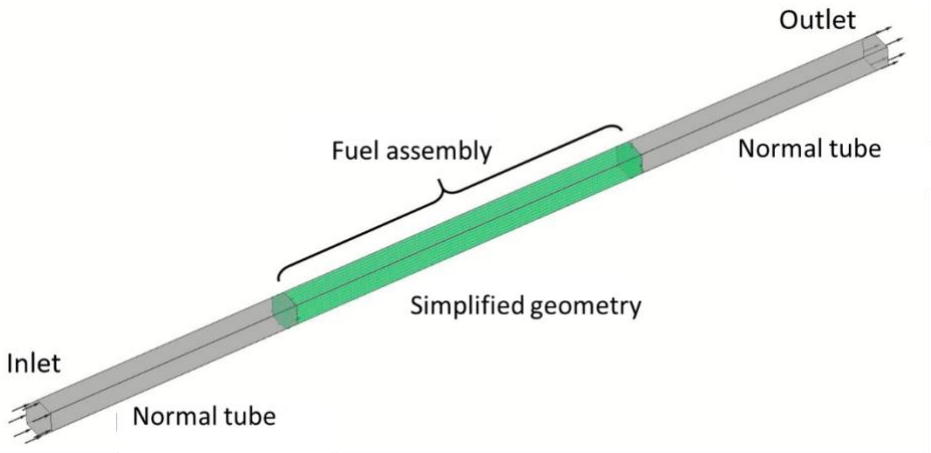

Figure 8: geometry used in STAR-CCM+ to model the COMPLOT bundle

A series of steady state calculations was made using different mass flows and temperatures in order to cover the range of Reynolds numbers and temperature of the experimental sets. The following figure shows the pressure profile (from STAR-CCM+ calculation) along the channel for Re = 50,000 and T = 350 °C. The fuel bundle starts at Z = 1m and ends at Z = 2.4m. The sudden change in pressure at the entrance and exit of the bundle is caused by the sudden change in flow area. From this data, the friction factor is calculated using Equation 3. This procedure is repeated for each Reynolds number and temperature that was tested.

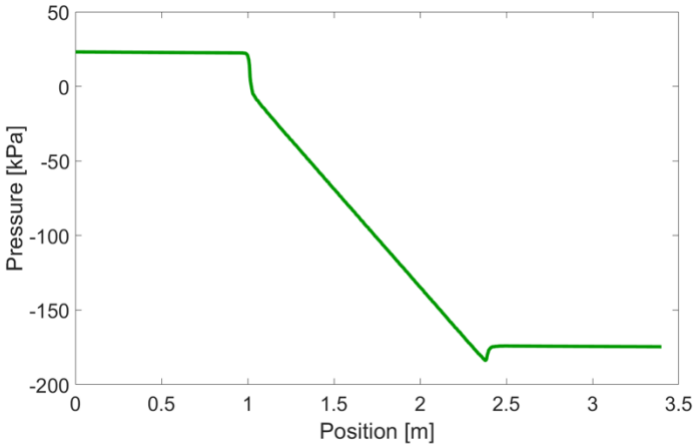

Figure 9 Pressure profile from a STAR-CCM+ calculation of the COMPLOT bundle at Re = 50,000 and 350 °C

All the results are compiled on the next figure. The blue and red circles and diamonds are the experimental sets from COMPLOT, which operated at two different temperatures: 200 °C (blue) and 350 °C (red). The dashed green line is the friction factor calculated with UCTD. The red line is the fit of the UCTD and it's the friction factor that is actually used in STAR-CCM+. The very small difference between the fit and the UCTD is negligible compared to the uncertainty from the experimental data. The cyan squares are the friction factors derived from the results of the CFD calculations. As expected, they fall exactly on the fit since the latter is used to calculate the momentum source in STAR-CCM+.

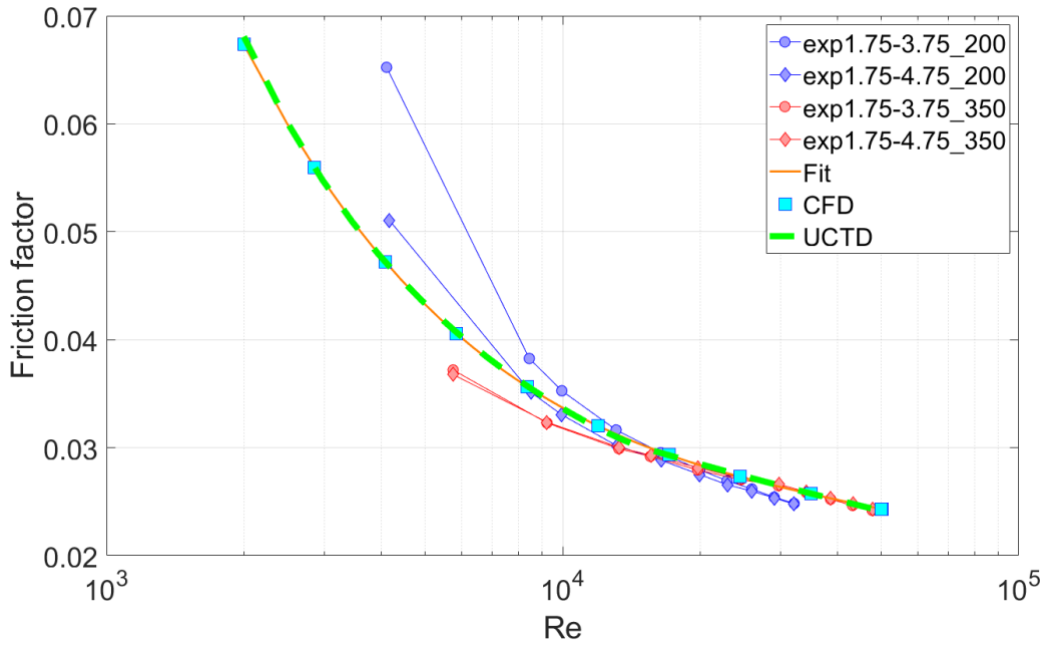

Figure 10 Friction factor from experimental data, UCTD correlation, fit of the UCTD correlation and CFD calculations

3.2.2 Heat transfer in the fuel pins

Heat transfer in the fuel pins is solved by a custom script programmed in Matlab. This solver takes coolant temperature and velocity, and fission power as inputs, and calculates the pin temperature distribution and pin-coolant heat transfer for the new time step. Since it is assumed that all the pins in one assembly have the same temperature distribution, only one fuel pin per assembly needs to be solved for, which greatly simplifies the calculations. This simplification somewhat deviates from reality given that the neutron field decreases radially sharply. However, this is compatible with the approach used for the reactor core which is analogous to a system code.

The method used to solve heat transfer inside fuel pins is to divide the length of the pin into slices, and then divide each slice into “rings”. Since the gap between fuel and clad is very thin, it is assumed that convection is negligible and the gap is simply treated as a solid. It

is also assumed that everything is uniform around each ring. In this case, solving heat transfer in one slice is a 1D problem. Figure 11 shows a schematic of how geometry is divided and the different variables that are used. Note that the amount of cells is for illustration purposes. For most of the tests, fuel pins were divided in 10 slices and 30 rings (10 for fuel, gap and clad).

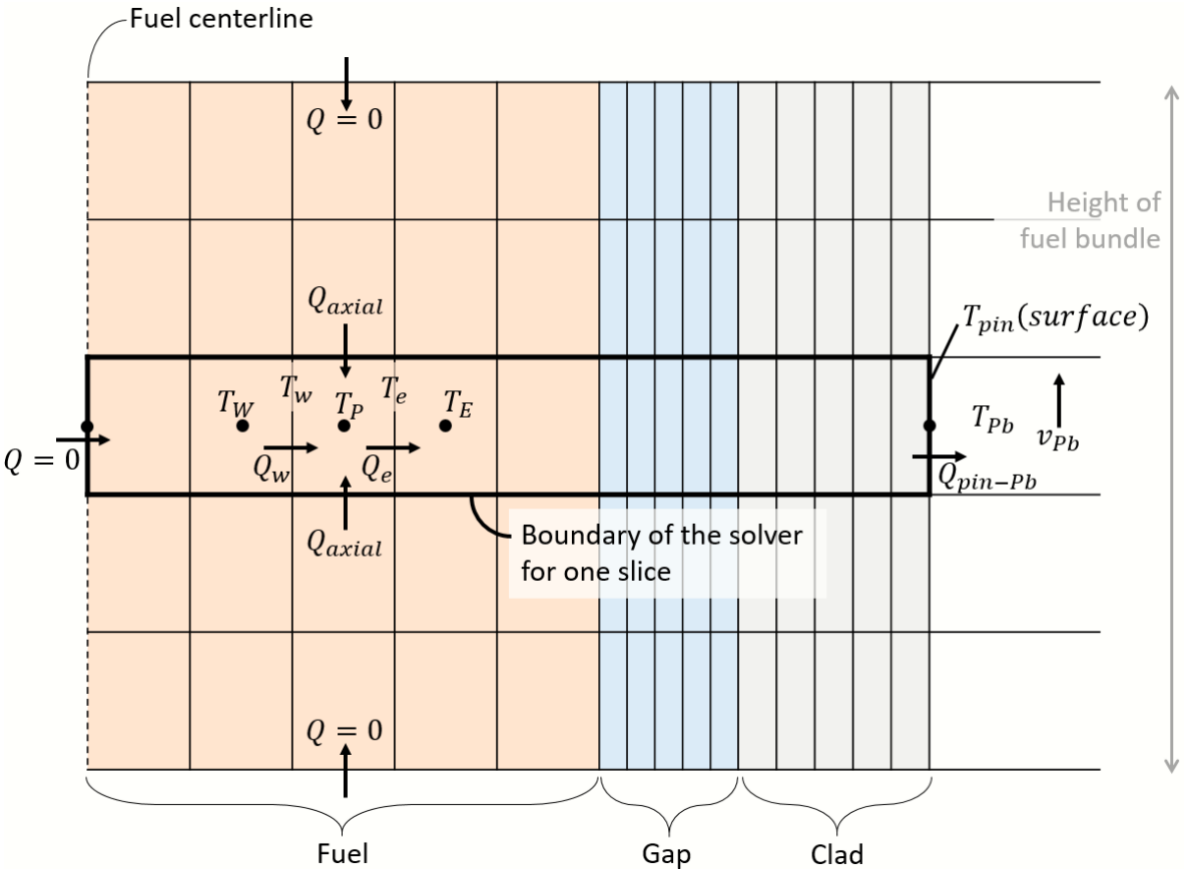

Figure 11 Schematic of the heat transfer solver

Slice solver

The building block for solving heat transfer inside fuel pins is the subroutine that solves temperature distribution in one pin slice, called the "slice solver". This is a 1D heat transfer solver. In Figure 11, it corresponds to the area surrounded by a thick black line. This solver

is based on a general control volume approach where every ring (control volume) is governed by the following equation:

$$\rho c_P V \frac{T_P - T_P^0}{\Delta t} = Q_w - Q_e + Q_{axial} + Q_{source}$$

Equation 5

Where:

ρ is the density

c_P is the heat capacity

T_P is the current temperature at the center of the control volume (variable to solve)

T_P^0 is the temperature at the center of the control volume of previous time step

Δt is the length of each time step

Q_w is the heat [W] going into the control volume from the west control volume (inner ring)

Q_e is the heat [W] going out from the control volume from to the east control volume (outer ring)

Q_{axial} is the total heat [W] coming from the control volumes in the slices above and below

Q_{source} is the heat [W] generated in that control volume (from fission)

When executing the slice solver subroutine, only T_P is solved, all other quantities listed above are constant (for a given control volume). Variations and temperature dependency of those quantities are taken into account iteratively running the slice solver, as will be explained in the next section.

Q_w and Q_e are calculated with the face temperatures T_w and T_e:

$$Q_w = -k_P A_w \frac{T_P - T_w}{\frac{\Delta x_P}{2}} \qquad Q_e = -k_P A_e \frac{T_e - T_P}{\frac{\Delta x_P}{2}}$$

Equation 6

Where:

k_P is the thermal conductivity of this control volume

A_w and A_e are the surface area of the west and east faces respectively

Δx is length of the control volume (thickness of the ring in the radial direction)

Since the thermal conductivity changes significantly between fuel, gap and clad, the face temperatures cannot be approximated to the simple average between the center temperature of two adjacent control volumes. Thus, face temperatures are calculated by taking thermal conductivity into account:

$$Q_e = -k_P A_e \frac{T_e - T_P}{\frac{\Delta x_P}{2}} = -k_E A_e \frac{T_E - T_e}{\frac{\Delta x_E}{2}}$$

Equation 7

$$\Longrightarrow \qquad T_e = \frac{\frac{k_E}{\Delta \mathrm{x_E}} T_E + \frac{k_P}{\Delta x_P} T_P}{\frac{k_P}{\Delta x_P} + \frac{k_E}{\Delta x_E}}$$

Equation 8

Equation 8 and an analogous one for T_w are substituted into Equation 6, which themselves are substituted back into Equation 5. The final set of equations (one for each control volume) is of the form:

$$a_P T_P = a_w T_W + a_e T_E + b$$

Equation 9

Where the coefficients a_P, a_w, a_e and b only depend on geometry, material properties and previous time step. For this sub-solver, the boundary conditions on the left (centerline) is adiabatic and the one on the right (surface of clad) is a set temperature. The set of equations is solved directly with the TDMA algorithm. This is part B2 on Figure 16.

Coupling slices and accounting for temperature dependency of material properties

To solve for the whole length of the fuel pin (the 2D problem), the slices are coupled together through an iterative process where Q_{axial} (see Figure 11) of the current iteration is calculated from the temperature distribution of the previous iteration. This corresponds to part B1 on Figure 16.

Since material properties are dependent on temperature, a few iterations of the slice solver are required to obtain a converged solution. In every iteration, the material properties of every control volume correspond to the temperature of the previous iteration. In practice, the same iteration loop is used to couple the slices and to take into account the temperature dependency of the material properties.

In order to validate the slice solver and the coupling of slices, it was compared against a CFD simulation using a relatively fine mesh (see Figure 12). The same dimensions and material properties were used in both solvers. In CFD, the gap was set as a solid (even if it's helium) in order to solve the same problem as in the custom Matlab solver.

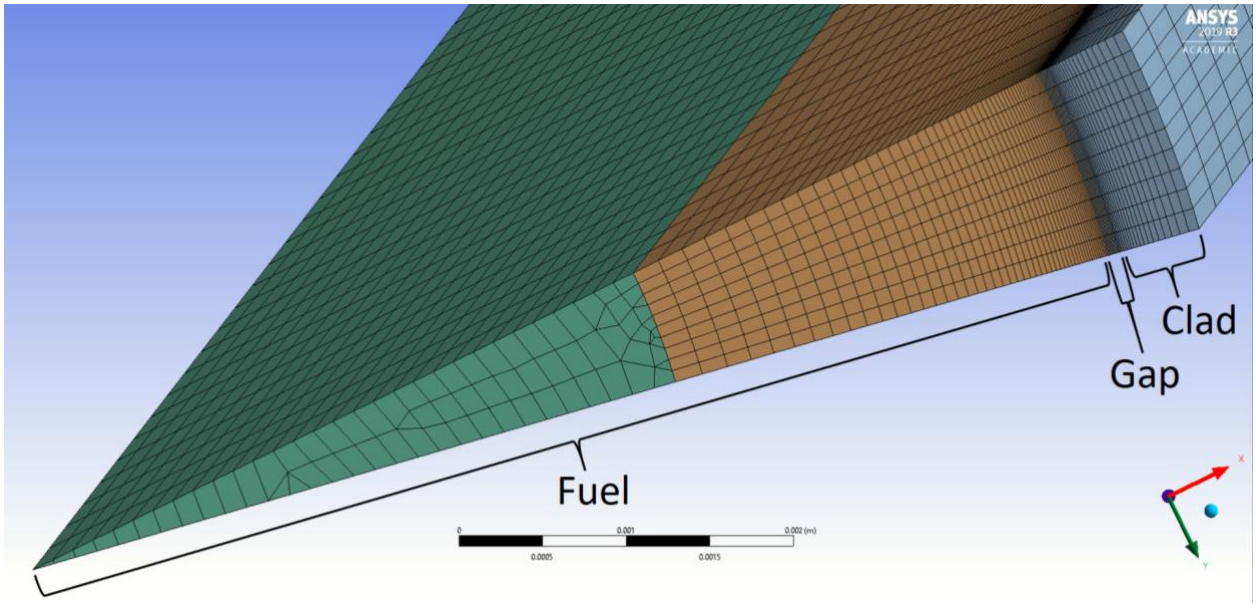

Figure 12 Mesh used to solve heat transfer inside a fuel pin with CFD

The boundary condition on the clad surface was set at 400 K. Initial conditions were also 400 K everywhere. The problem is a transient where power increases linearly from zero to maximum amplitude in 5s, followed by a 60s plateau, then decreases linearly to zero in 5s (see gray line in Figure 13). The maximum amplitude corresponds to 0.66 MW for the whole bundle, which is the steady state power of the central bundle in the SEALER reactor. The results of the test are shown in Figure 13 to Figure 15. The CFD solution and the slice solver (Matlab code) are essentially identical.

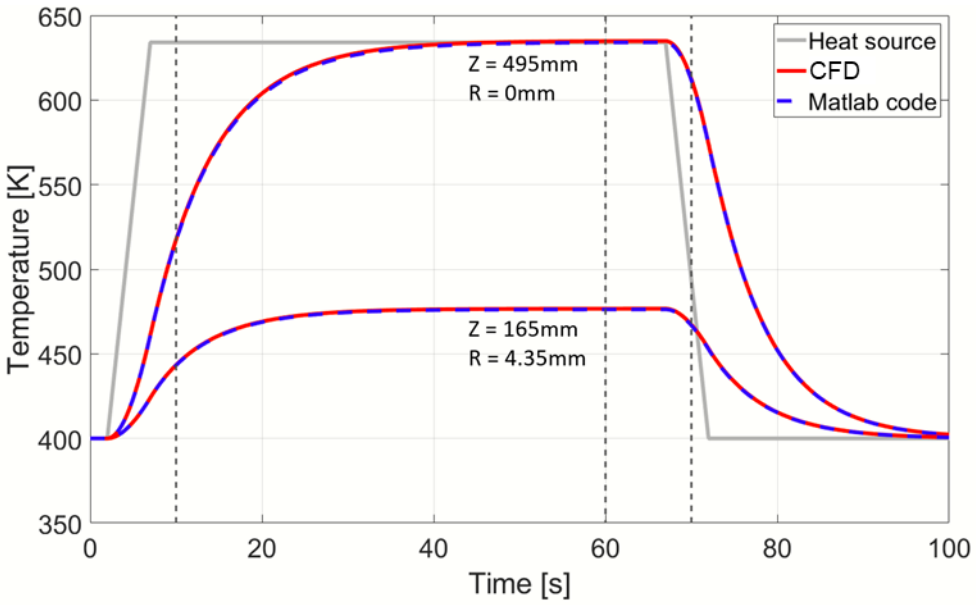

Figure 13 Validation of the fuel pin external solver with CFD: temperature at two different points throughout the transient

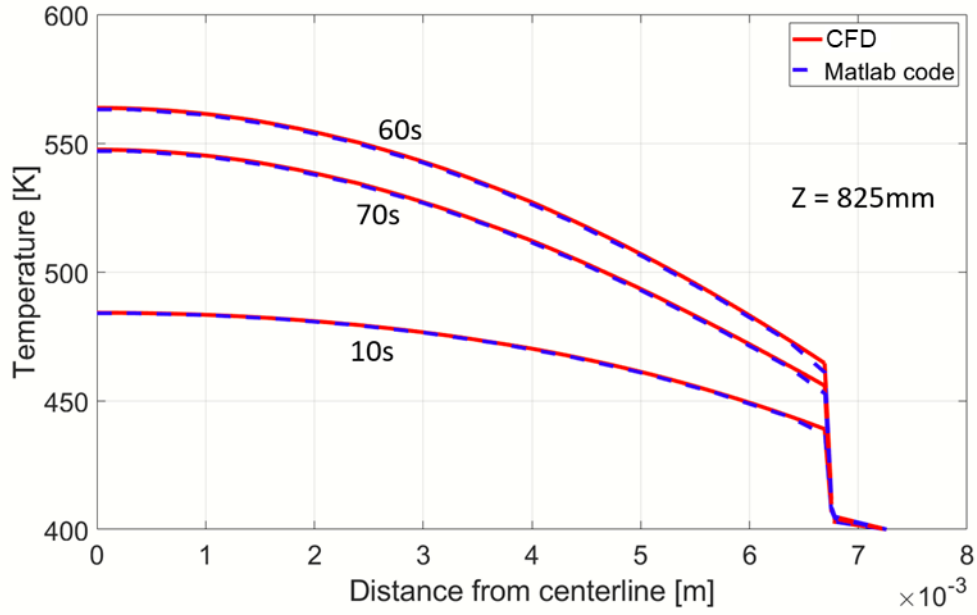

Figure 14 Validation of the fuel pin external solver with CFD: radial temperature distribution at three different times

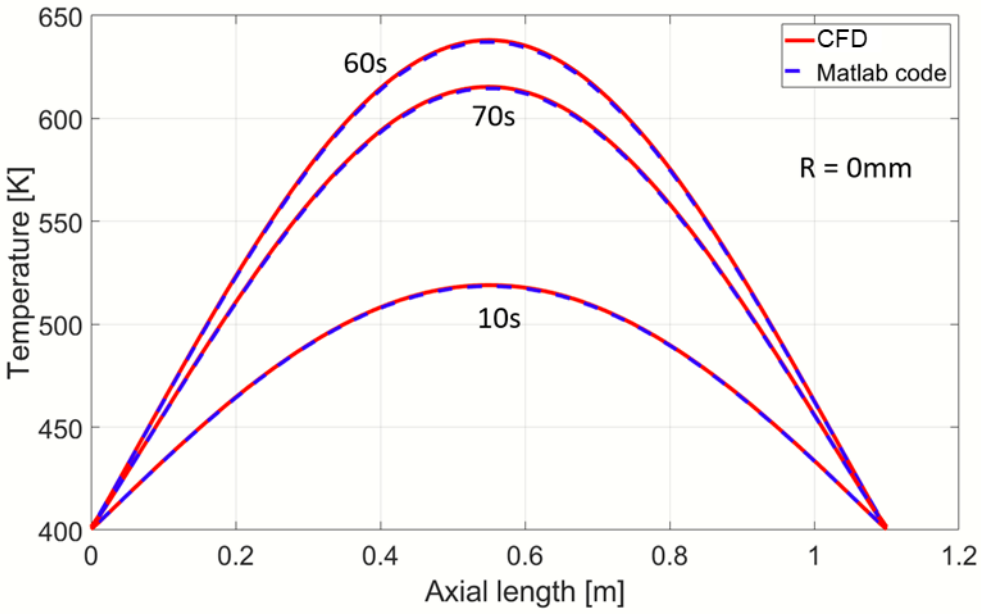

Figure 15 Validation of the fuel pin external solver with CFD: centerline temperature at three different times

Using coolant temperature and velocity as boundary conditions

The solver described so far uses a fixed temperature on the clad surface as a boundary condition. However, in order to couple the heat transfer solver with the CFD simulation, coolant temperature and velocity need to be used as boundary conditions. The key element for establishing this connection is the Nusselt number:

$$Q_{pin-Pb} = Nu \frac{k_{Pb}\left(T_{pin}(surface) - T_{Pb}\right)}{D_h} A_{pin}$$

Equation 10

Where:

Q_{pin-Pb} is the heat transfer [W] from pin to coolant

k_{Pb} is the thermal conductivity of the coolant

$T_{pin}(surface)$ is the clad surface temperature

T_{Pb} is the coolant temperature

D_h is the hydraulic equivalent diameter of the bundle

A_{pin} is the total surface area between pins and coolant

The Nusselt number Nu is a function of pin pitch to diameter ratio and Peclet number. The correlation used here is the Kazimi and Carelli correlation used for sodium systems, which has been successfully compared against LBE wire-wrapped bundles (Pacio et al., 2018).

$$Nu = 4.0 + 0.33\left(\frac{P}{D}\right)^{3.8} \cdot \left(\frac{Pe}{100}\right)^{0.86} + 0.16\left(\frac{P}{D}\right)^{5.0}$$

Equation 11

Valid for $1.1 \leq \frac{P}{D} \leq 1.4$ and $10 \leq Pe \leq 5000$.

The Nusselt number is ultimately dependent on geometry and coolant temperature and velocity.

The slice solver cannot take a heat flux as a boundary condition on the clad surface, because the adiabatic boundary condition at the centerline is already a heat flux boundary condition.

Therefore, the strategy adopted here is to use a temperature boundary condition, and iteratively update that temperature until Equation 10 is respected. At every iteration, clad to coolant heat transfer is calculated by two different ways. One uses Equation 10 with current clad surface temperature, and the other derives it from temperature gradient near clad surface. The two heat transfer values are averaged and Equation 10 is used to obtain the new clad surface temperature. The pin temperature distribution is solved again with the new boundary condition (same time step) and this process is repeated iteratively until the clad surface temperature does not vary anymore. This process is also included in the same iterative loop that updates Q_{axial} and material properties. It corresponds to steps B3 and B4 in Figure 16.

Figure 16 shows how the fuel pin heat transfer solver iterates through its different components. To determine convergence, the maximum difference between current and previous pin temperature and Q_{axial} are tracked from iteration to iteration. When both of those two differences stop decreasing, convergence has been reached.

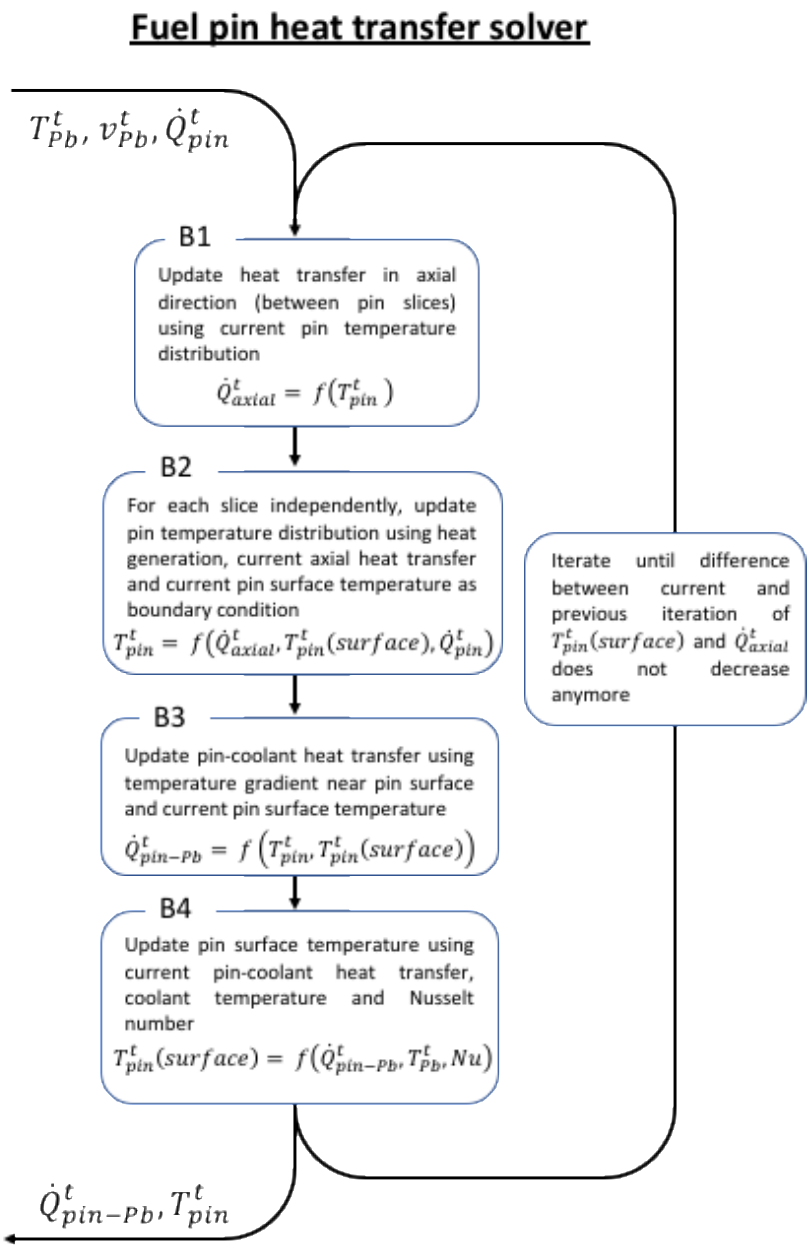

Figure 16 Structure of the fuel pin heat transfer solver

3.2.3 Coupling of all the solvers

Reactor simulations are performed by coupling all the solvers: coolant thermal-hydraulics (CFD), fuel pin heat transfer, neutronics and pump flywheel. Figure 17 shows the algorithm used to couple all the solvers. At the beginning of each time step, current pump rotational speed is calculated using data from previous time step, and the coolant temperature and velocity in the core is updated by extrapolating from previous three time steps. This extrapolation reduces the number of CFD runs which reduces computing time. Then, two iteration loops are used to find a converged solution for thermal-hydraulics, pin temperature and neutronics. The reason for using two loops instead of one, is to reduce the number of CFD runs in order to reduce computing time. Pin heat transfer and neutronics require very little computing time so a partial solution is first calculated by iterating those two solvers. That partial solution is fed into the CFD software and convergence is tested. For the latter, the coolant temperature of every control volume (as defined by the fuel pin heat transfer solver) is tracked for every iteration. The difference between current and previous iteration is calculated, and when the control volume with the maximum difference is below a threshold (0.01 K), convergence is reached. All relevant data is saved at each time step. STAR-CCM+ is the CFD software used in this work. Everything else, including the coupling algorithm, is programmed in Matlab. Communication between STAR-CCM+ and Matlab is achieved by writing and reading text files and CSV files.

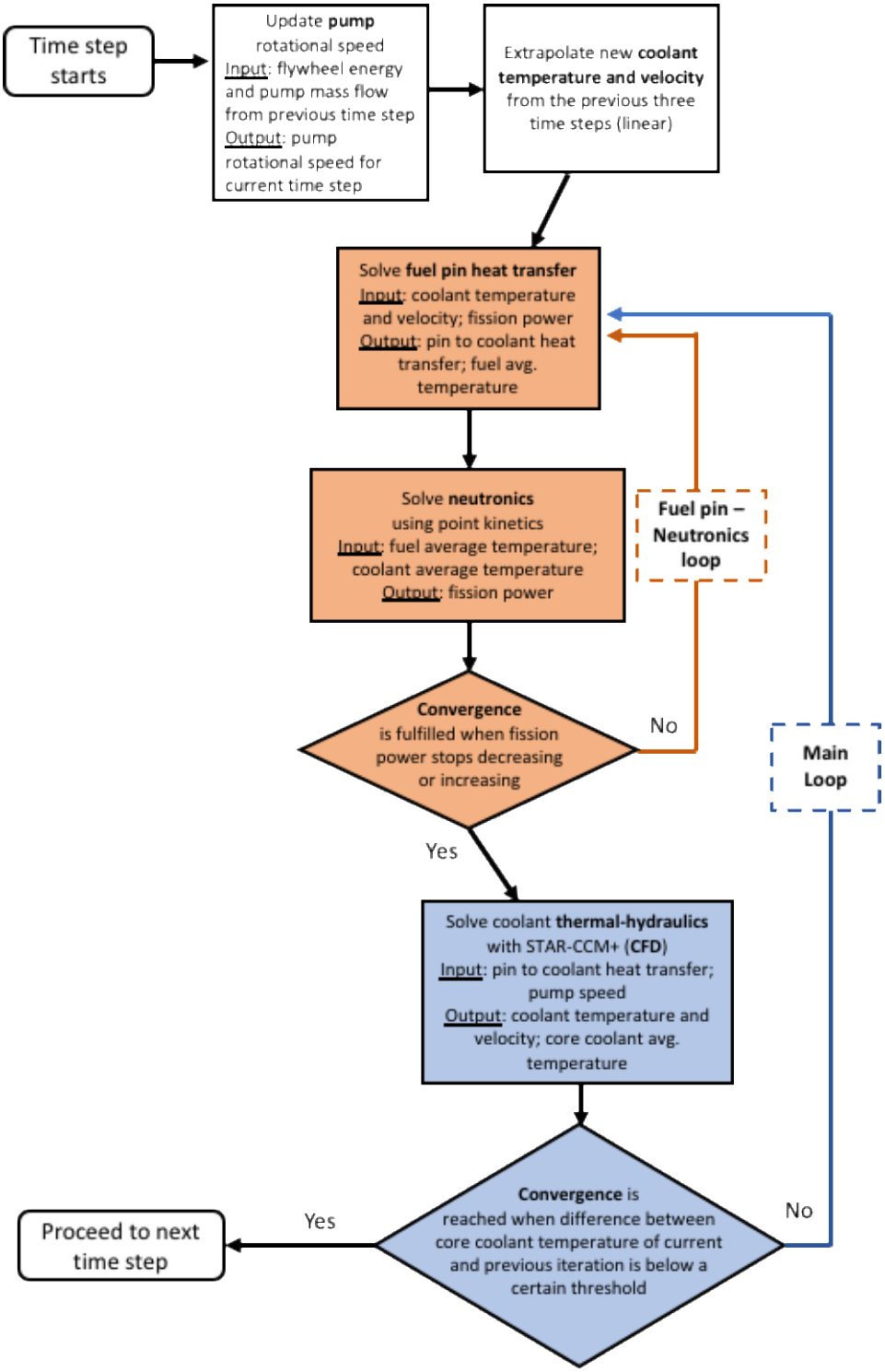

Figure 17 Algorithm used to couple all the solvers

Before implementing the entire reactor model, a small test was performed by coupling only the fuel pin heat transfer solver with CFD for only one fuel channel. It is a transient problem driven by a pulse heat source (instead of fission power from neutronics) and the main purpose is to test conservation of energy. The heat transfer from pin to Pb (coolant) and inlet outlet enthalpy balance was tracked during the transient. The results are shown on Figure 18. By integrating the power over time, we can compare the total heat that was injected into the fuel, transferred from pin to Pb and coming out of the channel. The relative difference is less than 0.02%, which confirms conservation of energy.

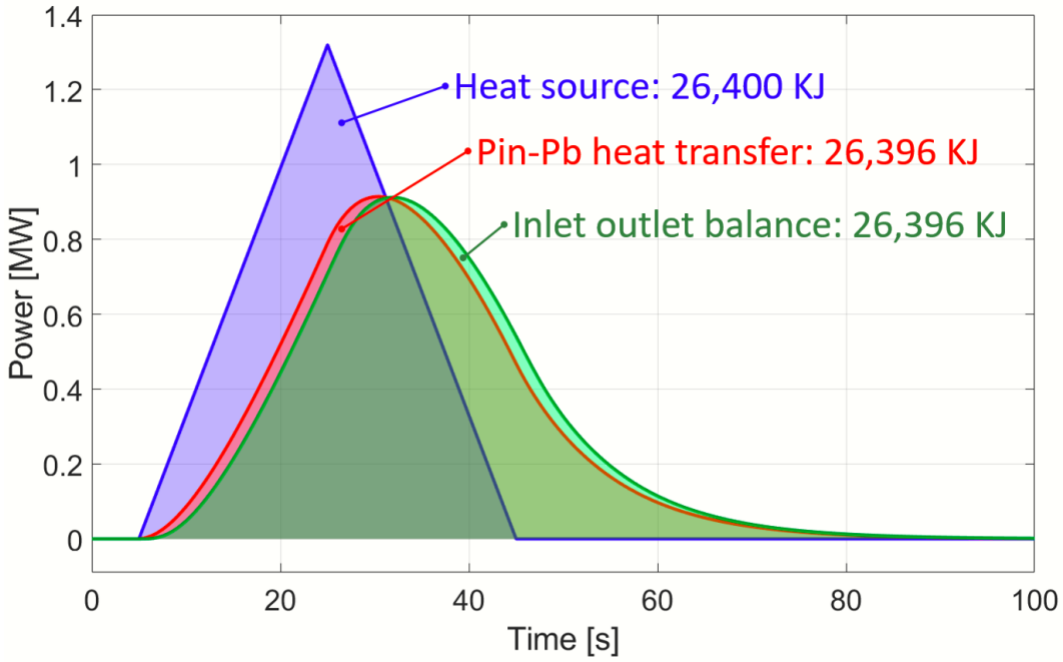

Figure 18 Heat transfer in different parts of the channel during a transient calculated with the whole solver

Chapter 4 - Article I

4.1 Publication Details

C. R. Hernandez, J. Wallenius, J. Luxat, "Dynamic sensitivity and uncertainty analysis of a small lead cooled reactor," Annals of Nuclear Energy, vol. 144, p. 10, 2020, doi: 10.1016/j.anucene.2020.107512

The model used in this article to simulate transients of the SEALER reactor was developed at KTH and provided to the author by Dr. Wallenius in the form of a Mathematica script. The translation of that script into Matlab and all the scripts necessary to the uncertainty and sensitivity analysis were entirely written by the author. Dr. Luxat provided help on the methodology and structure of the study. Dr. Wallenius provided a lot of insights into understanding the mass flow disturbance. The section on the "Exploration of the limits of certain parameters" was also done in close collaboration with him. The writing of the article and the production of all the figures were done by the author. Dr. Wallenius and Dr. Luxat provided some feedback to improve the quality of the article.

4.2 Preface

Prior to starting this thesis, the authors of the SEALER design had already performed transient calculations with a lumped-parameter model. One particular issue that they identified was a fluctuation of the mass flow in the pumps at the beginning of a loss of flow transient. Therefore, one of the main objectives of this thesis became to investigate that issue. The first step in that process was to use the previously mentioned lumped-parameter model to perform an uncertainty and sensitivity analysis. Different types of parameters were tested in that study: geometry, material properties, correlations and neutronics. The effect of those parameters was studied on two transients: an unprotected loss of flow and an unprotected overpower. The uncertainty analysis concluded that all the relevant temperatures remain well within safety limits throughout the transients. However, with respect to the mass flow fluctuation issue, it was found that varying some parameters in a

realistic manner could cause reverse flow at the pumps. All that study is presented in this article.

4.3 Article

The following pages contain the original article.

Dynamic Sensitivity and Uncertainty Analysis of a Small Lead Cooled Reactor

Cuauhtemoc Reale Hernandez[a]*, Janne Wallenius[b], John Luxat[a]

[a] Department of Engineering Physics, McMaster University, 1280 Main St W, Hamilton, Canada

[b] Department of Nuclear Engineering, KTH, Brinellvägen 8, 114 28 Stockholm, Sweden

Abstract

A sensitivity and uncertainty analysis was performed on a small lead cooled reactor for two types of transients: an unprotected loss of flow (ULOF) and unprotected transient overpower (UTOP). Transients were simulated with the code BELLA, which is a point-kinetics and lumped-parameter model. A Monte Carlo based method was used with 5000 simulations. Input parameters are reactor dimensions, neutronics properties, material properties and thermal hydraulic properties. Outputs are maximum temperatures (clad, coolant and fuel), mass flow disturbance, natural convection mass flow, maximum power and energy deposition. For ULOF, it was found that the most sensitive parameters were the gap between fuel and clad, the flow area in the core, the friction factors in core and steam generator and the pump coastdown time. A deeper analysis recommends increasing pump coastdown time to avoid mass flow disturbances during coastdown. For UTOP, the most sensitive parameters are the gap between fuel and clad, the reactivity feedback coefficients, and to a lesser extent, fuel conductivity and fuel heat capacity. In any case, the uncertainties never bring the reactor beyond safety limits.

* Corresponding author, email address: realehec@mcmaster.ca

1. Introduction

Lead-cooled reactors present many advantages over other types of reactors. Several inherent properties of lead make it highly desirable as a reactor coolant; high thermal conductivity, very high boiling point (1749 °C), absence of violent reaction with air & water and the ability to function in the fast spectrum. In a big reactor, these properties translate into a fast breeder reactor without the safety concerns encountered by liquid sodium, and the possibility of natural circulation. A lead-cooled SMR might not be a breeder, but would still have a very high conversion ratio. This results in an SMR that would have very long refuelling periods, passive safety features, and a simple fuel pin design very similar to existing reactors. For these reasons, lead cooled reactors will very likely be part of tomorrow's nuclear landscape. For example, in 2019, Russia made a contact with the company that will be building the BREST 300 MWe lead cooled reactor("Russia awards contract to build BREST reactor," 2019). As part of the process to develop this type of reactors, it is necessary to assess their safety and stability during a transient. To our knowledge, a study of this type on a small lead cooled reactor which employs a model of the whole primary circuit is a premier.

This study presents a sensitivity and uncertainty analysis of an unprotected loss of flow accident (ULOF) and an unprotected transient overpower accident (UTOP) in the SEALER reactor (Wallenius, Qvist, et al., 2018). This reactor produces between 3 and 10 MWe and has a lifetime of between 30 and 10 years without refueling. It is intended to be deployed in Canadian arctic towns or remote mines.

2. Methods

2.1 BELLA

BELLA is a lumped parameter and point kinetics model to simulate transients in a small lead cooled reactor, in particular the SEALER design (Bortot et al., 2015). The model simplifies the temperature distribution to a total of 8 areas (4 in the coolant circuit, 2 in the fuel and 2 in the cladding). Then, the heat and mass transfer equations of these areas are coupled with the point kinetics and reactivity feedback equations. The model takes into account both forced flow and natural convection, so it can model a loss of flow accident. The details of BELLA and an analysis of the transients in the SEALER reactor have been published elsewhere (Wallenius, Bortot, et al., 2018). For the purpose of benchmarking with the code SAS4A/SASSYS-1, many material properties implemented in BELLA were chosen to match the ones used in SAS. The same material properties have been used here, for consistency. BELLA is used for all the calculations performed in this study. Two types of accidents are considered, unprotected loss of flow (ULOF) and unprotected transient overpower (UTOP).

2.2 Uncertainties

All the parameters used in the simulations can be divided into four categories: properties related to fabrication processes (dimensions, fuel porosity, etc.), neutronic properties, material properties and thermal-hydraulics correlations. **Table 1** lists all the parameters, their nominal value and their uncertainty. Note that for material properties, the nominal values are given for 700 K. In the subsequent calculations, the probability density function of each parameter is considered to be a uniform distribution where the distance between the mean value and the edges are the uncertainty values listed in **Table 1**. A uniform distribution is used in order to simplify the calculations. Although this assumption might not be exact, its effect can only be to exaggerate sensitivities and/or uncertainties so that any conclusions drawn from this study will be more conservative.

The uncertainty of the properties related to fabrication processes, which are mostly dimensions, have been set to ± 0.5 % for the most part. This approximated value was chosen

by considering the fact that any part for a nuclear reactor is manufactured with very high precision. The exceptions are the steam generator flow area, which has a larger uncertainty because it was not calculated from the geometry but rather chosen to be equal to the core flow area; and the cold pool volume because it's a rough estimate.

The uncertainties of the neutron generation time, delayed neutron fraction and decay rate of neutron precursors are assumed to be similar to other type of reactors (Gajev et al., 2014). Concerning the reactivity feedback coefficients, a precise estimate of their uncertainties is not available. Considering that they incorporate a series of uncertainties (materials properties, geometry, cross section data, Monte Carlo calculations), a conservative large value of ±10% was attributed to them.

Material properties uncertainties were determined from available experimental data in the literature for lead (*Handbook on Lead-bismuth Eutectic Alloy and Lead Properties, Materials Compatibility, Thermal-hydraulics and Technologies*, 2015), fuel (Carbajo et al., 2001), clad (Leibowitz & Blomquist, 1988) (Banerjee et al., 2005) and helium (Petersen, n.d.) (Tsederberg et al., 1971). The value of the uncertainty was determined in such a way that the upper and lower limits enclose the experimental data in the relevant temperature range.

The Rehme and Moody correlations are used to calculate the pressure drop in the core and steam generator, respectively. Rehme recommends an uncertainty of 5% (Rehme, 1973). To take into account friction factor, a total uncertainty of 10% was assumed for pressure drop correlations. This uncertainty is taken into account by modifying the core and steam generator friction factors. The uncertainty on the Nusselt number is ±1.9 (Mikityuk, 2009). Since the pump for SEALER has not been selected yet, the nominal value for the pump coastdown time constant is a gross estimate, so its uncertainty is set to 10% to test its sensitivity rather then to take into account the actual uncertainty of the pump.

Table 1 List of parameters and corresponding uncertainties

	Parameter name	Nominal value	Uncertainty
Fabrication process	Clad diameter outer	14.52 mm	±0.4%
	Clad thickness	0.500 mm	±0.5%
	Fuel diameter	13.38 mm	±0.5%
	Pitch of pins	16.37 mm	±0.5%
	Fuel height	1100 mm	±0.5%
	Hexcan diameter inner	160.0 mm	±0.5%
	SG elevation	1.50 m	±0.5%
	SG height	300 mm	±0.5%
	Barrel diameter inner	1708 mm	±0.5%
	Barrel diameter outer	1748 mm	±0.5%
	Vessel diameter inner	2648 mm	±0.5%
	Cold pool volume	3.30 m^3	±5%
	SG flow area	0.130 m^2	±2%
	Fuel clad gap pressure	100.0 kPa	±0.5%
	Fuel porosity	4.0 %	±13%
Neutronics	Effective neutron generation time	0.212 μs	±1%
	Delayed neutron fraction β	682 pcm	±1.2%
	Decay rate of group i λ_i	-	±1%
	Doppler feedback	-259 pcm	±10%
	α Pb feedback	-0.35 pcm/K	±10%
	α radial feedback	-0.52 pcm/K	±10%
	α axial feedback	-0.33 pcm/K	±10%

Materials (at 700 K)	Pb density	10.46 g/cm^3	±1.5%
	Pb heat capacity	146 J/(kg·K)	±3%
	Pb viscosity	2.04 mPa·s	±7%
	Pb conductivity	15.8 W/(m·K)	±20%
	Clad density	7.92 g/cm^3	±1%
	Clad conductivity	19.9 W/(m·K)	±10%
	Clad heat capacity	554 J/(kg·K)	±30%
	He (gap) heat capacity	5193 J/(kg·K)	±0.5%
	He (gap) conductivity	0.28 W/(m·K)	±7%
	Fuel relative thermal expansion	0.42 %	±3%
	Fuel density	10.49 g/cm^3	±0.2%
	Fuel conductivity	4.74 W/(m·K)	±10%
	Fuel heat capacity	301 J/(kg·K)	±10%
	Fuel emissivity	0.9	±10%
TH	Core friction factor	-	±10%
	Steam generator friction factor	-	±10%
	Nusselt number (at s.s.)	6.63	±1.9
	Pump coastdown time	10 s	±10%

2.3 Uncertainty and sensitivity analysis methods

In the context of this study, uncertainty refers to the variability of a simulation output when taking into account the uncertainty of every parameter (input). The results are expressed in standard deviation or histogram of a specific output. If the output of interest is a state variable function of time, it can be shown as a band (superposition of curves) that includes all possible outcomes. On the other hand, the sensitivity analysis performed in this study aims at identifying the parameters (inputs) whose uncertainty causes a large impact on the output uncertainty. Once those parameters are identified, an additional analysis is done in order to ensure that the reactor remains safe even if the uncertainty of those parameters was

underestimated. In this study, the notion of *sensitivity* is defined as the degree to which an input uncertainty contributes to the output uncertainty.

First, a Monte Carlo based method with 5000 simulations is used to determine the uncertainty of the outputs. In each simulation, each parameter is chosen randomly inside its uncertainty range (uniform distribution). The calculation procedure for each simulation is described in the next section. From each simulation, different outputs (refered to as Quantity Of Interest or QOI) are calculated (i.e maximum temperatures, maximum power, etc). Section 2.5 describes the different QOIs.

The sensitivity of each parameter is then calculated using a standardised regression coefficients method (Saltelli et al., 2004). The variation of the QOI (output) value is assumed to be a linear function of parameter variations:

$$\Delta y = b_1 \Delta p_1 + b_2 \Delta p_2 + \cdots + b_n \Delta p_n \quad (1)$$

where:

$\Delta y = y - \bar{y}$ is the variation of the QOI from its mean value

$\Delta p_x = p_x - \overline{p_x}$ is the variation of parameter x from its mean value (there are n parameters)

b_x's are the regression coefficients.

The value of the $b_x's$ is determined by performing a linear regression using the data from the 5000 simulations to fit equation (1). The quality of the regression was determined by calculating R^2:

$$R^2 = \frac{\sum_{i=1}^{N} (\Delta \hat{y}_i)^2}{\sum_{i=1}^{N} (\Delta \mathrm{y_i})^2} \quad (2)$$

Where $\Delta \hat{y}_i$ is the QOI variation predicted by the regression, $\Delta \mathrm{y_i}$ is the actual QOI variation and i represent each simulation ($N = 5000$). For all the QOIs, except one, the minimum value of R^2 was 0.98, so the linear assumption in equation (1) is deemed acceptable. The exception is the flow disturbance amplitude, which has $R^2 = 0.86$. This is due to the fact that the flow disturbance amplitude is floored at 0. Some input combinations yield a flow evolution that presents no disturbance, in those cases the disturbance is set at 0.

Finally, coefficients b_x's are multiplied by the standard deviation of the parameter (to take into account its uncertainty) and divided by the standard deviation of the QOI to have a normalized value. The result is the standardised regression coefficients (SRC):

$$SRC_x = b_x \sigma_x / \sigma_y$$

The SRCs are a measure of how much the uncertainty of a particular parameter (input) affects the overall uncertainty of an output, they are calculated for every parameter and for every QOI. They are used to determine which parameters have the highest sensitivity.

2.4 Calculation procedure for each simulation

A calculation consists of simulating a transient in the reactor (either ULOF or UTOP) with a specific set of parameters (selected randomly). The initial conditions of the transient are steady state, so the first step of the calculation is to find the steady state that corresponds to the specific set of parameters. This is achieved by performing a series of simulations while adjusting the pump head iteratively so that the power is 8 MWth. The core outlet temperature is fixed at 432 °C and the temperature difference of the lead going across the steam generator is fixed at 42 °C. Once the initial conditions have been calculated, the actual simulation of the transient can be performed. In ULOF, the transient is driven by decreasing the pump head exponentially. In UTOP, this is achieved by inserting 0.5$ of reactivity gradually during one second. The results of the simulations consist in a series of state variables that are function of time. The ones that are considered in this study are the mass flow, power, reactivity and temperatures (fuel, clad and coolant).

2.5 Quantity of Interest (QOI)

In order to calculate the SRCs, one or two QOIs (output) are calculated from each state variable. These QOIs have been selected because they are important from a safety perspective. For the temperatures, the QOI is the maximum temperature attained during the transient. Those QOIs are used both for ULOF and UTOP. Two QOIs are calculated from the mass flow in ULOF simulations, one is the flow at 600 s (natural convection flow), and

the other is the amplitude of a disturbance that occurs at the beginning of the transient as the pump is coasting down, see **Figure 19**. For the power, it is the maximum power and the energy deposited in the reactor during the first 5 min of the transient (in GJ). Only the power above the steady state power is considered in the energy deposition calculation, see **Figure 20**. For the reactivity, the QOI is simply the maximum reactivity. Power and reactivity QOIs are used in UTOP only.

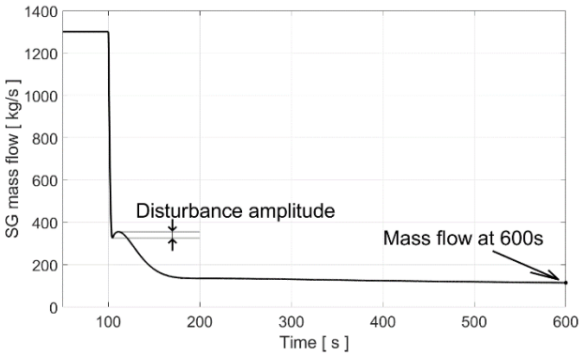

Figure 19 QOIs from the mass flow in ULOF simulations

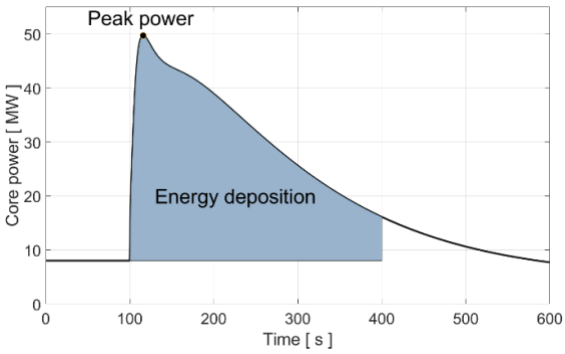

Figure 20 QOIs from the core power in UTOP simulations

3. Results: ULOF

3.1 Sensitivity analysis

Figure 21 presents the results of the sensitivity analysis for a ULOF. It lists the SRC of every parameter and for every QOI. A green bar indicates that a positive change in the parameter value will cause a positive change on the QOI value (directly proportional). A red bar indicates that it's inversely proportional.

Figure 21 SRCs in a ULOF transient, measured with five different QOIs

A few parameters have a significantly larger sensitivity. In the fabrication process category, there are two main factors: the flow area in the core and the thickness of the helium gap between fuel and clad. The flow area is not a direct input but is calculated from the clad diameter (outer) and the hexcan diameter. The helium gap thickness is calculated from the fuel diameter, clad thickness and clad diameter. Other calculations (not shown here) show that if the fuel diameter and clad thickness are varied without changing the gap thickness and clad outer diameter, there is nearly no effect on the QOIs. Besides, changing the clad diameter without changing the gap thickness has a large effect. This shows that the main factors are the flow area and the thickness of the gap. This is expected since in a natural circulation mode, small changes in pressure drops, which depend on flow area, can have a rather large effect on the flow. Also, the fuel clad gap is very thin (nominal value is 68 μm), so a small relative change in fuel or clad diameter will cause a very large relative change on the gap thickness.

Reactivity feedback coefficients have a moderate sensitivity. Lead density and heat capacity also have a moderate sensitivity. Fuel conductivity is sensitive only for the maximum fuel temperature. This is expected since fuel is a UO2 ceramic with low conductivity. The core friction factor is the most sensitive parameter for almost every QOI. Again, this is also expected in a natural convection mode. The pump coastdown time constant is also very sensitive, especially for the mass flow disturbance.

3.2 Uncertainty analysis

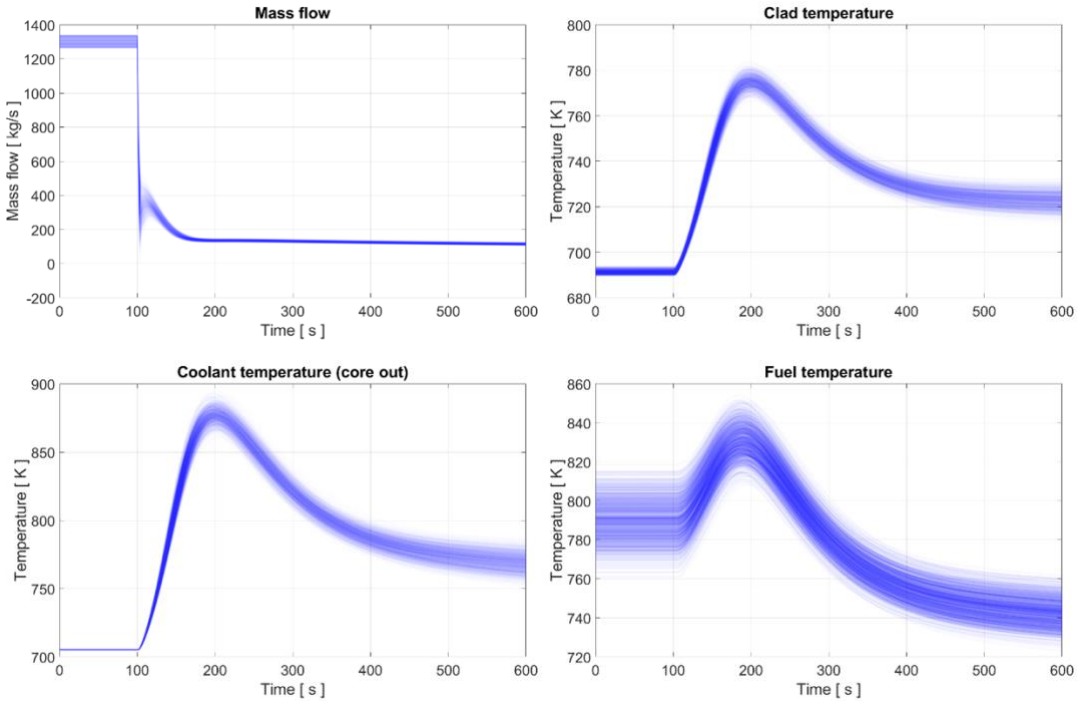

Figure 22 Uncertainty of 4 selected state variables in a ULOF transient

Figure 22 and **Figure 23** present the results of the uncertainty analysis. The purpose of this second part, is to assess the influence on the state variables and QOIs by taking into account the uncertainty of all the parameters at the same time. Figure 4 shows the mass flow, the fuel temperature, the clad temperature and the coolant temperature (coming out of the core) for first 500 s after the transient initiation (ULOF), which starts at 100 s. Each curve is a superposition of 1000 curves (randomly selected among the 5000 simulations). Note that the curves don't all start from the same point since the initial conditions correspond to steady state, which can vary if the parameters are changed. Thus, these graphs also show the uncertainty of the steady state. Furthermore, by looking at the QOIs of each state variable (e.g. the maximum temperatures), it is possible to construct the distribution of these QOIs. This is shown on **Figure 23**.

In the mass flow, both the steady state and the disturbance that occurs right after the transient starts have a relatively wide distribution. Once the flow stabilizes to natural

convection, the distribution shrinks to values between 105 and 125 kg/s, as can be seen on **Figure 23**. The distributions of maximum temperatures are relatively narrow. The maximum fuel temperature is the widest one, with a standard deviation of 8.3 K. In any case, maximum temperatures never get close to unsafe zones.

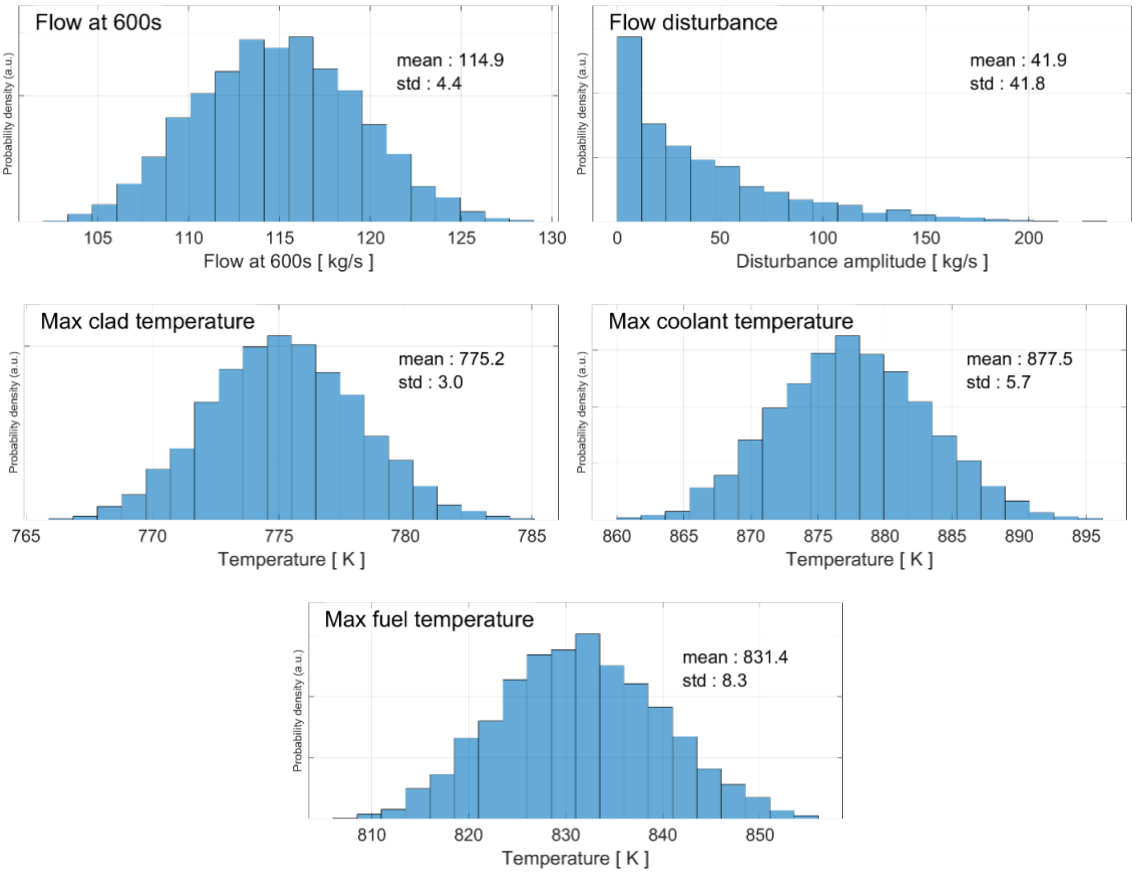

Figure 23 Distribution of 5 QOIs in a ULOF transient

3.3 Analysis of the mass flow disturbance

A feature of importance for safety analysis is the flow disturbance that occurs shortly after the beginning of the transient. As the pump is coasting down, one would expect the flow (at the steam generator) to decrease monotonically until it reaches the natural convection

flow rate. Instead, the flow rate goes through a dip, then increases a bit, then slowly decreases until it reaches natural convection (see **Figure 19**). The flow rate is positive throughout the transient, but the uncertainty analysis shows that for specific sets of parameters, the dip or oscillation can be large enough to cause a reverse flow. Although this only affects the flow at the steam generator (core flow always decreases monotonically), having a reverse flow or oscillations is always a safety concern.

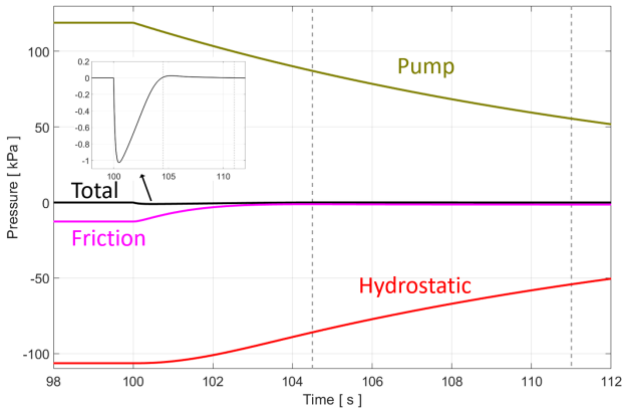

Figure 24 Pressure contributions to the SG mass flow

The rate of change of the mass flow rate is proportional to the pressure. **Figure 24** shows the different pressure contributions (pump, hydrostatic and friction) at the steam generator when the disturbance occurs. The gray dashed lines enclose the time during which the mass flow is increasing, thus the minimum of the dip occurs at the first gray line. The negative hydrostatic pressure at steady state comes from the fact that the pump head causes the free surface level of the cold leg to be higher then the free surface level of the hot leg. When the transient starts, the pump head starts decreasing immediately and follows an exponential decay. The free surface levels do not move immediately since they are moved by gravity. In the first two seconds, this results in a strong negative total pressure (see insert) which causes the flow rate to decrease very quickly. Right after this, the hydrostatic pressure starts decreasing (in amplitude) at an increasing rate, while the pump head is decreasing at a decreasing rate, and the friction is very low. This creates the conditions for a few seconds

where the pump head is slightly greater than the hydrostatic pressure and friction, and so the flow rate increases. In short, the flow disturbance is mainly the result of a dynamics between the hydrostatic pressure and the pump coastdown. The natural convection does not have any influence on this phenomenon as it can be inferred by looking at the coolant temperature at 104 s on **Figure 22**.

3.4 Exploration of the limits of selected parameters

As a further analysis of the mass flow disturbance, the most sensitive parameters were modified in both directions to the extent where the disturbance disappears or reaches reverse flow. The parameters in question are pump coastdown time constant, core flow area, steam generator friction factor and core friction factor. Note that the core flow area is modified by changing the clad outer diameter and the hexcan inner diameter. All other parameters were used at nominal value. Results are compiled on **Figure 25**.

We are interested in eliminating the disturbance in order to have a monotonous decreasing mass flow during the transient. Modifying any of the presented parameters individually can accomplish this, though it may be difficult to implement it in practice or cause negative impact on something else. The exception is the pump coastdown time constant. Changing it from 10 to 13 sec eliminates the disturbance while also lowering the maximum temperatures. This can easily be accomplished by increasing the weight of the flywheels.

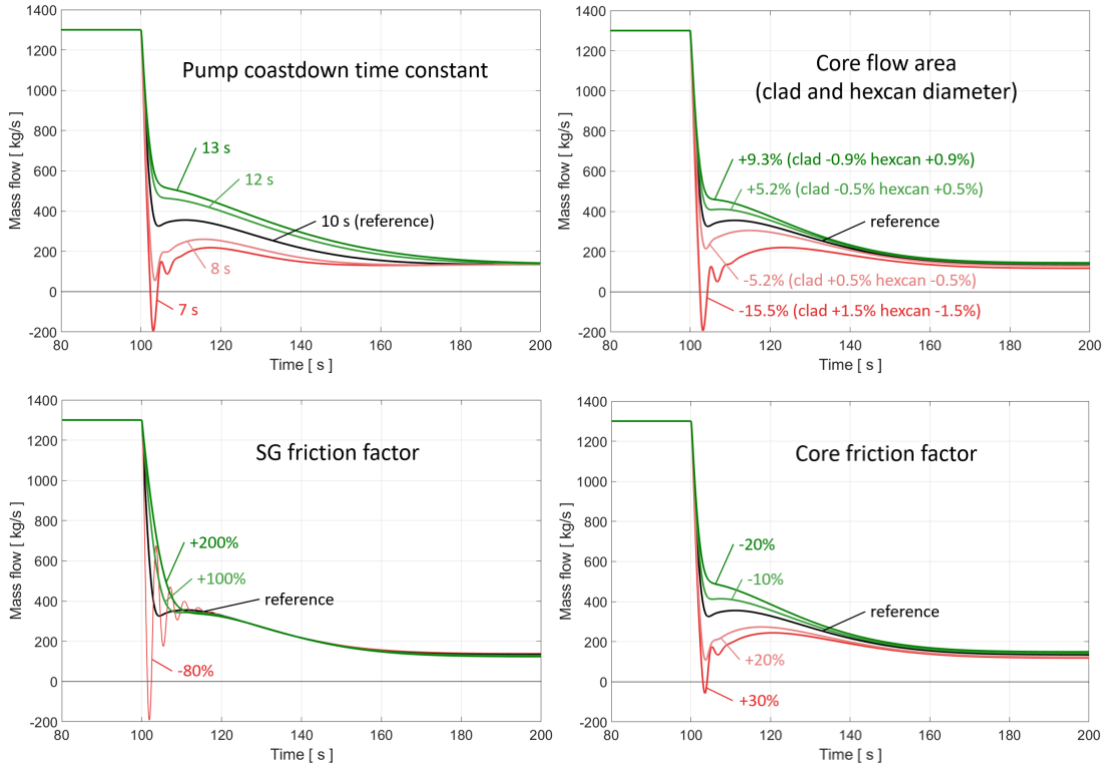

Figure 25 Lead mass flow at the steam generator for limiting conditions of four different parameters

4. Results: UTOP

4.1 Sensitivity analysis

The same analysis that was performed on ULOF was also performed on UTOP, with the only difference being that the QOIs are not the same. **Figure 26** presents the results of the sensitivity analysis. The QOIs are peak power, energy deposition, max fuel temperature, max clad temperature and max coolant temperature. A green bar indicates that a positive change in the parameter value will cause a positive change on the QOI value (directly proportional). A red bar indicates that it's inversely proportional.

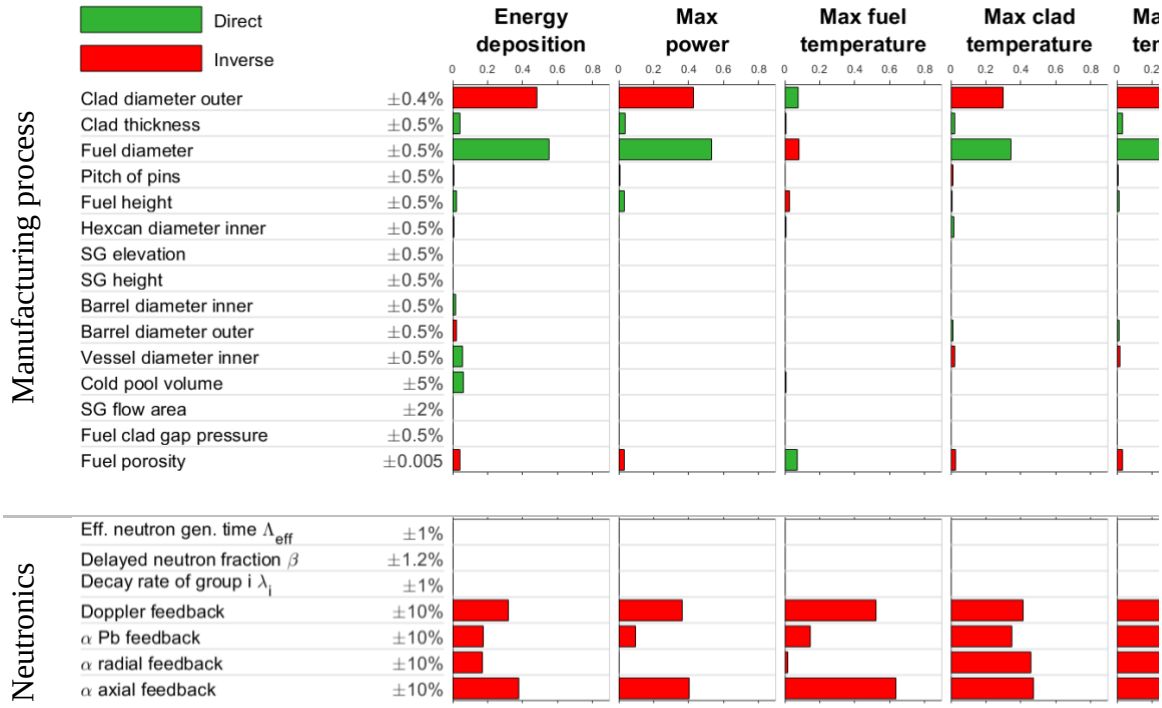

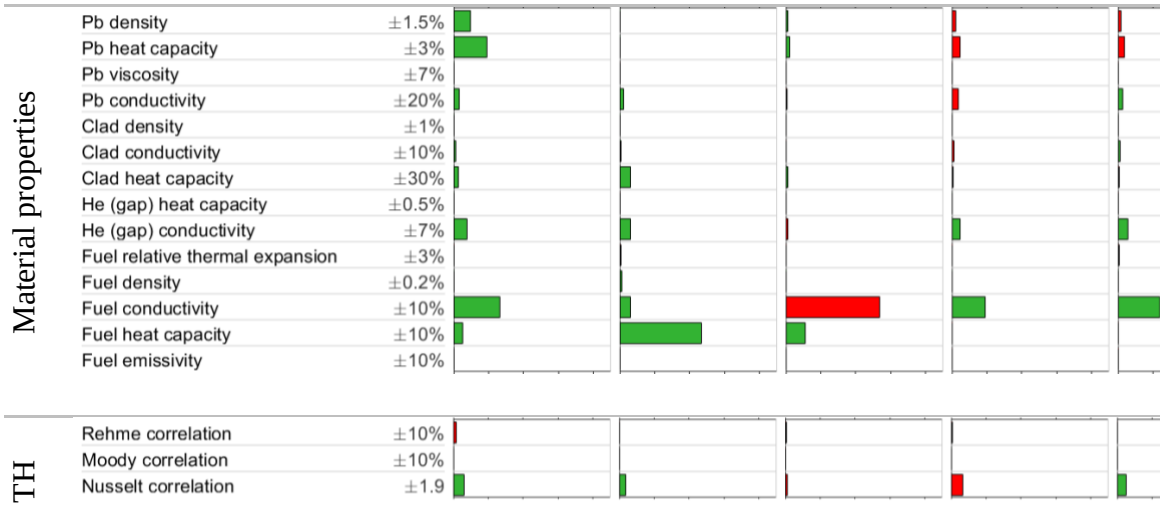

Figure 26 SRCs in a UTOP transient, measured with five different QOIs

Among the properties related to fabrication process, the helium gap between fuel and clad has by far the highest sensitivity. Although it is not a primary input (since it is calculated from fuel diameter, clad thickness and clad diameter), it can be inferred by looking at the SRC of the clad diameter and the fuel diameter. Increasing the clad diameter directly increases the gap thickness, and decreasing the fuel diameter also directly increases the gap thickness. The fuel clad gap is very thin (nominal value is 68 µm), so a small relative change in fuel or clad diameter will cause a very large relative change on the gap thickness. Adding that to the low thermal conductivity of helium, it's high sensitivity is expected. In UTOP, there is only forced convection, so the flow area is not a sensitive parameter as is the case in a ULOF event.

The reactivity feedback coefficients have a high sensitivity as can be expected by their high uncertainty and by the fact that they are part of the main parameters driving the UTOP transient. Nevertheless, their sensitivity is comparable to other parameters. This, and the fact that total uncertainty on QOIs (see **Figure 28**) is low, highlight the stability of the reactor.

In the material properties, the fuel thermal conductivity and heat capacity are the main sensitive parameters. The thermal hydraulic correlations have a very low sensitivity in UTOP since the flow is forced convection and it doesn't change very much throughout the transient.

4.2 Uncertainty analysis

Figure 27 and **Figure 28** present the results of the uncertainty analysis. The purpose is to assess the effect on the state variables from all the uncertainties combined. The state variables under consideration are power, reactivity and maximum temperatures (fuel, clad and coolant). Each graph shows the superposition of 1000 curves (out of the 5000 simulations). From each simulation, one set of the following QOIs can be calculated: maximum core power, maximum reactivity, energy deposition and maximum temperatures (fuel, clad and coolant). By taking all the 5000 simulations into account, it is then possible to construct the distribution of those QOIs, see **Figure 28**. Among the maximum temperatures, the fuel temperature has the largest standard deviation, about 42 K. Nevertheless, considering that UO_2 melting point is above 3000 K, maximum fuel temperature doesn't get any close to melting temperature even by taking three standard deviations. Clad and coolant maximum temperatures have a relatively small standard deviation and their uncertainty do not present any safety issue.

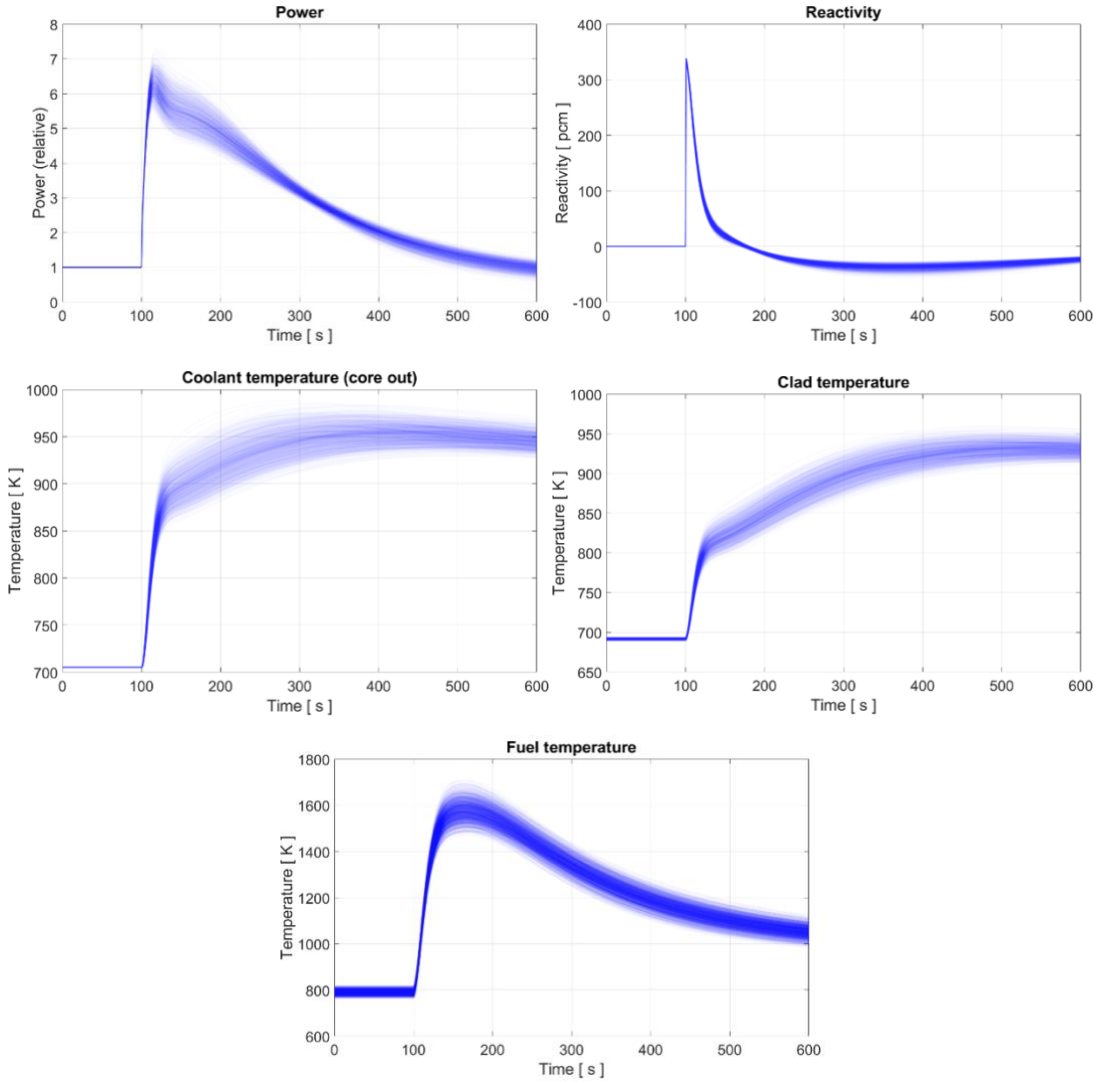

Figure 27 Uncertainty of 5 selected state variables in a UTOP transient

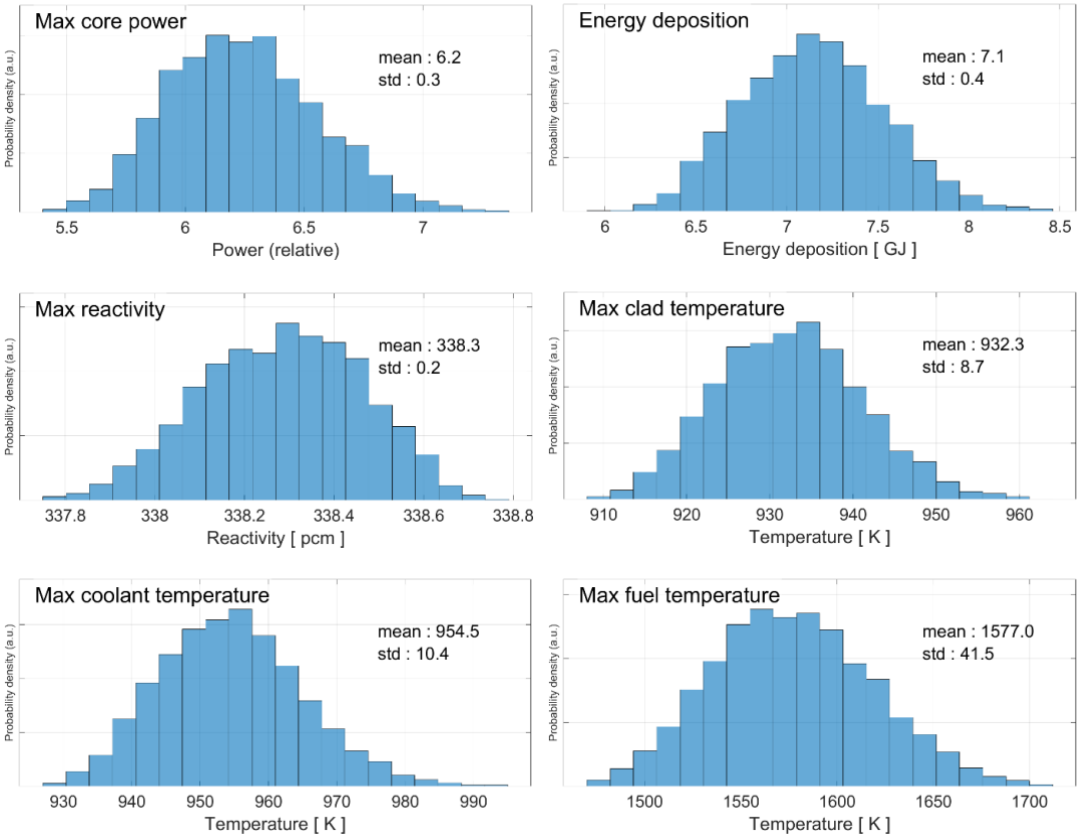

Figure 28 Uncertainty of 6 QOIs in a UTOP transient

4.3 Exploration of the limits of selected parameters

The two most sensitive parameters, reactivity feedback coefficients and fuel clad gap, were modified to extreme values in order to test the limits of those parameters. The results, presented on **Figure 29**, shows that even if we half all the reactivity feedback coefficients, maximum fuel temperature does not reach melting temperature. They have to be reduced by 70% to reach melting temperature, which is unrealistic. In this extreme case, the clad temperature, not shown here, gets close to 1600K which is still below melting temperature. This illustrates that even if uncertainty of feedback coefficients is much larger than what is estimated here, the reactor remains stable.

The clad and fuel diameters were modified up to 5% (in opposite direction), which increased the gap thickness up to about tenfold. This had the effect of increasing the maximum fuel temperature to about 1900 K, which is well below melting point. Since the temperature of the fuel increases faster, the maximum power is lower due to the negative temperature feedback. In short, modifying the most sensitive parameters beyond their estimated uncertainty does not produce adverse behavior.

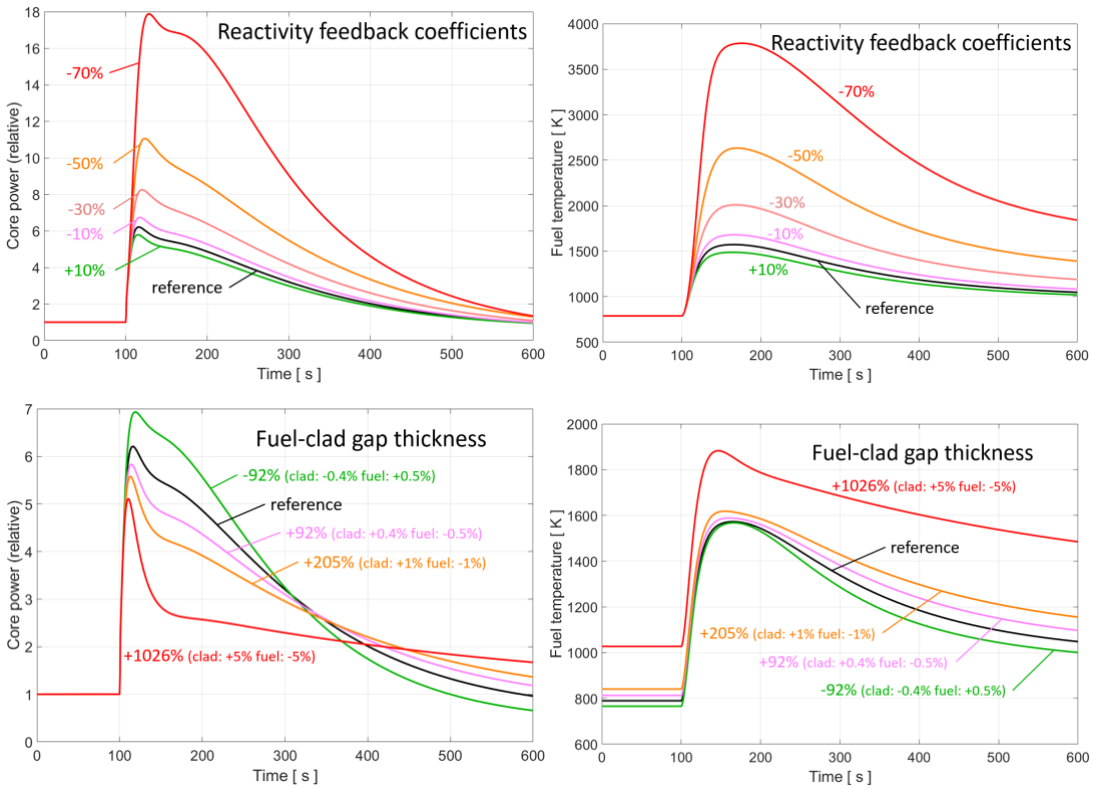

Figure 29 Effect of extreme parameter variations (feedback coefficients and fuel-clad thickness) on core power and fuel temperature

5. Conclusion

A sensitivity and uncertainty analysis of a transient in small lead cooled reactor was performed using a point kinetics – lumped parameter model called BELLA. The transients in consideration were an unprotected loss of flow (ULOF) and an unprotected transient overpower (UTOP). For ULOF, it was found that the most sensitive parameters were the gap between fuel and clad, the flow area in the core, the friction factors in core and steam generator and the pump coastdown time. For UTOP, the most sensitive parameters are the gap between fuel and clad, the reactivity feedback coefficients, and to a lesser extent, fuel conductivity and fuel heat capacity. In any case, the uncertainties never bring the reactor beyond safety limits. The largest uncertainty that was found is the maximum fuel temperature in a UTOP, with a standard deviation of 42 K (mean value 1542 K), which still remains far below the melting point of UO_2 (above 3000 K).

A further analysis was performed where the most sensitive parameters were modified beyond their uncertainty limits until a limiting scenario. In a ULOF, it was found that the disturbance of the flow mass during pump coastdown can be eliminated by increasing the pumps coastdown time. This is easily achieved by increasing the weight of the flywheel. In a UTOP, it was found that fuel melting temperature is not attained even by decreasing by 50% all the feedback coefficients or by increasing by tenfold the fuel clad gap thickness.

6. Acknowledgements

We thank Ignas Mickus who provided very insightful comments on the statistical methods and the mechanism of the pump coastdown disturbance.

Funding: This work was supported by NSREC-UNENE (Natural Sciences and Engineering Research Council of Canada, and University Network of Excellence in Nuclear Engineering) [grant number IRCPJ309310-14].

7. References

Banerjee, A., Raju, S., Divakar, R., Mohandas, E., Panneerselvam, G., & Antony, M. P. (2005). Thermal property characterization of a titanium modified austenitic stainless steel (alloy D9). *Journal of Nuclear Materials*, *347*(1–2), 20–30. https://doi.org/10.1016/j.jnucmat.2005.06.009

Bortot, S., Suvdantsetseg, E., & Wallenius, J. (2015). BELLA: A multi-point dynamics code for safety-informed design of fast reactors. *Annals of Nuclear Energy*, *85*, 228–235. https://doi.org/10.1016/j.anucene.2015.05.017

Carbajo, J. J., Yoder, G. L., Popov, S. G., & Ivanov, V. K. (2001). A review of the thermophysical properties of MOX and UO2 fuels. *Journal of Nuclear Materials*, *299*(3), 181–198. https://doi.org/10.1016/S0022-3115(01)00692-4

Gajev, I., Ma, W., & Kozlowski, T. (2014). Sensitivity analysis of input uncertain parameters on BWR stability using TRACE/PARCS. *Annals of Nuclear Energy*, *67*, 49–58. https://doi.org/10.1016/j.anucene.2013.10.016

Handbook on Lead-bismuth Eutectic Alloy and Lead Properties, Materials Compatibility, Thermal-hydraulics and Technologies. (2015). 950.

Leibowitz, L., & Blomquist, R. A. (1988). Thermal conductivity and thermal expansion of stainless steels D9 and HT9. *International Journal of Thermophysics*, *9*(5), 873–883. https://doi.org/10.1007/BF00503252

Mikityuk, K. (2009). Heat transfer to liquid metal: Review of data and correlations for tube bundles. *Nuclear Engineering and Design*, *239*(4), 680–687. https://doi.org/10.1016/j.nucengdes.2008.12.014

Petersen, H. (n.d.). The Properties of Helium: Density, Specific Heats, Viscosity, and Thermal Conductivity at Pressures from 1 to 100 bar and from Room Temperature to about 1800 K. 46.

Rehme, K. (1973). Pressure Drop Correlations for Fuel Element Spacers. *Nuclear Technology*, *17*(1), 15–23. https://doi.org/10.13182/NT73-A31250

Russia awards contract to build BREST reactor. (2019, December 5). *World Nuclear News*.

Saltelli, A., Tarantola, S., Campolongo, F., & Ratto, M. (2004). *Sensitivity Analysis in Practice, A Guide to Assessing Scientific Models*. John Wiley & Sonds, Ltd.

Tsederberg, N. V., Popov, V. N., & Morozova, N. A. (1971). *Thermodynamic and thermophysical properties of helium*. Israel Program for Scientific Translations.

Wallenius, J., Bortot, S., & Mickus, I. (2018). Unprotected transients in SEALER: A small lead-cooled reactor for. 12.

Wallenius, J., Qvist, S., Mickus, I., Bortot, S., Szakalos, P., & Ejenstam, J. (2018). Design of SEALER, a very small lead-cooled reactor for commercial power production in off-grid applications. *Nuclear Engineering and Design*, *338*, 23–33. https://doi.org/10.1016/j.nucengdes.2018.07.031

Chapter 5 - Article II

5.1 Publication Details

C. Reale Hernandez, D. Grishchenko, P. Kudinov, J. Wallenius, and J. Luxat, "Development of a CFD-based model to simulate loss of flow transients in a small lead-cooled reactor," Nuclear Engineering and Design, vol. 392, p. 111773, Jun. 2022, doi: 10.1016/j.nucengdes.2022.111773.

This article is divided in two parts. The first part is about the development of CFD-based model for simulating transients. This part was entirely done by the author with some insights from different people. At the very beginning of the process, Dr. Novog indicated which scale is possible to model with CFD and suggested the use of 1D model for the fuel channels. Some work was done on developing a 1D model (including fuel and coolant) in C++. After a literature review and discussion with Paul Galpin (who was teaching an advanced CFD class), it became clear that coupling the mass and momentum equations of a 1D model with CFD would be very challenging. The solution was to include the fuel channels in the CFD model with a coarse mesh and simplified geometry and couple only heat transfer with a different solver. Dr. Luxat gave some general guidance on what the model should include.

The second part is a validation exercise where the CFD setup of the model is used to simulate experimental data. The latter is taken from the TALL-3D facility, which is an LBE loop located in KTH. Dr. Grishchenko and Dr. Kudinov provided all the necessary data and information. They were also very active in the reviewing process and suggested many corrections to ensure that the analysis was coherent.

5.2 Preface

Following the results of the first article, it was decided to develop a more accurate model for simulating the same type of transients. This would allow to confirm the results already obtained and to explore the effect of selected parameters. The development of this model

is the second part of the thesis and is divided into two articles. This article presents all the details of the methods used in the model and a validation work. The purpose of this article is to present all the background work that is necessary to understand how the model works and why it is viable. The other article will focus on the simulation results.

The model uses CFD to simulate the flow of lead in the entire primary circuit. The free surfaces are resolved by using multiphase (lead and helium) with the volume of fluid method. Similar to the porous medium, the complex components are replaced by a simple geometry with momentum and heat sources/sink. The CFD simulation is coupled with a custom-made code for fuel heat transfer and point kinetics for neutronics.

The validation exercise was performed to compare experimental results with CFD simulations. The experimental data was taken from the TALL-3D facility which contains a section specifically designed to validate CFD. The main phenomena targeted by this validation are temperature stratification and a jet into a plenum. The CFD case was set up exactly with the same configuration as for the model.

5.3 Article

The following pages contain the original article.

Development of a CFD-Based Model to Simulate Loss of Flow Transients in a Small Lead-Cooled Reactor

Cuauhtemoc Reale Hernandez[a*], Dmitry Grishchenko[b], Pavel Kudinov[b], Janne Wallenius[b], John Luxat[a]

[a] McMaster University, Hamilton, Canada

[b] KTH Royal Institute of Technology, Stockholm, Sweden

Abstract

With the deployment of advanced and small modular reactors (SMRs), it is important to develop the tools to assess their safety. This work presents the different components of a CFD based model for simulating transients in a pool-type small lead cooled reactor. The model encompasses the entire primary circuit with a simplification of the fuel channels, pumps and steam generators. Those parts are modelled through heat and momentum sources (or sinks), similar to the porous medium used in other studies. The CFD solver is coupled with a finite volume solver for fuel pin temperature and a point kinetics solver for neutronics. Free surface is modelled in CFD with multiphase volume of fluid method. The set of methods that is used in this work constitute a novelty for modelling lead cooled reactors. The goal is to have a model that is relatively simple to implement in order to study the effect of some parameters on reactor transients like an unprotected loss of flow. The focus of this study is to describe in detail every individual component of the model, namely the fuel channels, fuel pin temperature, neutronics, coupling strategy, pump and steam generators. In addition, CFD simulations are compared against experimental data from the TALL-3D facility. The purpose of this comparison is to verify that the models and parameters of the CFD software (STAR-CCM+) are capable of reproducing a flow of heavy metal. A future publication will provide the simulation results of an integrated model with all the components.

Keywords: heavy-metal reactors, SMR, CFD, transients

Abbreviations:

CFD: computational fluid dynamics

LBE: lead bismuth eutectic

SMR: small modular reactor

TC: thermocouple

EPR: European pressurized reactor

VOF: volume of fluid model

UCTD: Updated Cheng and Todreas Detailed correlation

*** Corresponding author**

email: realehec@mcmaster.ca

address: 1280 Main St W, Hamilton, Canada

1. Introduction

Heavy metal-cooled fast reactors are a promising technology for the future of nuclear energy. The high boiling point of lead, absence of violent chemical reactions in case of leakage and its ability to have a fast neutron spectrum place it in a unique position. Large fast lead -and lead-bismuth- cooled reactors would have the capability to breed fuel and close the fuel cycle. Currently, at least one lead-cooled breeder is under construction("Russia starts building lead-cooled fast reactor," 2021). Lead-cooled small modular reactors (SMRs) might not be breeders but would still have a high fuel efficiency and exhibit excellent safety features. Independently of that, the SMR market is slowly starting to take off and many prototypes are expected to be seen in the next 10 years.

For these reasons, it is important to study the safety of these reactors. This work focuses on developing a tool for simulating transients in a lead-cooled SMR. The reference reactor used here is the SEALER-arctic reactor (J. Wallenius et al., 2018), a small pool-type SMR intended for remote off-grid operation. It has a power of 3 to 10 MWe and its lifetime is between 10 and 30 years, without refueling. See Figure 30 for a schematic of the reactor. This work is part of a collaboration with the owner of the SEALER design, Janne Wallenius' team at KTH, who provided the necessary design data.

Previous work has been done on modelling the SEALER reactor and other heavy-metal reactors. Bortot et al. developed a code called BELLA for simulating different types of transients. It is a lumped parameter model coupled with point kinetics (Bortot et al., 2015). That model was used by the authors of this study to perform a sensitivity and uncertainty analysis[4]. One of the findings was that for a set of parameters not very far from nominal values, reverse flow is possible during an unprotected loss of flow accident. That has motivated the development of a more accurate model based on CFD.

Roelofs et al. developed a CFD model for SEALER-arctic (Roelofs et al., 2019) and SEALER UK Demo (Zwijsen et al., 2020). It contains the entire primary circuit and simplifies some of the components with porous media and specified momentum and heat

sources. That CFD model is for calculating steady-states, so neither the free surface, the fuel pin temperature nor the neutronics are modelled.

Moreau et al. elaborated a CFD model for the MYRRHA reactor, which is an accelerator driven system (ADS) cooled by lead-bismuth eutectic (LBE) (Moreau et al., 2019b). Many components, including the fuel assemblies, are replaced by a porous medium. The coolant in the fuel channels is thermally coupled with the fuel which occupies the same volume but whose physical properties were modified to take into account the real mass. That coupling incorporates a characteristic time to produce the right heat transfer delay during transients. For cases where transients are driven by reactivity feedbacks like in this study, a more accurate fuel temperature model would be required.

Fiorina et al. developed a CFD model based on the open source software OpenFOAM (Fiorina et al., 2015). It is aimed at simulating transients in different types of reactors. The fuel channels and other components are also replaced with a porous medium, fuel temperature is solved with finite elements and a diffusion model is used for neutronics. This code has extended capabilities like coupling with thermal mechanics.

The aim of the model that is presented in this study is to have a tool for simulating transients that is more accurate than a lumped-parameter or pure STH code, while remaining relatively simple to implement and utilize. One of the main objectives is to explore the effect of certain parameters on an unprotected loss of flow accident. Using CFD is necessary for the areas of the reactor that exhibit complex 3D flows, like in the plenums. Traditionally, for large reactors, STH codes have been coupled with CFD to obtain accurate solutions. In the case of the SEALER reactor, which is more compact and where all the components are integrated into a smaller pool, it is beneficial to model the entire circuit in the same CFD code. This has the advantage of eliminating the need for coupling STH with CFD. Similar to the models mentioned previously, the main strategy is to simplify the geometry of the main components (fuel channels, pump, steam generators) and to add momentum and heat sources (or sinks) which are derived from correlations. Those components are thus treated just like in an STH code, but their integration with the rest of

the circuit (which requires CFD) is easier and faster. The free surface is modelled with CFD by using multiphase. Fuel temperature is solved in a custom code along with point kinetics for neutronics. This combination of methods constitutes a novelty in the field of heavy-metal reactors modeling.

The purpose of this article is to provide background work on the modelling methods and to show that the model is viable. The first two sections present a general description of the model and provide the details of each component which includes: fuel channels, fuel pin temperature, neutronics, coupling method, steam generators and pump. The last section compares CFD simulations against experimental data from the TALL-3D facility. The purpose is to ensure that the parameters of the CFD software, which is STAR-CCM+, are appropriate to model a general flow of heavy metal. Although it is not directly connected to the reactor model, this section is a necessary building block in the development of a lead-cooled reactor model.

Results from reactor simulations where all the components are integrated will be presented in a future publication.

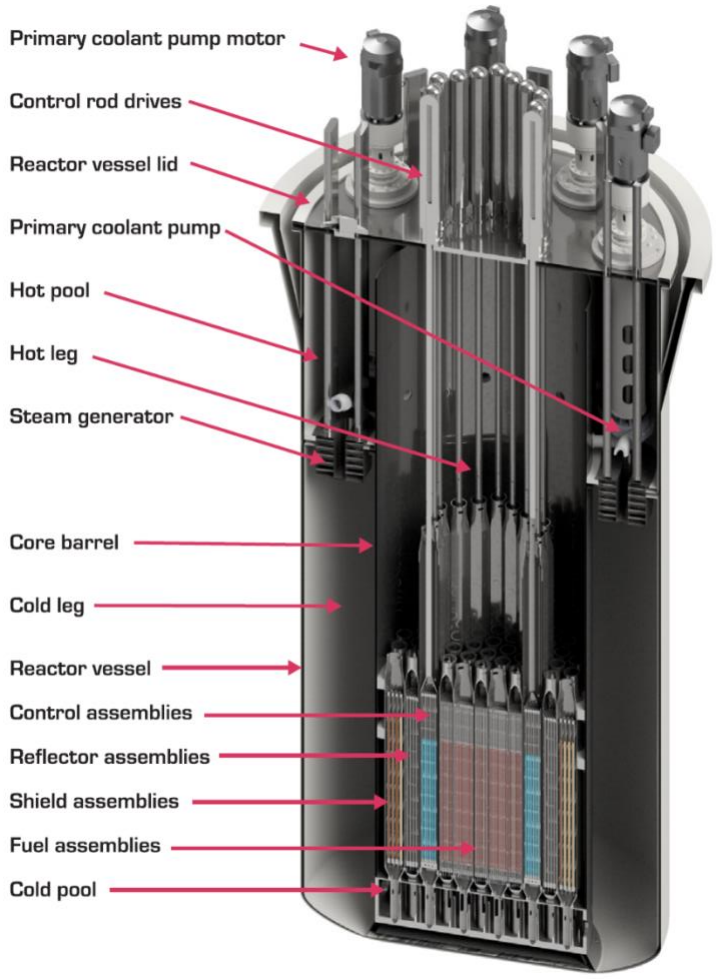

Figure 30 CAD rendering of the SEALER reactor, used as a reference in this study

2. General description of the model

The schematic in Figure 31 illustrates the geometry of the reactor and the main components. The dashed line represents the centerline of the vessel which has a cylindrical geometry. A barrel divides the reactor vessel in two concentric regions, the middle one contains the cold pool, reactor core and hot leg (or upper plenum), and the outer region contains the pumps, steam generators and cold leg. During normal operation, the coolant will move from the cold pool upwards into the fuel channels, where it is heated and then discharged into the

upper plenum. From there, the coolant is moved to the outer region through 8 holes on the barrel, each connected to a pump. On the outer region, lead moves downwards through the steam generators and then to the cold leg. Finally, the cold leg connects to the cold pool through holes on the barrel. The free surface is higher on the outer region because of the pressure generated by the pumps.

The physics of the model are separated in three parts:

- Thermal-hydraulics of the entire primary circuit (except the fuel), solved with CFD
- Fuel pin temperature, solved with a finite volume method for solid heat transfer
- Neutronics, solved with point kinetics

The solvers for the fuel pin temperature and point kinetics are both programmed in Matlab. The coupling of those two solvers with STAR-CCM+ is also done through Matlab. Text files and CSV files are used for interfacing Matlab with STAR-CCM+.

Thermal-hydraulics is itself divided into a few parts. Although the entire circuit is part of the same CFD simulation, the components with a complex geometry are simplified and each has a specific heat and momentum source (or sink). This is due to the impossibility for CFD to capture every detail because of computing limitations. The different parts of the CFD geometry and their corresponding color on Figure 31 are as follows:

- Fuel channels: heat source and momentum sink, red
- Fuel channel foots (orificing): momentum sink, not shown on the figure
- Pumps: momentum source, blue
- Steam generators: heat and momentum sink, green
- Upper plenum, cold pool and cold leg: free flow, gray

Using heat and momentum sources is very similar to using a porous medium, which is becoming standard practice for modelling the entire primary circuit with CFD (Roelofs et al., 2019), (Moreau et al., 2019b), (Fiorina et al., 2015). The reason for not using an actual porous medium is elaborated in the section on fuel channels.

The free surface is modelled by using multiphase with volume of fluid (VoF). The two phases are lead and helium. The boundaries in contact with helium are walls. The control rods, reflector and shield assemblies also contain coolant (black components on Figure 31), but since the flow is nearly stagnant, they are treated as solid and not included in the fluid domain.

The following section describes in detail each component of the CFD geometry: fuel channel, pump and steam generator. It also describes the model for fuel pin temperature, neutronics and the coupling strategy.

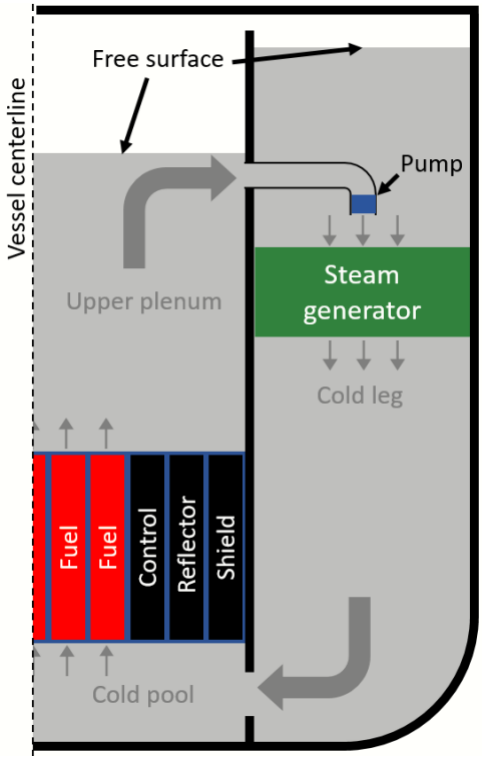

Figure 31 Schematics of the geometry of the primary circuit

3. Description of CFD components and physics models

3.3 Fuel channels

3.3.1 General description

The reactor core contains 19 hexagonal fuel channels, see Table 2 for a list of assembly and fuel pin parameters. The fuel channels are part of the same CFD mesh that is used for calculating thermal hydraulics of the entire primary circuit. However, a special treatment is necessary. Modelling the full geometry of the fuel assemblies would be computationally prohibitive since the mesh would require enough detail to properly calculate the heat transfer and friction from every of the 91 pins per assembly. Therefore, the geometry is simplified to what is shown on the right of Figure 32. The hollow triangular areas are there to replace the space occupied by the fuel pins so that the flow cross section area is the same (i.e. the coolant moves through the area highlighted in yellow). A momentum source and an energy source are used to take into account the heat transfer and friction (pressure drop) between coolant and pins, see next sections for details.

Adjacent assemblies are not in contact, so cross-flow is impossible. That is coherent with the design of SEALER, where assemblies are wrapped in hex-cans to avoid cross-flow. Also, in the first implementation of the reactor model, only the fluid will be modelled, so there is no heat conduction between assemblies either. In the SEALER design, heat conduction is possible but plays only a minor role since velocities are adjusted so that the temperature gain is the same in every channel. If heat conduction becomes an important aspect to model, it could be calculated externally and fed to the CFD simulation through the heat source.

Using a porous hexagonal tube, where the porosity takes into account the space occupied by the fuel pins, was considered for this model. STAR-CCM+ has two ways of modelling porosity, one is using a Porous Region, and the other is the Porous Media Model. Only the latter produces the correct velocity which is necessary for calculating the coefficients for heat transfer and pressure drop. Indeed, STAR-CCM+ recommends using the Porous Media Model for modelling heat exchangers. However, that model is not compatible with

VOF (volume of fluid) model, which is needed for the free surface. Thus, using the described geometry resulted in the best solution. Similar approaches have also been used elsewhere, like in CFD simulations of the EPR (Martinez and Galpin, 2014).

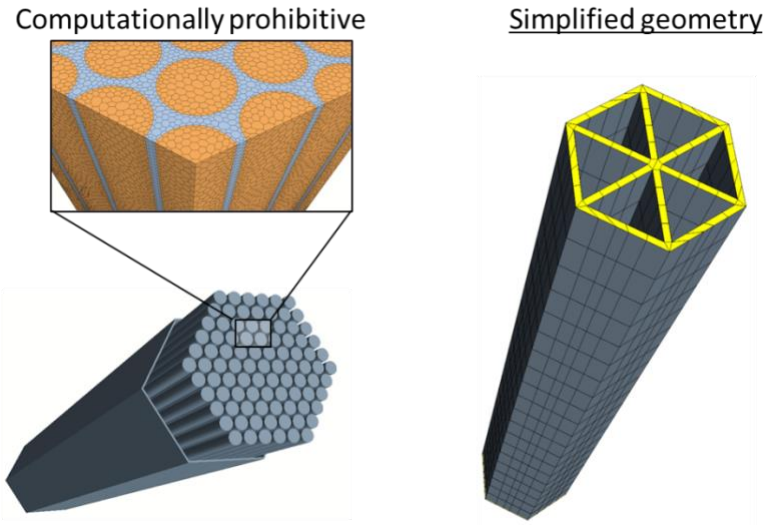

Figure 32 The geometry of the fuel assembly used in CFD is simplified by keeping the same flow cross section

Table 2 Assembly and fuel rod design of SEALER

Item	Value
Fuel assemblies	19
Fuel pins per assembly	91
Fuel pin pitch	16.37 mm
Fuel pin (P/D) (hot)	1.127
Fuel composition	UO2
U-235 enrichment	19.75 wt%

Fuel pellet diameter (cold/hot)	13.30/13.40 mm
Fuel column height (cold/hot)	1100/1106 mm
Clad outer diameter (cold/hot)	14.44/14.52 mm
Fuel rod length	1590 mm

3.3.2 Momentum sink

Pressure drop is taken into account by introducing a momentum sink in STAR-CCM+. That sink is calculated from the following relation:

$$\frac{\Delta P}{L} = f(Re)\frac{\rho \cdot v|v|}{2 \cdot D_e} \quad \left[\frac{kg}{m^2 s^2}\right]$$

Equation 12

where $\frac{\Delta P}{L}$ is the momentum sink (pressure drop per unit length), $f(Re)$ is the friction factor, which is a function of Reynolds number, ρ is the coolant density, v is the coolant velocity, and D_e is the equivalent hydraulic diameter of the fuel assembly.

The main task is to obtain the right value for the friction factor. Many empirical correlations exist to calculate the friction factor as a function of the Reynolds number and the dimensions of the fuel bundle (Bubelis and Schikorr, 2008). The one used in this work is the Updated Cheng and Todreas Detailed (UCTD) correlation (Chen et al., 2018). This correlation was developed for wire wrapped bundles (like SEALER) and has been tested against many experimental data sets.

The procedure to obtain the friction factor is not a simple equation, but rather a series of steps that would be too complicated to implement in STAR-CCM+. Therefore, the strategy adopted here is to calculate the friction factor using UCTD for a range of relevant Reynolds number and for one specific set of assembly dimensions. That data is then fitted with a function of the following form:

$$f(Re) = \frac{A}{\log Re} + B + C(\log Re) + D(\log Re)^2$$

Equation 13

where A, B, C and D are the fitted parameters. The equation only depends on the Reynolds number and can be easily implemented in STAR-CCM+.

3.3.3 Heat source

Heat transfer between the fuel pins and the coolant is replaced by a volumetric heat source in the CFD simulation. For each channel, the space which contains fuel is divided axially into 10 sections, each having a different value of volumetric heat source. A directed mesh is used in the fuel channels to ensure that the divisions between sections correspond to divisions between CFD cells, see Figure 32.

A table in the form of a CSV file containing the heat source of each section in each channel is prepared by an external code and read by STAR-CCM+ at each iteration.

3.4 Fuel pin temperature

The evolution of the fuel temperature distribution is calculated outside of the CFD simulation, in a Matlab code. All the material properties are temperature dependent (Carbajo et al., 2001), (Leibowitz and Blomquist, 1988). In addition, the material properties of the fuel pellets also depend on the porosity. To some extent, this allows for burnup to be taken into account since porosity depends on it. This solver requires two inputs: coolant temperature and velocity (provided by the CFD part), and heat generation (provided by neutronics). Its output consists of the average fuel temperature (used by neutronics) and heat transfer from clad to coolant (used by CFD).

In each assembly, it is assumed that all the pins have the same temperature distribution, so it is only necessary to solve one fuel pin per assembly. This greatly reduces the number of calculations. A finite volume approach is used where each cell is created by dividing the length of the pin into slices, and then each slice into rings. Since the gap between fuel and clad is very thin, it is assumed that convection is negligible and the gap is simply treated as a solid. Therefore, solving heat transfer in one slice is a 1D problem, and a 2D problem for the whole pin. Figure 33 shows a schematic of how geometry is divided and the different variables that are used. Note that the number of cells is for illustration purposes. In practice, fuel pins are divided in 10 slices and 30 rings (10 for fuel, gap and clad).

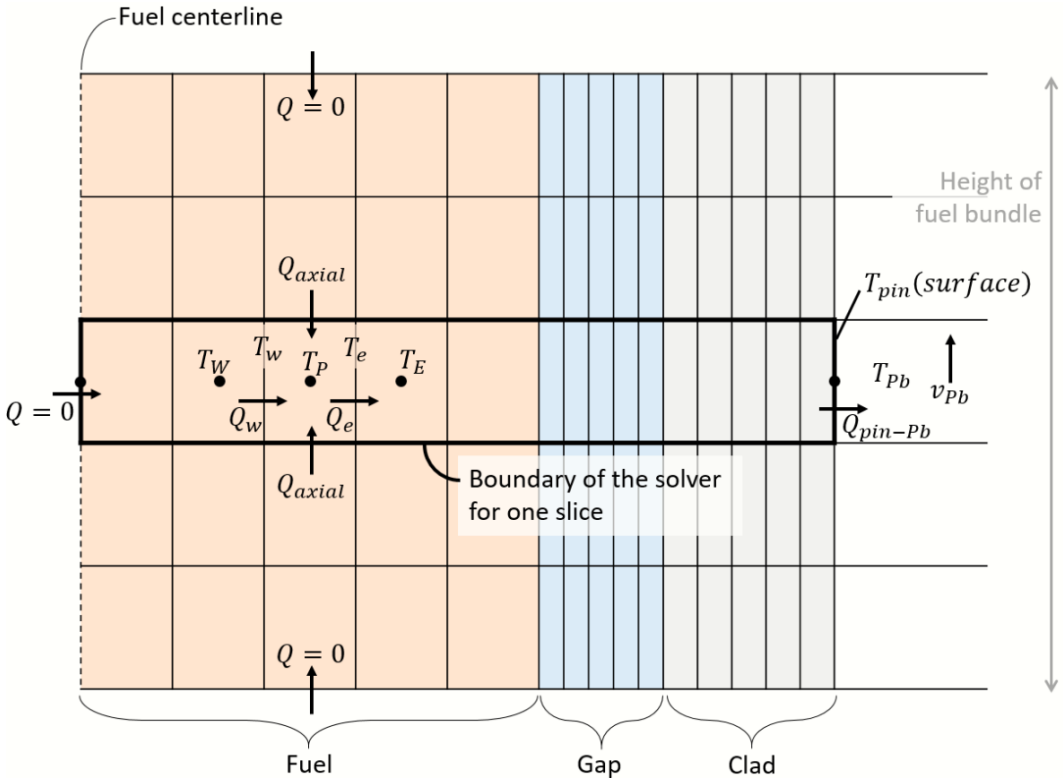

Figure 33 schematic of the fuel pin temperature solver

The fuel pin temperature solver is separated in two parts. The first part uses a fixed clad surface temperature as a boundary condition to calculate the evolution of the pin temperature distribution. That is achieved through straightforward numerical methods. This part was verified against a transient CFD simulation with a very fine mesh using the exact same geometry and material properties. The temperature profiles and temperature evolution were identical in the CFD simulation and this solver (not shown here for brevity).

The second part connects the clad surface temperature to the coolant temperature through the Nusselt relation:

$$Q_{pin-Pb} = Nu \frac{k_{Pb}\left(T_{pin}(surface) - T_{Pb}\right)}{D_h} A_{pin}$$

Equation 14

Where Q_{pin-Pb} is the heat transfer from pin to coolant, k_{Pb} is the thermal conductivity of the coolant, $T_{pin}(surface)$ is the clad surface temperature, T_{Pb} is the coolant temperature, D_h is the hydraulic equivalent diameter of the assembly, A_{pin} is the total surface area between pins and coolant.

The Nusselt number Nu is a function of pin pitch to diameter ratio $\frac{P}{D}$ and Peclet number. The correlation used here is the Kazimi and Carelli correlation used for sodium systems, which has been successfully compared against LBE wire-wrapped bundles (Pacio et al., 2018).

$$Nu = 4.0 + 0.33\left(\frac{P}{D}\right)^{3.8} \cdot \left(\frac{Pe}{100}\right)^{0.86} + 0.16\left(\frac{P}{D}\right)^{5.0}$$

Equation 15

Valid for $1.1 \leq \frac{P}{D} \leq 1.4$ and $10 \leq Pe \leq 5000$.

The solver iterates between the two parts. The second part will update the clad surface temperature by performing the following calculations. The heat transfer between clad surface and coolant is calculated in two different ways. One employs Equation 14 and clad surface temperature. The other derives it from the temperature gradient at the clad surface. Those two values are averaged together and the new heat transfer value is used with Equation 14 to calculate the new clad surface temperature for the next iteration. That process is repeated until the two values of heat transfer are equal.

Since neutronics are calculated with point kinetics, the heat generation data provided to the fuel pin solver is a single value corresponding to the total reactor fission power. The power distribution is obtained from Serpent simulations of the SEALER reactor. The discretization of the power distribution corresponds exactly to the discretization used in this fuel pin temperature solver. The power distribution is constant throughout any transient

simulation, only its amplitude changes to match the total reactor power provided by neutronics.

3.5 Neutronics

Neutronics are also calculated outside of CFD, in a Matlab code. Point kinetics are used with six precursor groups. The neutron density $n(t)$, which is proportional to the total power, is derived from the following equations:

$$\frac{dn(t)}{dt} = \frac{\rho(t) - \beta_{eff}}{\Lambda_{eff}} n(t) + \sum_{i=1}^{6} \lambda_i C_i(t)$$

Equation 16

$$\frac{dC_i(t)}{dt} = \frac{\beta_i}{\Lambda_{eff}} n(t) - \lambda_i C_i(t)$$

Equation 17

Where $\rho(t)$ is the time dependent reactivity, β_{eff} is the effective delayed neutron fraction, Λ_{eff} is the effective neutron reproduction time, $C_i(t)$ is the time dependent concentration of the delayed neutron precursor group i, β_i is the delayed neutron fraction of group i, and λ_i is the decay rate of group i.

The reactivity is approximated with the following equation:

$$\rho(t) = K_D \ln\left(\frac{T_{fuel}(t)}{T_{fuel}^0}\right) + \alpha_{axial}\left(T_{fuel}(t) - T_{fuel}^0\right) + \alpha_{Pb}(T_{Pb}(t) - T_{Pb}^0)$$

Equation 18

$T_{fuel}(t)$ and $T_{Pb}(t)$ are the temperature average of the entire core for the fuel and coolant, respectively. T_{fuel}^{0} and T_{Pb}^{0} are those same temperatures but at the beginning of the transient (steady state). K_D is the Doppler constant, α_{axial} is the reactivity coefficient due to fuel axial expansion, and α_{Pb} is the reactivity coefficient due to coolant expansion. Those three coefficients were calculated from Serpent simulations.

The equations are solved numerically using the Matlab function ode15s. The time step is automatically selected to reach a relative tolerance of 1e-6.

The inputs of this solver are the average fuel temperature (provided by the fuel pin temperature solver) and the average coolant temperature in the core (provided by CFD). The output is the total fission power which is used by the fuel pin temperature solver.

3.6 Coupling method

One of the key elements for solving transients consists in properly coupling the different physics involved in the model, namely thermal hydraulics (CFD), fuel pin temperature and neutronics. The schematics on Figure 34 illustrates how they are dependent on each other by providing the inputs and outputs required and provided by each solver.

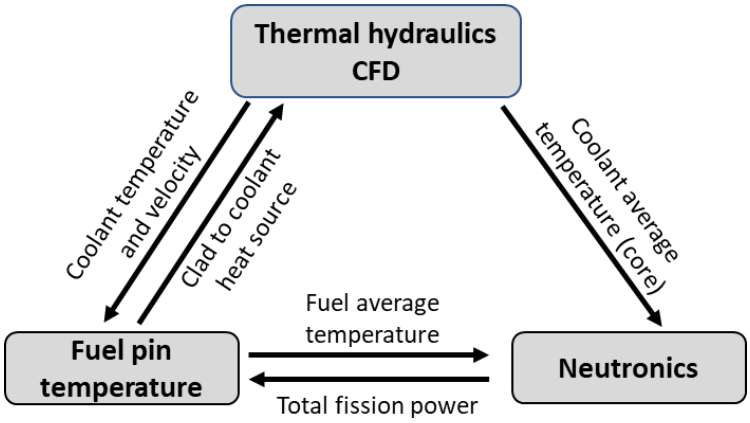

Figure 34 Interdependency of the different physics involved in the model

For every time step, an iterative process is used to reach a converged solution across all three solvers. Figure 35 presents a simplified flowchart of that process. The sequence of the algorithm is set up in a such way to minimize CFD runs and reduce computing time. Therefore, a partial solution is first obtained by iterating only the fuel pin and neutronics solvers. That small loop (orange on Figure 35) solves for fuel pin temperature and neutronics for a given coolant temperature and velocity, and it requires very little computing power. The main loop (all colored boxes in Figure 35) consists in iterating the small loop and the thermal hydraulics solver (CFD) to reach a complete solution.

An iterative process is necessary because a backward Euler method is employed, so the input variables used by every solver correspond to the new values (i.e. the ones that are being solved for). The first solvers to run in the main loop (fuel pin and neutronics) need an estimate of the new coolant temperature and velocity. That could simply be the value of the previous time step, but in order to reach a converged solution with less iterations, a linear extrapolation is made using the last three time steps.

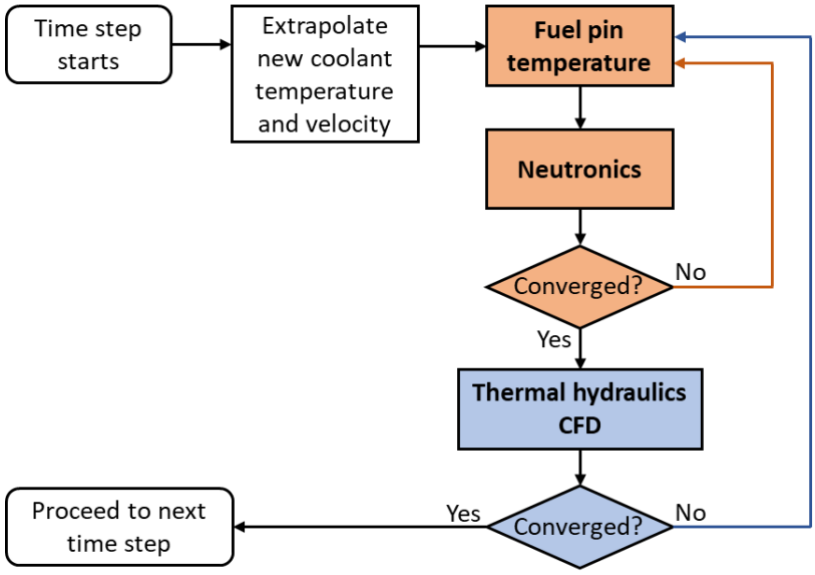

Figure 35 Simplified flowchart of the algorithm for coupling the different physics

The entire process, except for CFD, is programmed in Matlab. The communication between Matlab and STAR-CCM+ (the CFD software) is achieved through reading and writing of text files and CSV files. This reading and writing takes a considerable amount of time, so performing the coupling process at each CFD time step would take too much time. Instead, the coupling process takes place every 10 or 20 CFD time steps. For instance, the coupling time step is around 0.1s and the CFD time step around 0.01s. The time step of the fuel pin temperature solver is the same as the coupling time step. The neutronics solver automatically selects a time step small enough to reach a converged solution at a specified tolerance.

It is to be noted that the pump is also coupled to the rest of the simulation. That is not included in this section for simplicity and because there is no iteration between the pump and the rest. At the beginning of each time step, the pump properties (characteristic curve) are updated according to the volumetric flow rate of the previous time step. The details of the pump model are presented in the pump section.

3.7 Steam generator

The steam generators (SGs) are part of the thermal hydraulics (CFD) solver. Their geometry is a simple box located under the pumps. They occupy the whole cross section area of the cold leg, such that the flow will necessarily go through the SGs, see Figure 30 and Figure 31. Unlike the fuel channels, no special geometry was used to take into account the space occupied by the SG tubes, the coolant simply fills the whole space. A momentum sink and a heat sink are used to account for the pressure drop and heat transfer. The momentum sink is calculated from the following equation:

$$\frac{\Delta P}{L} = f_{SG}\frac{\rho \cdot v|v|}{2 \cdot D_e} \quad \left[\frac{kg}{m^2 s^2}\right]$$

Equation 19

Where f_{SG} is a constant friction factor calculated in such a way to obtain the pressure drop at the nominal mass flow specified in the design of SEALER[2], that is 12kPa at 1300kg/s for the whole reactor.

Since the focus of the model is on the primary circuit, the behavior of the SG is simplified to have a constant temperature drop. That is deemed sufficient for simulating loss of flow and overpower transients. More specifically, the actual volumetric heat sink in the CFD software follows the following equation:

$$\dot{q} = -h\left(T - \left(T_{pump} - \Delta T_{SG}\right)\right)$$

Equation 20

Where T is the coolant temperature, T_{pump} is the temperature of the coolant at the pump (used as inlet temperature of SG), and ΔT_{SG} is the specified temperature drop of 42 °C. The heat transfer coefficient h is a value high enough to ensure that all the coolant at the SG outlet is almost equal to $T_{pump} - \Delta T_{SG}$.

3.5 Pump

3.5.1 CFD implementation

The pump is part of the thermal hydraulics (CFD) solver. Its geometry is a cylinder located at the end of the tube that connects the hot leg with the cold leg, see Figure 31. The pump characteristic curves are used to calculate the momentum source. The dimensionless equations for the pump head and the brake-horse torque are as follows:

$$h = a^2 \left(p_0 + p_1 \left(\frac{\nu}{a}\right) + p_2 \left(\frac{\nu}{a}\right)^2 + p_3 \left(\frac{\nu}{a}\right)^3 \right)$$

Equation 21

$$b = a^2 \left(q_0 + q_1 \left(\frac{\nu}{a}\right) + q_2 \left(\frac{\nu}{a}\right)^2 + q_3 \left(\frac{\nu}{a}\right)^3 \right)$$

Equation 22

Where $a = \frac{\omega}{\omega_R}$ is the rotor speed ratio, $h = \frac{H}{H_R}$ is the pump head ratio, $b = \frac{T}{T_R}$ is the break-horse torque ratio, $\nu = \frac{Q}{Q_R}$ is volumetric discharge flow ratio. The equation coefficients p_i and q_i are listed on Table 3. Since the actual pump has not been selected yet, the values used for these coefficients are taken from the Maine Yankee reactor pumps (Kao, 1984; Todreas and Kazimi, 1990).

Table 3 Coefficients for the pump characteristic curves

p_0	p_1	p_2	p_3
1.8	-0.3	0.35	-0.85
q_0	q_1	q_2	q_3
1.37	-1.28	1.61	-0.7

In the SEALER reactor, the operating point for each pump is $0.016\ m^3/s$, $140\ kPa$, and $500\ rpm$. The reference points ω_R, H_R, T_R *and* Q_R are calculated in a way such that maximum efficiency occurs at the operating point and that efficiency is arbitrarily chosen to be 85%. The resulting pump characteristic curves are shown on next figure, at operating rotor speed.

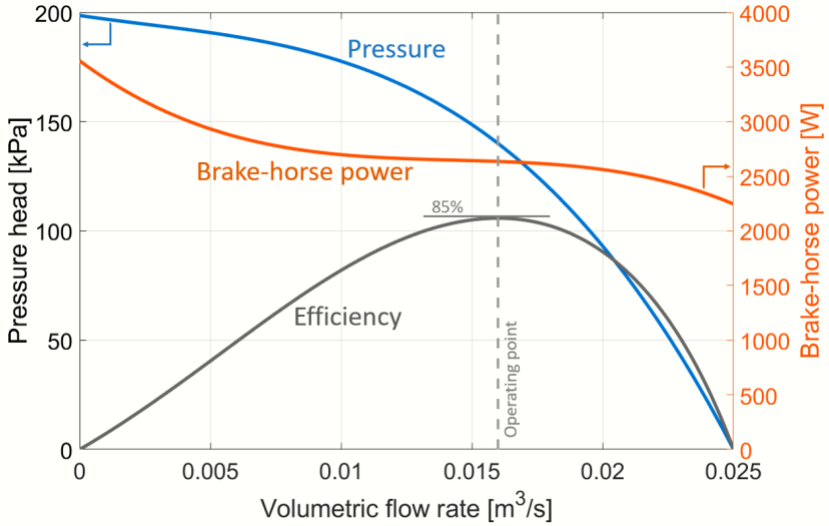

Figure 36: Pump characteristic curves at operating rotor speed

For a given rotor speed a, the momentum source corresponds to H/L, where L is the length of the pump region (a cylinder). That value is calculated by implementing a modified version of Equation 21 in STAR-CCM+, in which the momentum source is a function of flow velocity u:

$$\frac{H}{L} = \frac{H_R \cdot a^2}{L}\left(p_0 + p_1\left(\frac{A \cdot u}{Q_R \cdot a}\right) + p_2\left(\frac{A \cdot u}{Q_R \cdot a}\right)^2 + p_3\left(\frac{A \cdot u}{Q_R \cdot a}\right)^3 \right) \quad \left[\frac{Pa}{m}\right]$$

Equation 23

Where A is the cross section area of the pump region.

In a loss of flow accident, flow regime will change from forced to natural convection as the rotor speed a tends to zero. For very small values of a, it is not possible to use Equation 21, instead the following equation is recommended (Todreas and Kazimi, 1990) :

$$h = -4.181|\nu|\nu$$

Equation 24

The method described here is valid for the first quadrant only. However, the simulations are controlled to ensure that the flow and the pump head both remain positive.

3.5.2 Flywheel coupling for transient calculations

To perform pump coastdown calculations, the rotor speed is sometimes approximated as having an exponential decay. In this study, because of the change in free surface level, that approximation is not accurate. Instead, the kinetic energy contained in the flywheel is coupled with the brake-horse power and flow rate.

The calculation procedure is as follows. At the beginning, the kinetic energy of the flywheel is calculated from angular velocity (rotor speed) ω and moment of inertia I:

$$E = \frac{1}{2} I \omega^2$$

Equation 25

For any subsequent time step, the torque is calculated using the mass flow of the previous time step with Equation 22. Since that torque was all provided by the flywheel, its kinetic energy is decreased by the energy it provided from last to current time step. This corresponds to the flywheel kinetic energy of current time step, which is used with Equation 25 to calculate the current rotor speed, which is then used to calculate the current head characteristic curve for CFD. The losses due to friction in the mechanical parts of the pump are neglected.

The coupling is implemented in Matlab along the coupling with the other solvers. There is no iterative process, the pump head characteristic curve of current time step is exclusively derived from variables of the previous time step.

3.5.3 Test of pump dynamics

A CFD simulation case was setup to test this method. It consists of two tall boxes connected at the bottom by a pump (that moves the fluid from left to right) and pipe (that allows the fluid to go from right to left). The pressure loss in the lower pipe was adjusted to have a flow of about $0.016\,m^3/s$ (operating point of SEALER pumps). The boxes are also connected at the top to allow air to move when free surface levels change. In Figure 37, the left side presents the mesh that was used, and the right side shows the free surface levels and Pb velocity of the steady state.

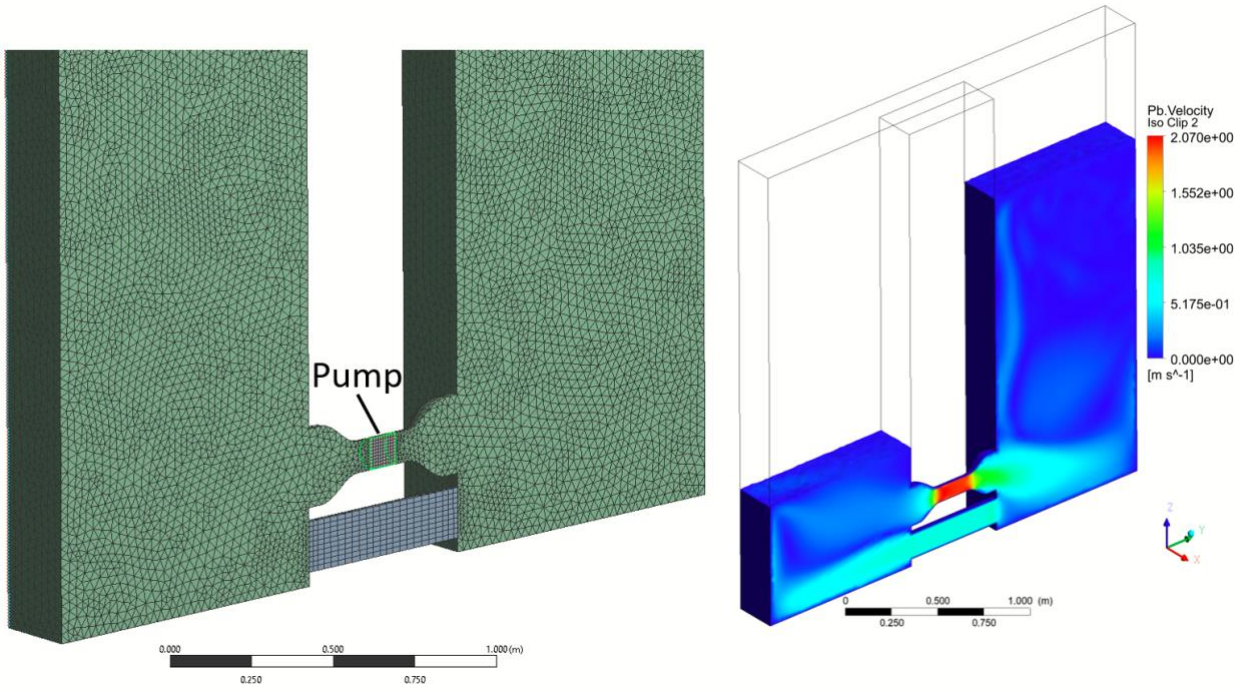

Figure 37: Mesh and steady state of the setup used to test the pump coastdown calculation method

A coastdown transient calculation was performed using the state showed in Figure 37 as initial conditions. Different flywheel moments of inertia were tested in order to find one that would cause the flow rate to decrease as quickly as possible without becoming negative (reverse flow). The results presented here were obtained with a flywheel that is a steel disc of 1m of diameter and 5cm thick.

Figure 38 shows the evolution of volumetric flow rate with time during the coastdown transient. At the start of the transient, the flow rate decreases very rapidly, attains a minimum, then increases and only from there, it starts decreasing slowly. This behavior is very similar to simulations of the SEALER reactor performed with a lumped parameter model (J Wallenius et al., 2018). It's the result of the interaction between the decreasing pump head and moving free surface levels.

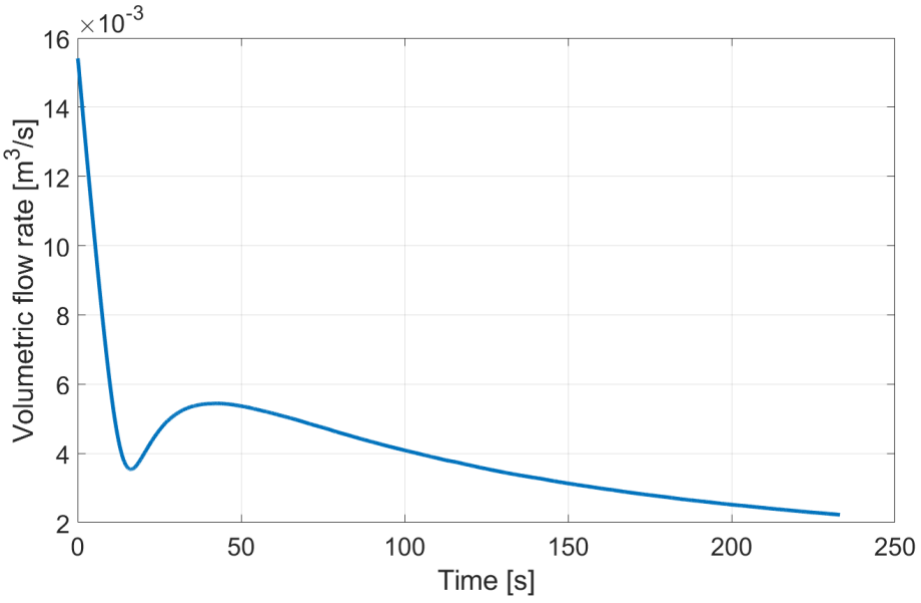

Figure 38: Volumetric flow rate during coastdown transient

Figure 39 shows the speed of the rotor during the transient. An exponential curve of the form $y = a \cdot \exp(b \cdot x)$ is also shown for comparison. We can see that it is not possible to

fit the rotor speed to that curve. Thus, in this case, the rotor speed does not follow an exponential decay.

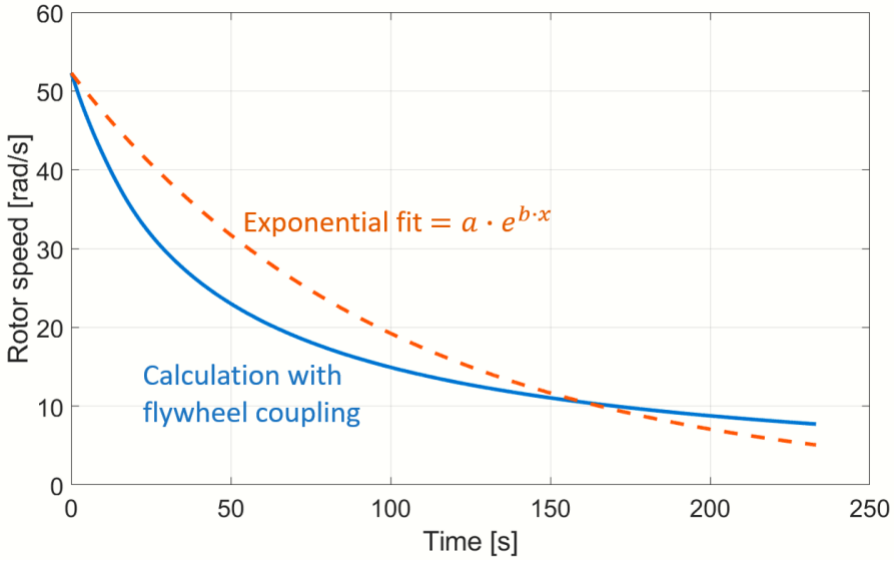

Figure 39: Rotor speed during coastdown transient, compared to an exponential decay

3. STAR-CCM+ comparison with experimental results from TALL-3D

Before setting up a CFD simulation of the SEALER reactor, it is necessary to test the capability of STAR-CCM+ to model a general flow of lead. More specifically, is it important to verify that the STAR-CCM+ parameters and models that are intended to be used for SEALER are capable of reproducing experimental results of a simple geometry. This section presents a comparison between STAR-CCM+ simulations and experimental results from the TALL-3D facility. The main phenomena of interest are the mixing of a hot jet into a plenum and temperature stratification.

3.1 Description of the facility

TALL-3D (Kudinov et al., 2017) is a lead-bismuth-eutectic (LBE) loop located at the KTH Royal Institute of Technology in Stockholm. The 3D test section of the TALL-3D facility

is very well suited for the purpose of this study. In the recent years, a battery of tests has been performed and used in benchmarks to validate system codes, CFD (Jeltsov et al., 2019) and the coupling of both (Grishchenko et al., 2020), (Grishchenko et al., 2015). This was done as part of the European SESAME project, which stands for thermal-hydraulics Simulations and Experiments for the Safety Assessment of Metal cooled rEactors.

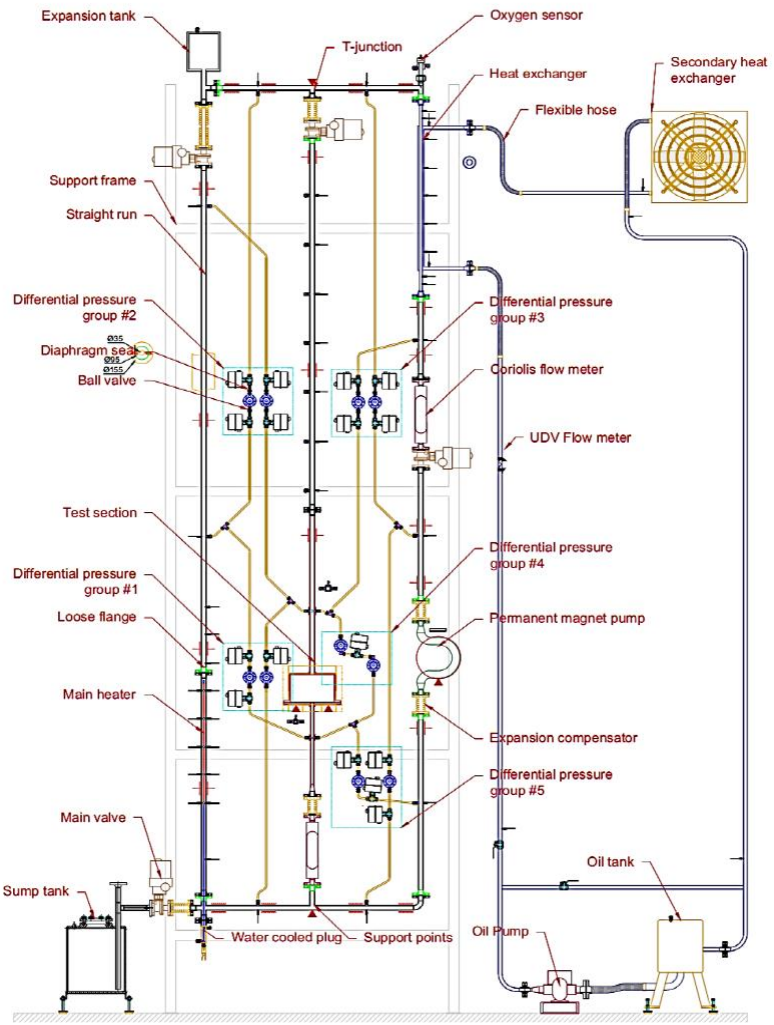

Figure 40 TALL-3D facility main components

Figure 40 shows a diagram of the facility. It consists of three vertical legs of about 6m in height. In the right (“cold”) leg, which contains a heat exchanger and a pump, the coolant typically flows downwards. In the left (“hot”) leg, which contains a rod heater, the flow is

usually upwards. The middle leg contains a 3D test section which was designed to compare with CFD codes. Thermocouples, pressure sensors and flow meters are placed at all the relevant locations in order to obtain a complete characterization of the thermal-hydraulics in the loop.

The work presented in this study addresses only the 3D test section since the rest of the loop is typically modelled using system thermohydraulic codes. A diagram of the 3D test section is shown in Figure 41. The flow enters the cylindrical vessel from the bottom through a relatively narrow pipe. A circular plate (the inner plate) is placed inside the vessel at the top in order to reflect the jet in radial direction and to create more complex patterns in the flow. The flow leaves the vessel at the top through a pipe slightly wider than the inlet. Heating elements are placed on the outer cylindrical wall of the vessel as illustrated in the figure. In order to measure the temperature distribution inside the vessel, four vertical inner pipes are placed between the inner plate and the vessel wall, each containing nine thermocouples (inner pipes for in-pool TCs). The inner plate also contains a series of the thermocouples placed in a cross shape. A flow meter is located below the test section and thermocouples are placed at the inlet and outlet pipes.

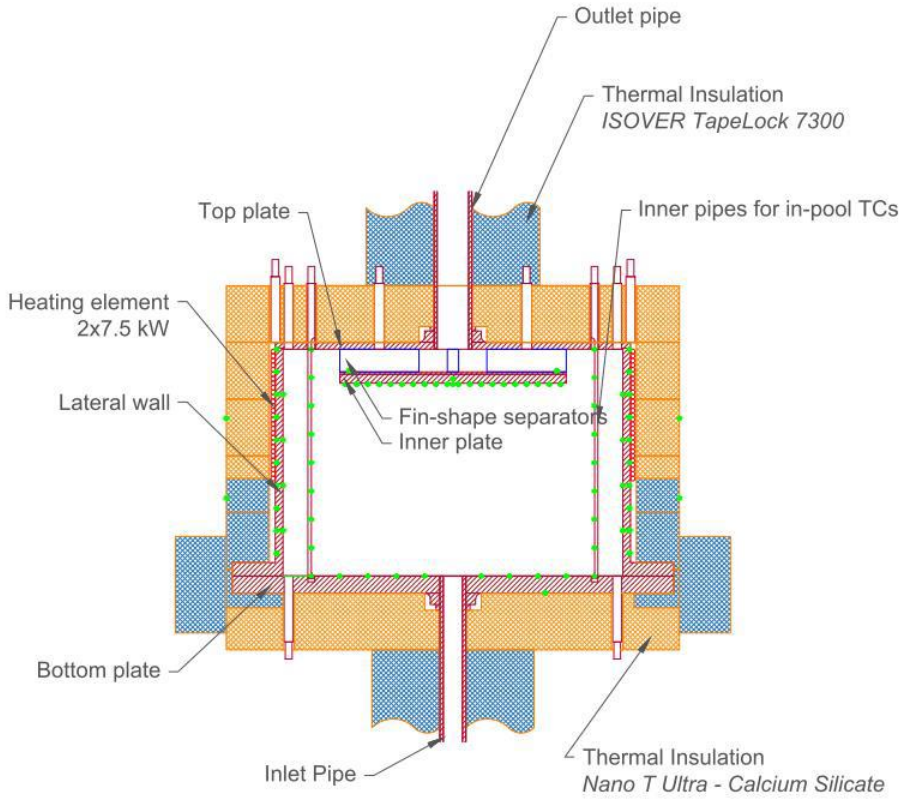

Figure 41 TALL-3D test section: components

3.2 Geometry

The CFD software used in this study is STAR-CCM+. Using its in-built 3D modeller, the geometry of the test section was constructed as it's shown in Figure 42. Some features of the actual test section were simplified in order to reduce the number of nodes: the inner pipes with thermocouples have a hexagonal base instead of circular to better fit the mesh, the grooves containing the thermocouples in the inner plate are not modelled, the fins holding the inner plate are not modelled, the bolts holding the upper and lower plates which constitutes the vessel are not modelled, the metal structure holding everything in place is not modelled. Although the test section has a square symmetry (almost cylindrical except for the four inner pipes), the geometry was not simplified to half or a quarter for reasons explained in the next sections. The length of the inlet and outlet pipes correspond to the location of the inlet and outlet thermocouples on the middle leg of the loop.

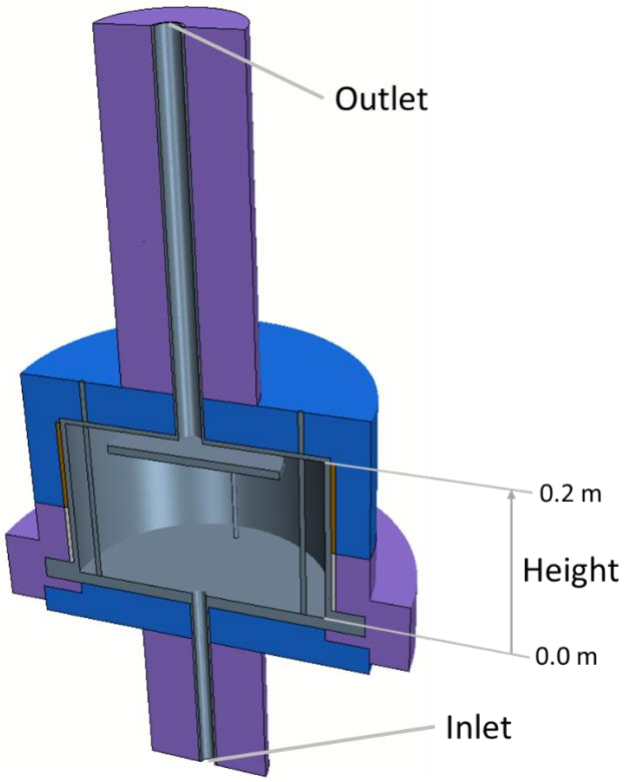

Figure 42 Cross section of the geometry used for CFD calculations

3.3 Physics models

The following physics models were selected in STAR-CCM+:

- Three dimensional flow
- Multiphase; Volume of fluid (VOF), Multiphase equation of state, multiphase interaction
- Segregated flow solver.
- Turbulent; Reynolds-Averaged-Navier-Stokes, K-Epsilon turbulence, Realizable K-Epsilon two-layer; Two-layer all y+ wall treatment
- Segregated multiphase temperature
- Gravity

It should be noted that in practice, all the simulations are single phase (LBE). However, the multiphase VOF model was selected because it will later be used to model the free surface

of SEALER. It is simply to ensure that the software configuration is stable. It does not, in any way, verify the proper modelling of a free surface. Indeed, there is no free surface in the TALL-3D simulations, the helium phase is always zero.

3.4 Material properties

The material properties of LBE were taken from the OECD's Handbook on LBE and lead (OECD, 2015). The material properties of the solid parts are taken from reports produced during the SESAME project (Moreau et al., 2019a). The vessel, inner pipes, inner plate and heater are all modelled with the same stainless steel properties. It should be noted that the thermal conductivity of some parts of the insulator were calibrated to achieve thermal balance. Namely, it was assumed that the departure from the reference values is due to the presence of the effect of thermal bridges created by the metal structures that hold the vessel and the thermocouples' cables. Therefore, the value of the thermal conductivity actually used is a weighted average between the pure insulator and stainless steel. The two insulator parts affected by this correction are the calcium silicate on the top plate and the mineral glass around the outlet pipe (see Figure 41). The weight of steel conductivity in the average is respectively 0.7% and 0.5%. All the simulations use the same correction.

3.5 Mesh

The mesh is composed of polyhedral cells. In the fluid area, the average cell diameter is about 2.5 mm (volume averaged). In the solid parts, it is about 8mm. The total number of cells is 3.3 M, where 1.9 M are in the fluid area. Figure 43 shows the mesh in a cross section.

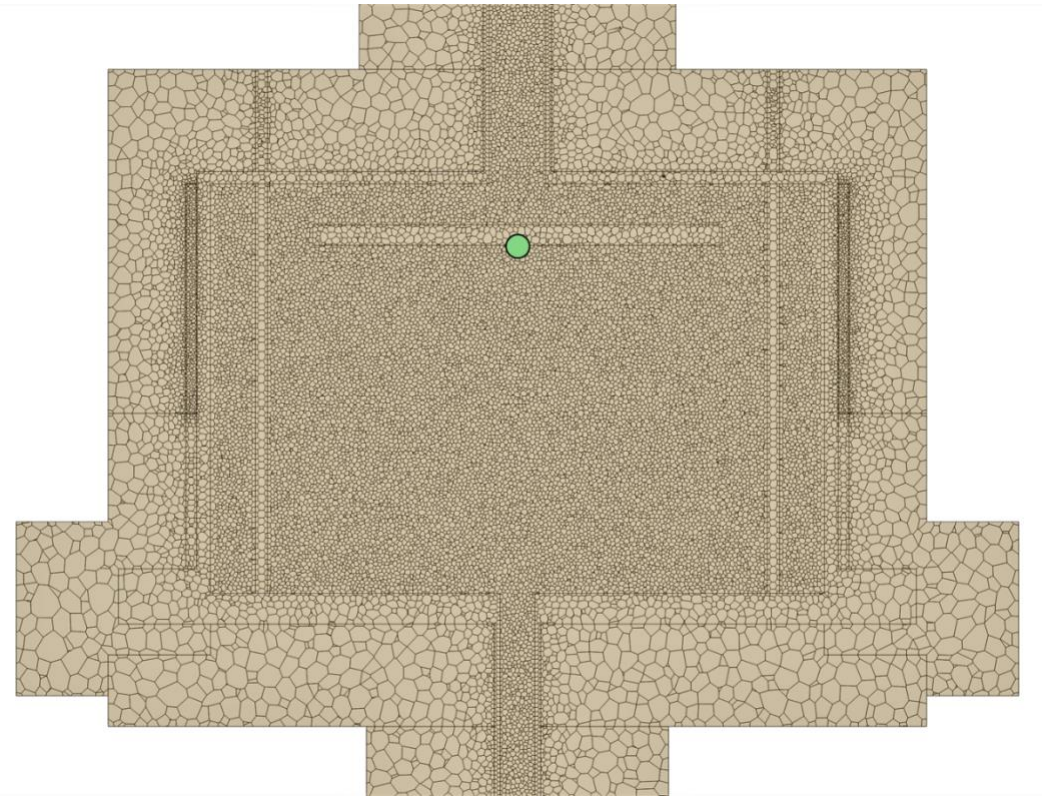

Figure 43 Mesh of the 3D test section

Two areas inside the vessel require a fine mesh: all the walls and the area where the jet is present. For simplicity, it was decided to have a fine mesh in the entire fluid region instead of using boundary offset layers on the walls and jet. The size of the mesh was determined through a mesh sensitivity study. Six different mesh sizes were tested using the conditions of the test TG03.S301.01 at forced flow (see next section for details). The quantity of interest is the average temperature on a small disc located on the lower surface of the inner plate, in the center, see the green dot on Figure 43. Under the selected conditions, the cool jet coming from the inlet pipe is very sensitive to the mesh size. See Figure 49 for an illustration of the jet. If the mesh is too coarse, numerical diffusion causes the temperature on the inner plate (quantity of interest) to be higher. The results of the mesh sensitivity are presented on Figure 44.

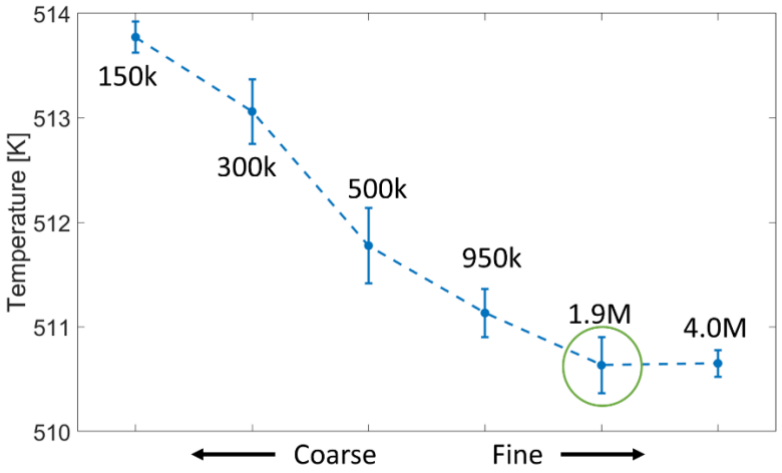

Figure 44 Mesh sensitivity analysis. The number of cells in the fluid domain is specified next to each point.

Since the "Two layer all y+ wall treatment" model is selected, there is no target y+ value. On the lower face of the inner plate (receiving the jet), y+ values vary between 50 and 200. On the vessel wall, it is between 5 and 60.

3.6 Steady-state calculations

The initial and final conditions of two TALL-3D tests were used in the steady-state calculations. In both tests, the initial conditions are forced flow, then the transient is initiated by tripping the pump, and finally the flow stabilizes into natural circulation. Table 4 lists the conditions of the four steady-states.

Table 4 List of the four steady state configurations

Test name	Flow regime	Mass flow [kg/s]	Heater power [kW]	Temperature at inlet [K]	Temperature increase [K]
TG03.S301.01	Forced	1.80	5.60	503	19
	Natural	0.33	5.58	452	104
TG03.S301.04	Forced	1.31	4.05	507	19
	Natural	0.27	4.03	473	94

The boundary conditions at the inlet are set according to the mass flow and inlet temperature measurements listed in Table 4. At the outer walls of the insulators, the boundary condition is a constant temperature of 300K. The insulator and pipe surfaces that are on the same plane as the inlet and outlet have adiabatic boundary conditions.

3.6.1 Natural circulation

Figure 45 shows the temperature profile on the inner pipes placed inside the vessel for the two natural circulation cases. For both the experimental and numerical results, the curve represents the average of the four inner pipes taken over a range of time/steps. Note that there are no significant differences between the TC measurements at the same elevations. The circular markers of the experimental data are the nine thermocouples placed on each pipe. The location of inlet, outlet and height are visually explained in Figure 42. Since the flow rate is low, thermal stratification develops inside the vessel, which is very well reproduced by the CFD calculations. Figure 46 shows the CFD results for the temperature and velocity on a cross-section of the vessel.

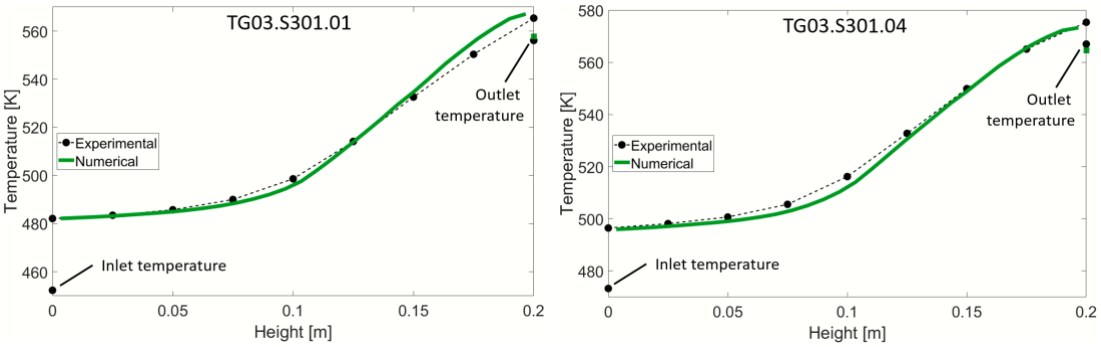

Figure 45 Natural circulation, steady-state, vertical temperature profile inside the test section

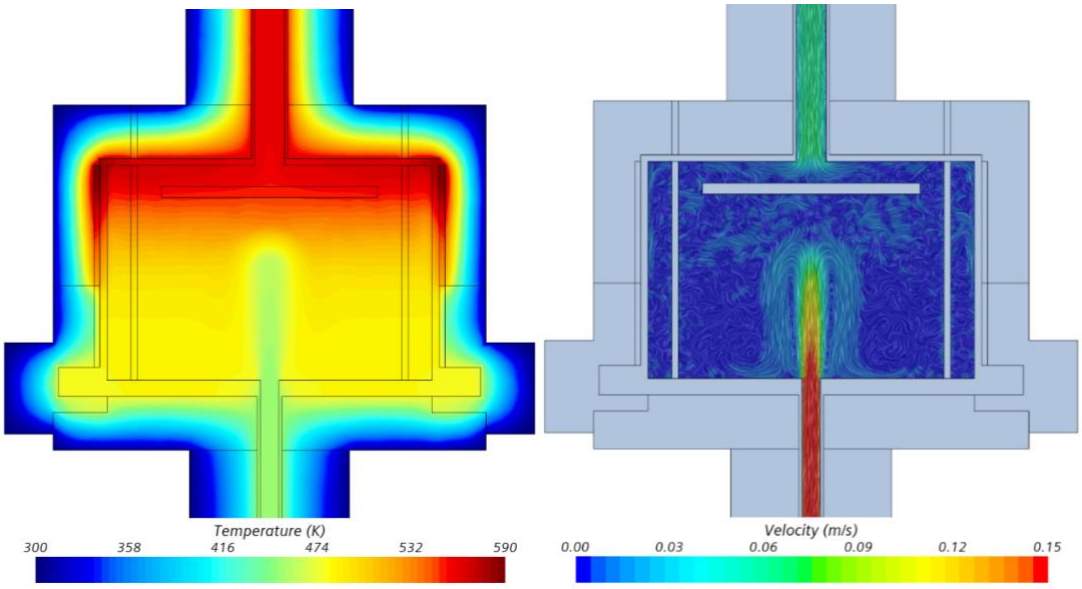

Figure 46 Natural circulation, steady-state; temperature and velocity distribution on a cross section of the test section, test TG03.S301.01

3.6.2 Discussion on the reference density

As was explained above, even if the vessel contains only LBE, the case was set up as multiphase since the target application requires that to model the free surface. For

multiphase cases, STAR-CCM+ recommends to use a reference density that is equal to the lowest density of all the phases, or simply zero. However, since LBE is very heavy, that approach does not produce the appropriate buoyancy forces, which results in an incorrect thermal stratification as can be seen in Figure 47. This problem, which is not specific to STAR-CCM+, has also been identified in other studies (Gallego-Marcos et al., 2019). For all the other calculations presented in this study, the reference density is that of LBE.

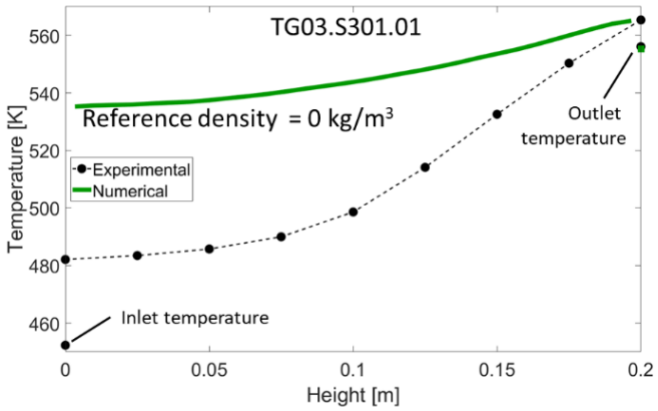

Figure 47 The reference density of 0 kg/m^3 does not yield the right thermal stratification. The density of LBE should be used as reference

3.6.3 Forced circulation

The results from the forced steady-state calculations are shown in Figure 48. Again, the computational domain is visually explained in Figure 42. In addition to the vertical temperature profile measured by the inner pipes, the horizontal profile measured by the inner plate is also presented. Experimentally, that is measured by TCs placed in a cross shape in grooves on the lower side of the plate (see Figure 41). Assuming cylindrical symmetry, the temperature profile of the four legs of the cross shape are averaged, resulting in one axis that goes from the center of the plate to the edge. Numerically, the whole area of the bottom surface of the plate is divided into many rings of different radii. One average temperature is computed for each ring.

In the case of forced circulation, there is mixing instead of thermal stratification, which is also well captured by CFD. Also, there is more variability in the temperature measurements. The band around the experimental and numerical curves represents two standard deviations ($\mu \pm 2\sigma$). The sample for the experimental data is about 500 seconds of data acquisition before the start of the transient. For the numerical data, it's 2000 steps (steady state mode). For both cases, the average of the four inner pipes was used. Figure 49 and Figure 50 shows the CFD temperature and velocity on the cross section of the vessel, also averaged over 2000 steps. By analysing the flow pattern, one can understand the shape of the temperature profile on the inner pipes. The part of the pipe that is next to the inner plate receives the flow coming from the inlet, and so that part is slightly cooler. That flow picks up the heat from the heater and is split into up and down directions, and that's why the bottom and top of the rods are hotter.

The temperature profile of the inner plate is also coherent with that flow pattern. The temperature is lowest in the center, which receives the cold jet coming from the inlet. As the flow travels from the center to the edges, its temperature increases gradually. Thus, even if the velocity field is not measured experimentally, it can be deduced from the temperature profile. The numerical results are able to reproduce the right temperature profile, even if there is an offset of up to 5 K. In the case of the inner plate, the offset is explained by the fact that the TCs in the experimental setup are placed slightly inside the plate, whereas the numerical results are taken from the surface. Since the other side (top side) is warmer, the temperature inside the plate should be higher than the bottom surface.

We conclude that CFD can reproduce the flow pattern correctly. Also, the CFD outlet temperature is very close the experimental one, in both tests.

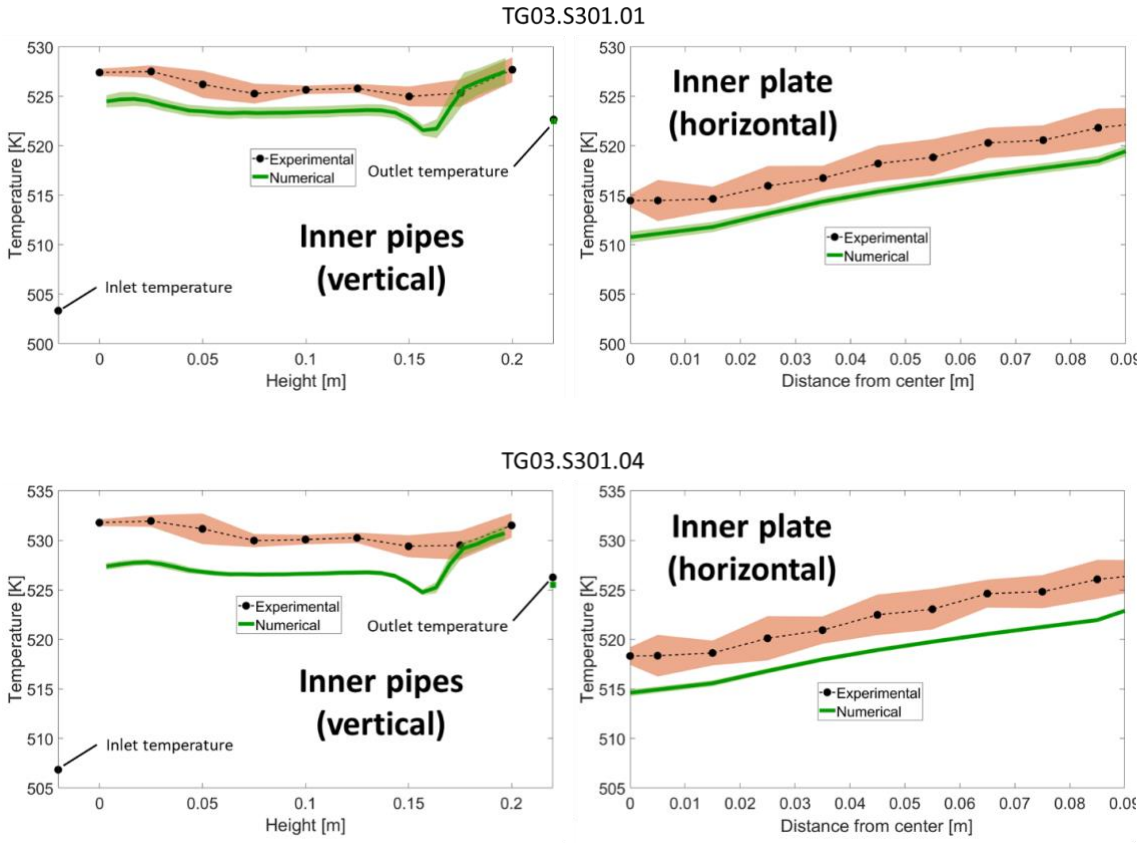

Figure 48 Forced circulation, steady-state: vertical and horizontal temperature profile inside the test section

On Figure 50, the horizontal cross sections have been included to check the presence of vortexes. When building the CFD geometry, one of the simplifications that was made included removing the fins placed between the inner plate and the top of the vessel. The function of those fins, aside from holding the inner plate, is also to avoid the formation of a vortex. Figure 50 confirms that there is no vortex that spans the entire cross section, only small local ones.

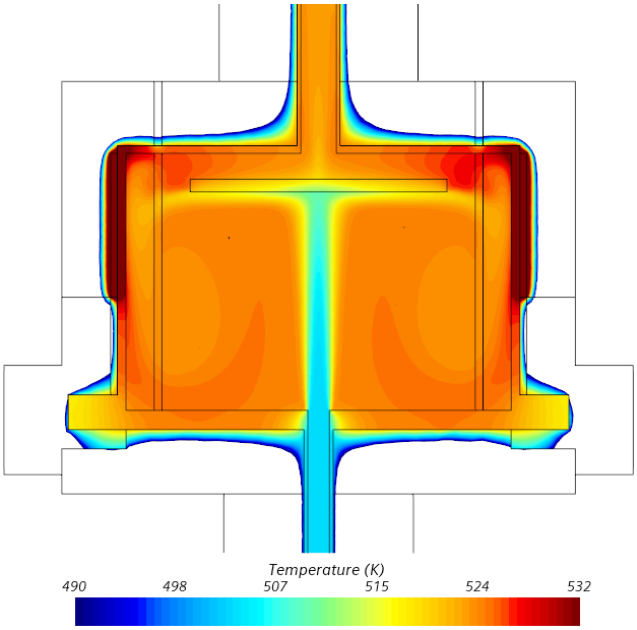

Figure 49 Forced circulation, steady-state: averaged temperature distribution a on vertical cross section, test TG03.S301.01

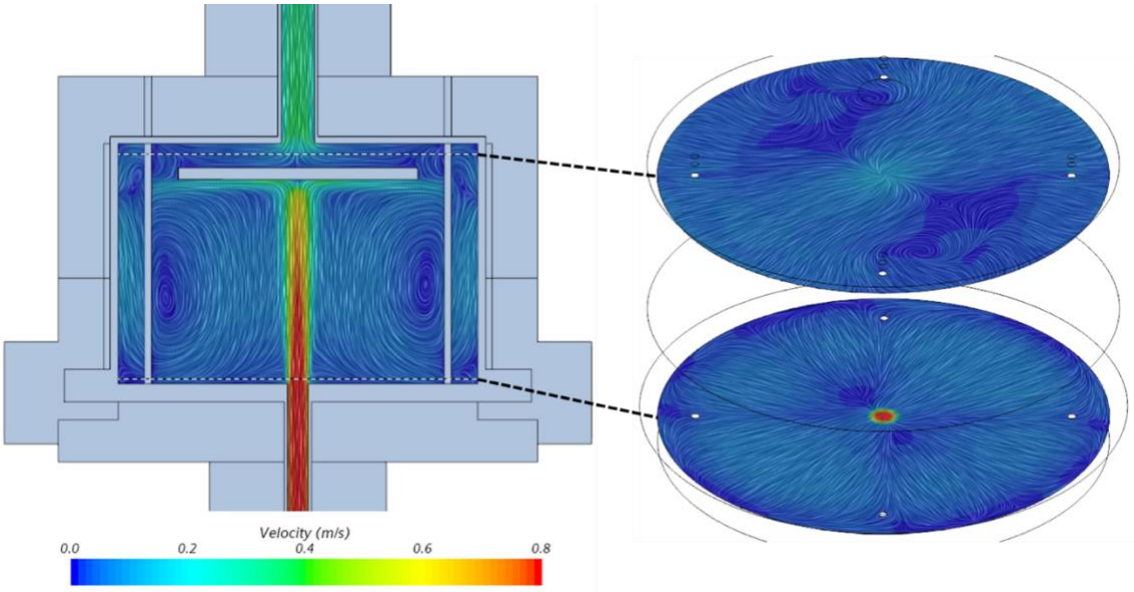

Figure 50 Forced circulation, steady-state: averaged velocity profiles on three cross sections, one vertical (left) and two horizontal (right), test TG03.S301.01

3.6.4 Discussion on the usage of a symmetry plane

Since the geometry has a perfect square symmetry (almost circular except for the four inner pipes), it would be computationally beneficial to model only a quarter or half of the vessel and use symmetry boundary conditions. Unfortunately, that approach was tested and it did not yield the expected results. Figure 51 shows the flow pattern on two planes of a CFD calculation where half of the geometry was modelled. The face on the left is the actual boundary of the geometry, where the symmetry condition is applied. The face on the right is a cross section of the geometry, i.e. inside the geometry. The flow pattern on those two faces is significantly different, which is not physically possible since the vessel has a square geometry. When modelling a reactor, such deviation from symmetry behavior might or might not occur, since the geometry is different. In any case it should be tested on a steady-state forced circulation before getting involved in long transient calculations.

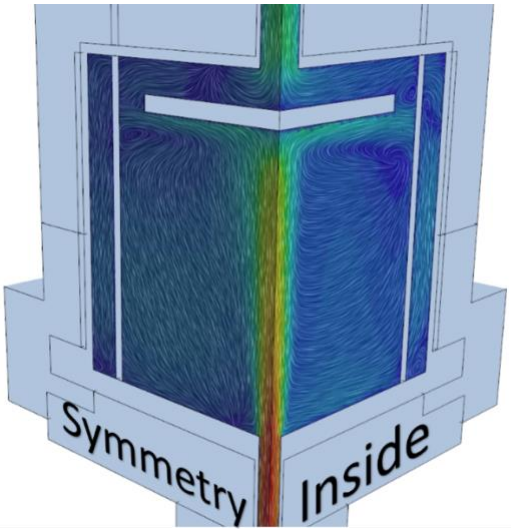

Figure 51 Modelling half of the test section with symmetry boundary conditions does not produce the right flow distribution

3.7 Transients

In order to test the capabilities of the CFD software to predict a transient we use TALL-3D test TG03.S301.01. The physics models are the same as previously described except that Implicit Unsteady was used instead of Steady study. The initial conditions are the forced circulation steady state for the corresponding test. The heater is maintained at a power of 5596 W throughout the transient. The inlet conditions (temperature and mass flow) vary over time and are set from the experimental data as shown in Figure 52 (temperature) and Figure 53 (mass flow). It should be noted that between around 90 and 160 seconds into the transient, the mass flow becomes negative. During that period, the inlet and outlet are inverted in the CFD software. The temperature boundary condition at the new inlet (top of the vessel) are calculated by shifting the experimental data so that there is no discontinuity when the flow becomes negative, see the dotted line on Figure 52.

The quantities of interest are the temperatures at the outlet and at the center of the inner plate, Figure 52 shows both of them compared against experimental data. We can see that there is generally a good agreement between the numerical and experimental curves. Between 700s and 800s, the numerical and experimental temperatures on the inner plate differ considerably. It should be noted that during that time, the experimental data fluctuates a lot which indicates that the flow is very unstable. Also, the numerical curve does exhibit the dip that is present in the experimental one, only less pronounced. The deviation from experimental data is similar to other CFD studies (Grishchenko et al., 2020), (Papukchiev et al., 2020)

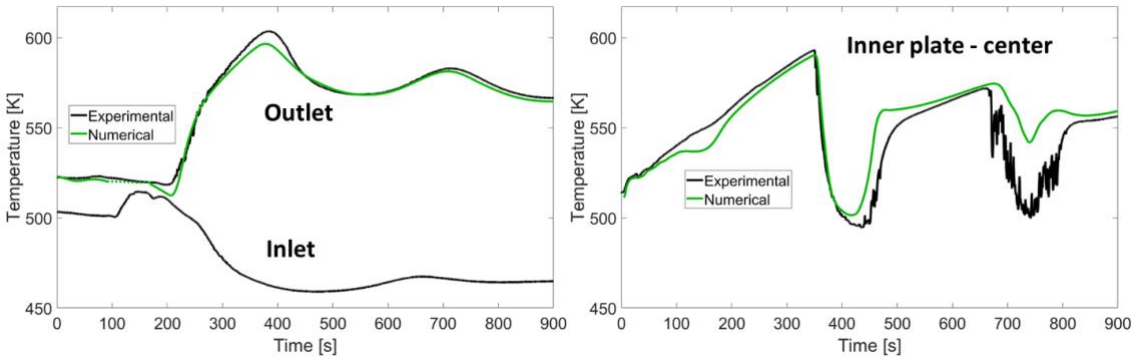

Figure 52 Transient results, comparison of numerical vs. experimental for outlet temperature and center of inner plate. Inlet temperature is a boundary condition.

The time step was adjusted along the transient to ensure that it's as large as possible but at the same time maintains the courant number below one. In the first 200s, the time step varied between 3ms and 50ms, from 200s till the end, it was maintained at 10ms. This was necessary because the velocity fluctuates a lot, specially at the beginning, and using a small time step for the entire transient would take too much computational time. To ensure that the time step is never too high, the maximum courant number was calculated at different times during the transient. That maximum excludes the 1% of the volume with the highest courant number to avoid outliers coming from cells that are abnormally small. The results are shown on Figure 53 and as it can be seen, the courant number is always below 1.

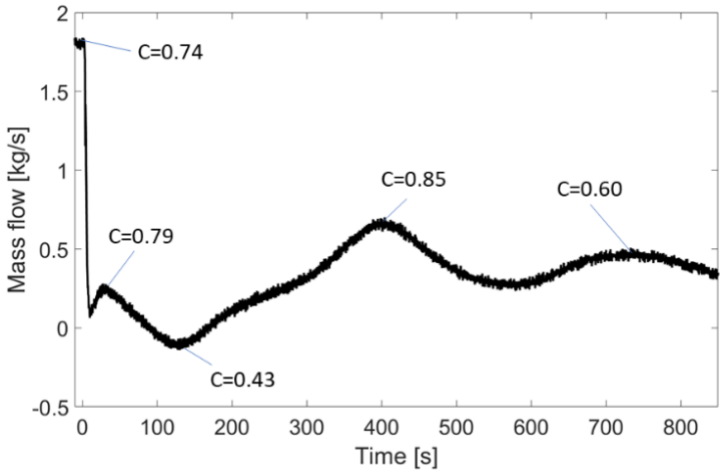

Figure 53 Mass flow during the transient (boundary condition) and courant number at different times

3.8 Lessons learned

There are a few takeaways from this exercise where CFD simulations are compared against a flow of heavy metal. First, the selected models and parameters are very well suited to model the desired coolant. Second, the reference density needs to be close or equal to the one of the heavy metal otherwise buoyancy effects are not well captured. Last, when reducing the geometry to half or a quarter with symmetry planes, it is important to ensure that the flow patterns on the symmetry planes are not altered by this simplification.

6. Conclusion

This work presented the different components of a CFD based model for simulating transients in a pool-type small lead cooled reactor. The fuel channels, the pumps and the steam generators use a simplified geometry with heat and/or momentum sources (or sinks). The fuel channels are coupled with a finite volume model for fuel pin temperature and a point kinetics model for neutronics. That is done through an iterative algorithm so that a converged solution is reached at every time step. The momentum source of the pump is calculated from its characteristic curve and is coupled with the kinetic energy of a flywheel to model loss of flow transients. This is more accurate than simply assuming an exponential decay of the rotor speed or pump head.

Finally, CFD simulations were successfully compared against experimental data from the TALL-3D facility. The purpose of this exercise is to ensure that the models and parameters used in the CFD software (STAR-CCM+) are capable of predicting a flow of heavy metal in general.

Results from an integrated model where transients of the entire reactor are simulated will be the work of a future publication. In addition, a validation exercise with an appropriate facility, like CIRCE (Zwijsen et al., 2019), will also be presented in a future publication.

7. Acknowledgments

Funding: This work was supported by NSREC-UNENE (Natural Sciences and Engineering Research Council of Canada, and University Network of Excellence in Nuclear Engineering) [grant number IRCPJ309310-14].

8. References

Bortot, S., Suvdantsetseg, E., Wallenius, J., 2015. BELLA: a multi-point dynamics code for safety-informed design of fast reactors. Annals of Nuclear Energy 85, 228–235. https://doi.org/10.1016/j.anucene.2015.05.017

Bubelis, E., Schikorr, M., 2008. Review and proposal for best fit of wire-wrapped fuel bundle friction factor and pressure drop predictions using various existing correlations. Nuclear Engineering and Design 238, 3299–3320. https://doi.org/10.1016/j.nucengdes.2008.06.024

Carbajo, J.J., Yoder, G.L., Popov, S.G., Ivanov, V.K., 2001. A review of the thermophysical properties of MOX and UO2 fuels. Journal of Nuclear Materials 299, 181–198. https://doi.org/10.1016/S0022-3115(01)00692-4

Chen, S.K., Chen, Y.M., Todreas, N.E., 2018. The upgraded Cheng and Todreas correlation for pressure drop in hexagonal wire-wrapped rod bundles. Nuclear Engineering and Design 335, 356–373. https://doi.org/10.1016/j.nucengdes.2018.05.010

Fiorina, C., Clifford, I., Aufiero, M., Mikityuk, K., 2015. GeN-Foam: a novel OpenFOAM ® based multi-physics solver for 2D/3D transient analysis of nuclear reactors. Nuclear Engineering and Design 294, 24–37. https://doi.org/10.1016/j.nucengdes.2015.05.035

Gallego-Marcos, I., Kudinov, P., Villanueva, W., Kapulla, R., Paranjape, S., Paladino, D., Laine, J., Puustinen, M., Räsänen, A., Pyy, L., Kotro, E., 2019. Pool stratification and mixing induced by steam injection through spargers: CFD modelling of the PPOOLEX and PANDA experiments. Nuclear Engineering and Design 347, 67–85. https://doi.org/10.1016/j.nucengdes.2019.03.011

Grishchenko, D., Jeltsov, M., Kööp, K., Karbojian, A., Villanueva, W., Kudinov, P., 2015. The TALL-3D facility design and commissioning tests for validation of coupled STH and CFD codes. Nuclear Engineering and Design 290, 144–153. https://doi.org/10.1016/j.nucengdes.2014.11.045

Grishchenko, D., Papukchiev, A., Liu, C., Geffray, C., Polidori, M., Kööp, K., Jeltsov, M., Kudinov, P., 2020. TALL-3D open and blind benchmark on natural circulation instability. Nuclear Engineering and Design 358, 110386. https://doi.org/10.1016/j.nucengdes.2019.110386

Handbook on Lead-bismuth Eutectic Alloy and Lead Properties, Materials Compatibility, Thermal-hydraulics and Technologies, 2015. 950.

Jeltsov, M., Grishchenko, D., Kudinov, P., 2019. Validation of Star-CCM+ for liquid metal thermal-hydraulics using TALL-3D experiment. Nuclear Engineering and Design 341, 306–325. https://doi.org/10.1016/j.nucengdes.2018.11.015

Kao, S.-P., 1984. A Multiple-Loop Primary System Model for Pressurized Water Reactor Plant Sensor Validation. MIT.

Kudinov, P., Grishchenko, D., Jeltsov, M., Koop, K., 2017. D3.1 - TALL-3D Test Setup (No. D3.1), SESAME.

Leibowitz, L., Blomquist, R.A., 1988. Thermal conductivity and thermal expansion of stainless steels D9 and HT9. International Journal of Thermophysics 9, 873–883. https://doi.org/10.1007/BF00503252

Martinez, P., Galpin, J., 2014. CFD modeling of the EPR primary circuit. Nuclear Engineering and Design 278, 529–541. https://doi.org/10.1016/j.nucengdes.2014.08.013

Moreau, V., Profir, M., Grishchenko, D., Jeltsov, M., 2019a. D3.5 - TALL-3D: CFD models and validation (No. D3.5), SESAME.

Moreau, V., Profir, M., Keijers, S., Van Tichelen, K., 2019b. An improved CFD model for a MYRRHA based primary coolant loop. Nuclear Engineering and Design 353, 110221. https://doi.org/10.1016/j.nucengdes.2019.110221

Pacio, J., Daubner, M., Wetzel, T., Di Piazza, I., Tarantino, M., Martelli, D., Angelucci, M., 2018. Experimental Nusselt Number in Rod Bundles Cooled by Heavy-Liquid Metals, in: Volume 6B: Thermal-Hydraulics and Safety Analyses. Presented at the 2018 26th International Conference on Nuclear Engineering, American Society of Mechanical Engineers, London, England. https://doi.org/10.1115/ICONE26-82213

Papukchiev, A., Grishchenko, D., Kudinov, P., 2020. On the need for conjugate heat transfer modeling in transient CFD simulations. Nuclear Engineering and Design 367, 110796. https://doi.org/10.1016/j.nucengdes.2020.110796

Roelofs, F., Zwijsen, K., Uitslag-Doolaard, H., Alcaro, F., Stempniewicz, M., Wallenius, J., 2019. Validation of Thermal Hydraulic Design Support and Safety Methodology and Application to SEALER. Presented at the IAEA BENEFITS AND CHALLENGES OF SMALL MODULAR FAST REACTORS, INTL ATOMIC ENERGY AGENCY, Milan, Italy.

Russia starts building lead-cooled fast reactor, 2021. . World Nuclear News.

Todreas, N.E., Kazimi, M.S., 1990. Nuclear systems II. Hemisphere Pub. Corp, New York.

Wallenius, J, Bortot, S., Mickus, I., 2018. Unprotected transients in SEALER: A small lead-cooled reactor for 12.

Wallenius, J., Qvist, S., Mickus, I., Bortot, S., Szakalos, P., Ejenstam, J., 2018. Design of SEALER, a very small lead-cooled reactor for commercial power production in off-grid applications. Nuclear Engineering and Design 338, 23–33. https://doi.org/10.1016/j.nucengdes.2018.07.031

Zwijsen, K., Dovizio, D., Moreau, V., Roelofs, F., 2019. CFD modelling of the CIRCE facility. Nuclear Engineering and Design 353, 110277. https://doi.org/10.1016/j.nucengdes.2019.110277

Zwijsen, K., Uitslag-Doolaard, H., Roelofs, F., Wallenius, J., 2020. Thermal-Hydraulic Design Support and Safety Analyses of SEALER UK Demo 10.

Chapter 6 - Article III

6.1 Publication Details

C. Reale Hernandez, J. Wallenius, J. Luxat, "Simulation of a Loss of Flow Transient of a Small Lead-Cooled Reactor Using a CFD-Based Model". Article was submitted to Nuclear Engineering and Design on Oct 26th 2022, decision pending.

The entire work presented in this article was done by the author. This includes the conceptual design, all the Matlab scripts, the STAR-CCM+ simulations, the writing and the production of the figures. The geometry for the CFD simulations was produced inside STAR-CCM+ itself and used as reference the figures and dimensions of SEALER. Dr. Luxat provided some general guidance.

All the simulations were performed on the SHAKA cluster located in NRB (Nuclear Reactor Building, McMaster). PhD student Christopher Hollingshead helped me set up the connection to the cluster. He was also in charge of fixing the server when there was an issue.

6.2 Preface

This third and last article is the second article on the new CFD-based model. The first one (second of the thesis) presented the details of the methods used in the model and a validation work to support its viability. This article presents only a summary of the modelling methods and focuses on the simulation results. The mass flow fluctuation issue that was initially identified with the lumped-parameter model is also present in the simulations with the CFD-based model. However, the shape is different and the overall mass flow evolution is slower, meaning that it takes more time to reach natural circulation. This is the result of coupling the pump with a flywheel in the CFD-based model compared to a simple exponential pump coastdown in the lumped-parameter model. Temperature variations during the transient also tend to be less pronounced with the CFD-based model and always remain far from safety concerns. Most importantly, simulations were performed with

different flywheel sizes and it was found that the mass flow disturbance can be completely eliminated with a very reasonable size. Temperature variations with such a flywheel are also smoother.

6.3 Article

The following pages contain the original article.

Simulation of a Loss of Flow Transient of a Small Lead-Cooled Reactor Using a CFD-Based Model

Cuauhtemoc Reale Hernandez[a*], Janne Wallenius[b], John Luxat[a]

[a] McMaster University, Hamilton, Canada

[b] KTH Royal Institute of Technology, Stockholm, Sweden

Abstract

The recent development of small modular reactors needs to be followed by safety analysis using the newest available tools. This work focuses on one type of reactor, SEALER, which is a small lead cooled reactor intended for remote communities in Canada. Simulations of a loss of flow transients are performed using a CFD-based model that was specifically developed for this project. The CFD geometry includes the entire primary circuit with some simplifications. The fuel channel, steam generator and pumps use a simple geometry with momentum and heat source/sink. Free surface level is modelled with the multiphase volume of fluid (VOF) method. The CFD part of the model is coupled to a custom code for heat transfer in the fuel rods and point kinetics for neutronics. Transient results show that core temperatures do not increase significantly and stay well below safety limits. The CFD-based model presented here is compared against a lumped-parameter model using the same transient. It is shown that the evolution of the mass flow and temperature is significantly different and more accurate with the CFD-based model. Finally, the influence of the moment of inertia of the pump flywheel on the transient is explored.

Keywords: heavy-metal reactors, SMR, CFD, transients, loss of flow

Abbreviations:

CFD: computational fluid dynamics

SMR: small modular reactor

VOF: volume of fluid model

ULOF: unprotected loss of flow

SEALER: Swedish advanced lead reactor

QOI: quantity of interest

*** Corresponding author**

email: realehec@mcmaster.ca

address: 1280 Main St W, Hamilton, Canada

1. Introduction

In the recent years, the development of small modular reactors (SMRs) has been picking up speed and governments are beginning to consider them as a serious option. There is a wide variety of designs from different companies, ranging from 1 to 300 MWe, for different applications and using different technologies, like water cooled, metal cooled, molten salt, gas cooled, etc. In this context, it is important to assess the safety of these new types of reactors using the newest available tools. This study focuses on a small lead cooled reactor and presents loss of flow transients calculated with a CFD-based model.

The reference reactor used in this study is the SEALER-arctic reactor (Wallenius et al., 2018). It is a 3 to 10 MWe fast spectrum reactor that employs lead as the coolant. Having a lifetime of 10 to 30 years without refueling, it is intended for remote communities in the north of Canada or for mines. The fuel is uranium oxide enriched to about 20%. A cross-section of the reactor is shown on Figure 54.

To perform the simulations, a CFD-based model that was specifically developed for this project is used. The entire primary circuit is modelled with CFD using several simplifications. Fuel channels, steam generators and pumps are replaced by a simple geometry with appropriate momentum and heat source/sink. This method is very similar to a porous media approach, which has been used in other studies (Fiorina et al., 2015; Moreau et al., 2019; Roelofs et al., 2019). Fuel temperature and neutronics are solved in a separate custom-made code and are coupled to the CFD calculations. The volume of fluid (VOF) method is used in CFD to model the free surfaces. Extensive details and background work on this model have been published elsewhere (Reale Hernandez et al., 2022).

The transient that is investigated in this work is an unprotected loss of flow (ULOF). Previously, a lumped-parameter model was developed to calculate transients in reactors like SEALER (Bortot et al., 2015). Results from that work showed that during the first seconds of a ULOF transient, the mass flow at the pumps undergo a fluctuation that is not desirable (Hernandez, 2020). The authors of this work then used that lumped-parameter

model to perform a sensitivity analysis and found that negative flow at the pump can occur by modifying some parameters in a realistic manner. Among other reasons, this prompted the development of a more accurate model based on CFD.

The article first presents the geometry of the reactor and a summary of the modelling methods. Then, some details about setting up the simulation are provided, namely the mesh and the search for steady state. The main and final sections present the transient results, a comparison with the lumped-parameter model and the effect of the pump flywheel.

2. Geometry

Figure 54 shows the cross-section of the SEALER-arctic reactor and the different components. The reactor is divided in two concentric regions. The reactor core is placed in the inner one, at the bottom, has a hexagonal geometry and is composed of 19 fuel assemblies, surrounded by control and shut-down assemblies, themselves surrounded by reflector assemblies, and themselves surrounded by shield assemblies. The coolant flows through the reactor core upwards into the hot leg. Eight pumps move the coolant from the hot leg to the outer region (cold leg) which contains the steam generators. Then, the coolant moves downwards in the outer region until it enters the cold pool which is placed at the very bottom of the inner region, from where it moves back into the reactor core.

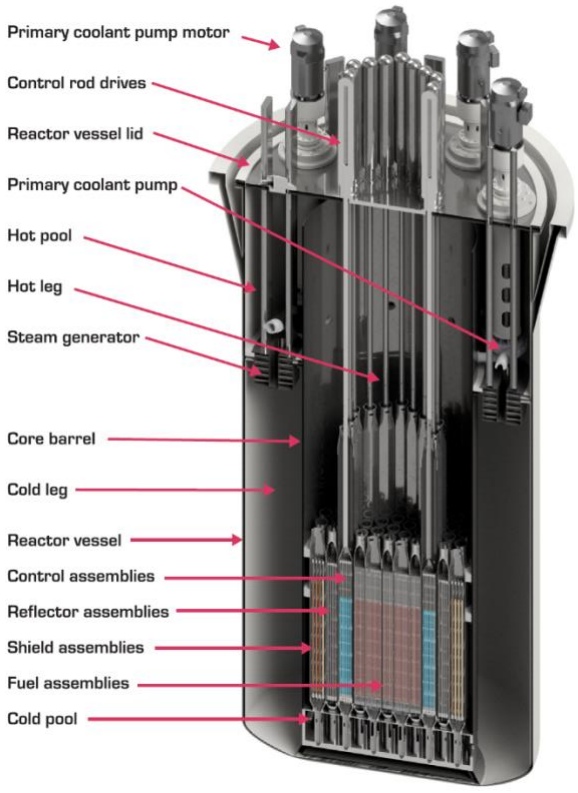

Figure 54 Cross-section of the SEALER-arctic reactor

For building the CFD model, many components had to be simplified. Figure 55 shows the solid parts of the geometry used in the CFD model. Note that the actual domain used in the

simulations corresponds to the negative space of that figure. The solid parts are not modelled in this version of the model, only the fluid. Also, the simulations were carried out using one quarter of the reactor, see Figure 56 in the mesh section for an exact representation of the CFD domain.

The pumps were replaced by elbow pipes in which a momentum source is applied. The solid components of the steam generators were removed completely, instead the area where they are located contains a heat and momentum sink. The structure and tubes above the pumps and steam generators were removed. All the control, shut-down, reflector and shield assemblies were replaced by solid. Although coolant does flow through them, the mass flow is so slow that it can be approximated to being stagnant. The guides and holding rods of the control and shut-down assemblies are present.

Every assembly sits on a cylindrical foot that contains different levels of orificing to adjust the velocity required in each assembly. In the CFD model, the foots were approximated to hexagonal prisms instead of cylinders to better fit the mesh. The foots of the control, shut-down, reflector and shield assemblies are full solid since we assume stagnant flow in those assemblies. For the fuel assemblies, it is not possible to model the actual orifices since that would require a very fine mesh and optimizing the size to obtain the right velocities would be very time consuming. Instead, the foot is a hexagonal prism that doesn't extend all the way to the bottom and whose side walls have no thickness but are impermeable. The coolant must enter from below the foot and cross its length before entering the assembly. Using a momentum sink in the foot area allows the velocities to be well adjusted. See Figure 59 in the mesh section for an illustration.

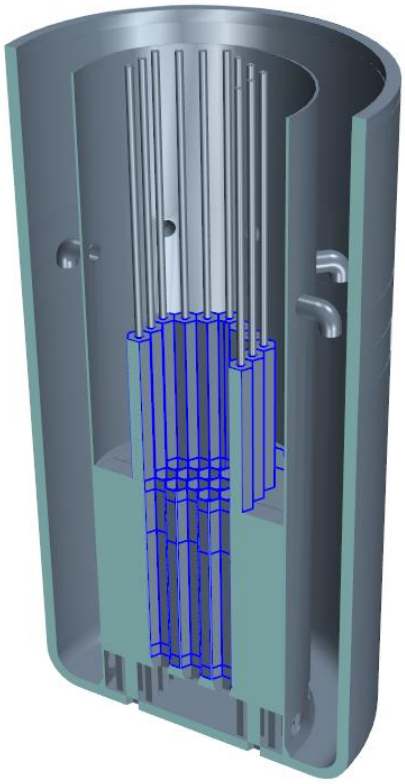

Figure 55 Geometry used for the CFD model

For the fuel channels, using CFD to model the 91 fuel pins per assembly would not be possible since it would require a really fine mesh and incredible amounts of computing power to obtain the right heat transfer and friction between the coolant and the fuel pins. Therefore, the fuel channels consist in a relatively simple prism which have the geometry shown on Figure 56. Note that the coolant flows through the yellow area, the hollow parts correspond to the volume occupied by the fuel pins. Maintaining the same flow cross sectional area is necessary for the implementation of pressure drop and heat transfer correlations. The other criteria for the selection of this geometry was to be simple and to have coolant flowing in and out more or less uniformly around the cross section (not only in the middle or edges).

Using a porous medium was considered for this model. In STAR-CCM+ (the CFD software used in this study), there are two ways of modelling porosity: using a Porous Region, or the

Porous Media Model. Only the latter would result in the right coolant velocity which is necessary for heat transfer and friction correlations. Indeed, the software manual states that Porous Media Model should be used for heat exchanger applications. However, that model is not compatible with multiphase volume of fluid (VOF), which is necessary for modelling the free surface at the top of the reactor. Therefore, a porous medium could not be used.

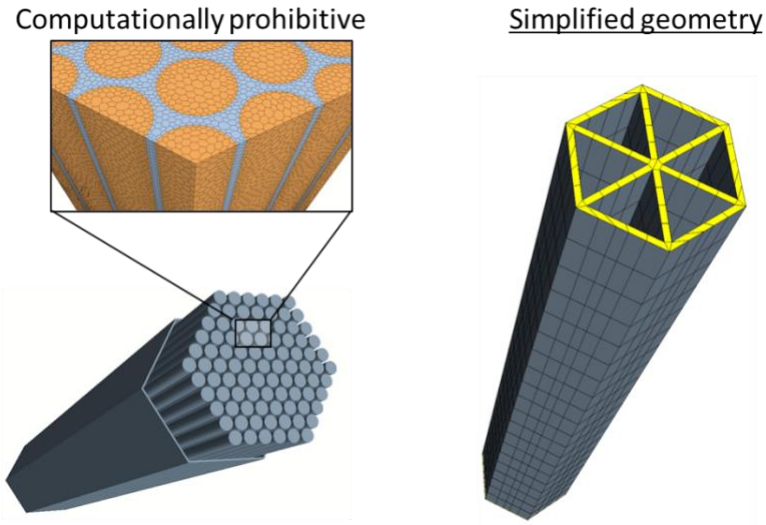

Figure 56 Geometry used for the fuel channels

3. Physics solvers

This section presents a short description of the modelling methodology. A detailed description has been previously published by the authors of this work (Reale Hernandez et al., 2022). The physics of the model are separated in three parts:

- Thermal-hydraulics of the entire primary circuit (except the fuel), solved with CFD
- Fuel pin temperature, solved with a finite volume method for solid heat transfer
- Neutronics, solved with point kinetics

Thermal-hydraulics (CFD) is itself divided into a few parts. Although the entire circuit is part of the same CFD simulation, the components with a complex geometry are simplified and each has a specific heat and momentum source (or sink). This is due to the impossibility for CFD to capture every detail because of computing limitations. The schematics on Figure 57 illustrates the different parts of the CFD geometry and their interaction with the other solvers. The type of source and the corresponding color of each CFD part is as follows:

- Fuel channels: heat source and momentum sink, red
- Fuel channel foots (orificing): momentum sink, not shown on the figure
- Pumps: momentum source, blue
- Steam generators: heat and momentum sink, green
- Upper plenum, cold pool and cold leg: free flow, gray

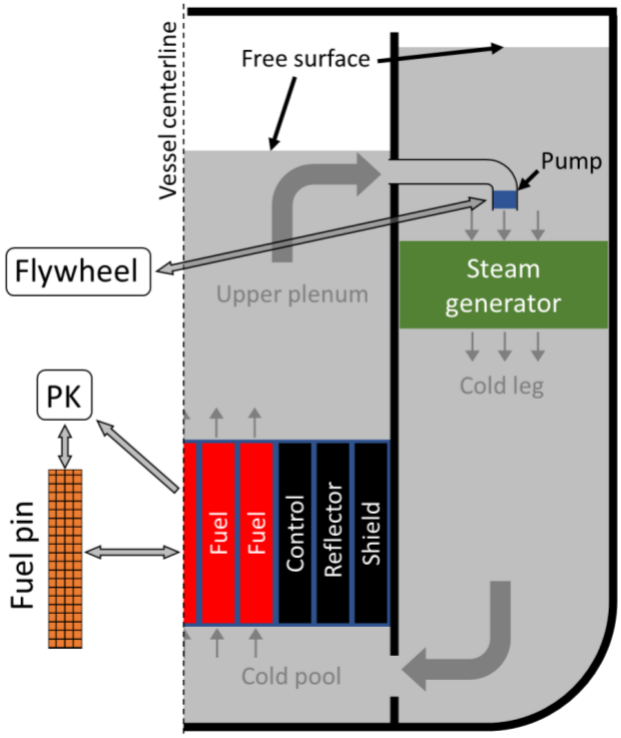

Figure 57 Schematics of the CFD geometry and the interaction with the other solvers

STAR-CCM+ is the CFD software employed in this model with the following configuration:

- Implicit unsteady, Three-dimensional flow
- Multiphase; Volume of fluid (VOF), Multiphase equation of state, Multiphase interaction
- Segregated flow solver
- Turbulent; Reynolds-Averaged-Navier-Stokes, K-Epsilon turbulence, Realizable K-Epsilon two-layer; Two-layer all y+ wall treatment
- Segregated multiphase temperature
- Gravity

The fuel pin temperature is solved separately in a custom-made code using a control volume approach. For each channel, it is assumed that the 91 pins of the assembly have the same

temperature distribution, so it is only necessary to solve one fuel pin per channel. The control volumes are created by dividing every fuel pin lengthwise into 10 pieces and radially into 30 rings. Straightforward numerical methods are employed to solve the resulting 2D heat transfer problem. This is done iteratively so that the temperature dependency of material properties is taken into account. The fuel pin temperature solver uses the coolant temperature and velocity (from CFD) as well as the fission power (from neutronics) as an inputs, and calculates the new pin to coolant heat transfer (for CFD) and average fuel temperature (for neutronics) as outputs.

Neutronics is calculated with point kinetics using six precursor groups. Three reactivity temperature feedback coefficients are used: the Doppler constant, fuel axial expansion and coolant expansion. They were all calculated from Serpent simulations and provided by the authors of the SEALER design. The neutronics solver uses the average fuel temperature (from fuel pin temperature) and the average coolant temperature in the core (from CFD) as inputs and generates the new total fission power (for fuel pin temperature) as an output. The fission power profile inside the reactor core is also calculated from Serpent simulations and is constant throughout any transient, only its amplitude changes.

The fuel temperature solver, the neutronics solver and their coupling with CFD is all programmed in Matlab. At each time step, an iterative process is used to ensure that the inputs and outputs of all the solvers are consistent with each other. The coupling time step is 100 ms, whereas the time step of the CFD calculations is 5 ms. Figure 58 presents a simplified flowchart of the iterative coupling process.

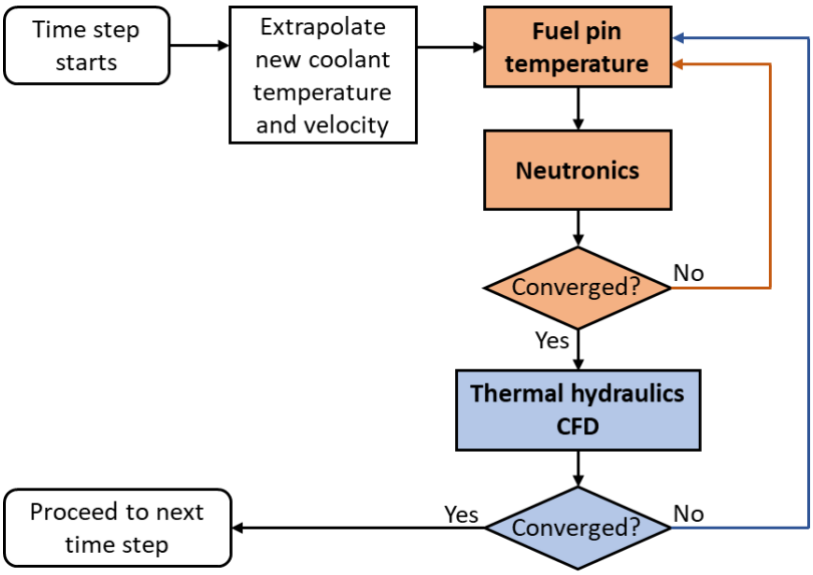

Figure 58 Simplified flowchart of the algorithm for coupling the different physics

In the CFD simulation, the pump is a simple cylinder with a specified momentum source. The latter is calculated from the pump characteristic curves. During a loss of flow transient, the pump head curve is modified at each time step according to the energy left in the flywheel. The torque curve and the volumetric flow of the previous time step are used to calculate the flywheel energy decrease. This way of proceeding is more realistic than simply assuming that the rotor speed or pump head decreases exponentially. There is no iterative process for the pump-flywheel coupling, the head curve of the current time step is exclusively dependent on the last time step.

4. Mesh

The CFD mesh was built in STAR-CCM+ and it covers the entire area that contains coolant and cover gas. The solid parts are not included in this version of the model. Only one quarter of the reactor is modelled using symmetry planes. Figure 59 shows the mesh and the different components that require momentum and/or heat source or sink. Most of the volume is filled with polyhedral cells and was created using the Automated Mesh tool using a base size of 5 cm. The entire volume contains 320,000 cells with an average diameter of 6.4 cm (volume averaged).

The mesh above the pump is composed of prisms that are uniformly stacked. This helps to have a sharp and stable free surface since it will be parallel to the cell faces. The base of the prisms are irregular polygons which are conformal to the polyhedral mesh beneath it. This portion of the mesh was created using the Directed Mesh tool in STAR-CCM+.

The fuel channels mesh is also made of prisms created with the Directed Mesh tool, see Figure 56 in the geometry section for a close-up view. Since in that area heat transfer and pressure drop are taken into account by correlations, it is not necessary to have a fine mesh. Additionally, using prisms allows to have long cells in the direction of the flow, which reduces the courant number. This is particularly important in the fuel channels because velocity is high. In the fuel area, the number of vertical divisions is chosen to ensure that the divisions used in the heat transfer solver fall precisely on the CFD cell divisions.

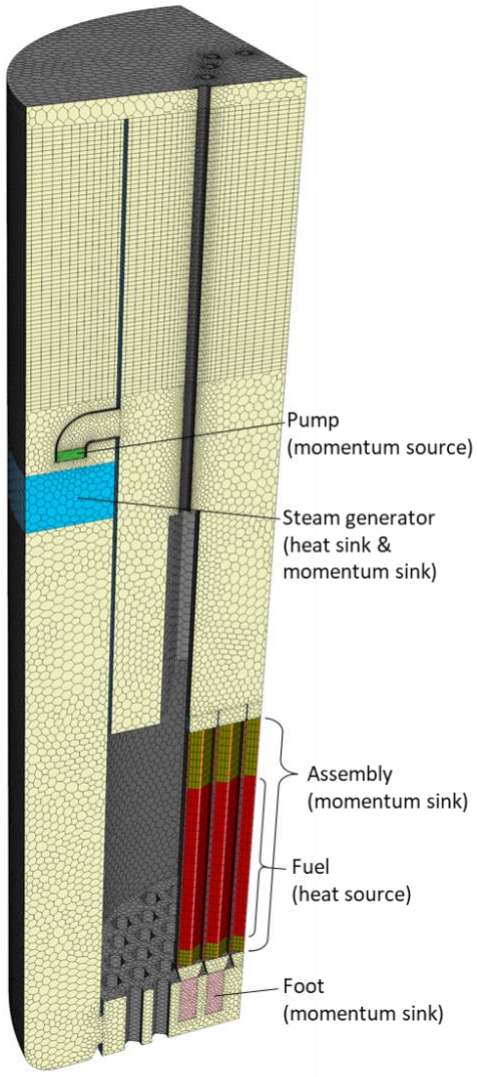

Figure 59 Mesh of the CFD model and the different components which use momentum and heat sources and sinks

The mesh size was determined using a sensitivity analysis were both the mesh size and time step were investigated. The quantity of interest (QOI) is the minimum pump mass flow that occurs at the beginning of the transient, see Figure 60. That QOI is more sensitive than other important quantities like the maximum fuel temperature. Four different mesh sizes were used, from base size of 8 cm to 1.5 cm, in total number of cells it corresponds to 180,000 and 1,300,000 respectively. For each mesh size, three different CFD time steps

were used: 10, 5 and 2 ms. Note that this is the time step used in the CFD calculations, not the time step at which coupling between CFD and the other solvers occurs.

The results are compiled on Figure 61. For the simulations performed with a time step of 10 ms, the QOI varies significantly with the mesh size. On the other hand, for the time step of 2 ms, the QOI remains almost constant throughout the different mesh sizes. These results suggest that a fine mesh requires a smaller time step, but it will not yield more accurate results. Therefore, in order to speed up calculations, the selected mesh is the one with base size of 5 cm and the time step is 5 ms.

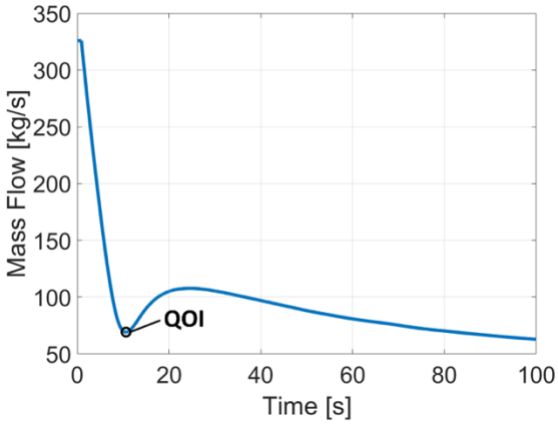

Figure 60 QOI used for the mesh sensitivity analysis

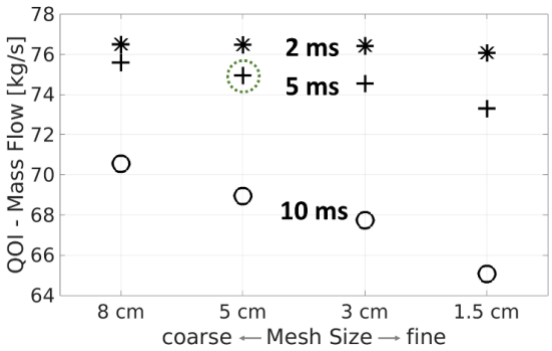

Figure 61 Mesh and time step sensitivity analysis

5. Steady state

Before calculating transients, it is necessary to obtain a steady state that can be used as initial conditions. The steady state should remain stable in transient mode (with all the feedback mechanisms) and should hit the design parameters (power, mass flow, velocities).

The parameters that need to be adjusted are the pump power and the friction factor of every fuel channel foot. This is done by first setting up a CFD simulation without any thermal effects (no heat source or sink) and a rough estimate for the pump and foot parameters. An automatic process is then used where a series of simulations are computed, and the parameters are corrected at every subsequent run until the quantities they control are very close to target values. The pump power controls the total mass flow, and the friction of every fuel channel foot control the coolant velocity in that channel (necessary to obtain the same temperature increase across all channels).

Once the hydraulics are running properly, a constant heat source is added in the fuel channels (with the appropriate power distribution) and the heat sink of the steam generator is activated. This case is ran for a very long time until all parts of the reactor have reached their steady state temperature. Finally, this CFD case is connected to the fuel temperature and point kinetics solvers. The entire system is ran in transient mode, but with steady state conditions (constant pump velocity), for a very long time until all parameters have stabilized.

6. Transient results

The transient that is investigated in this study is an unprotected loss of flow accident (ULOF). The initial condition is the steady state that is described in the previous section. At time = 1 sec, the transient is triggered by activating the pump-flywheel coupling, see section on solvers for details. The moment of inertia of the flywheel of each pump corresponds to a steel disc of 1m of diameter and 2cm thick. The initial rotational speed is 500 rpm. That value for the moment inertia was selected to obtain a mass flow at the pumps that clearly exhibits the fluctuation at the beginning of the transient while remaining far from reverse flow. Note that the real reactor would have a bigger flywheel to avoid the fluctuation altogether. The transient presented here is therefore a limiting case. The steam generators are modelled as having a constant temperature drop throughout the transient.

Figure 62 shows the mass flow through the pumps and the core during the transient. At the pumps, the previously mentioned fluctuation is clearly present between 10 and 20 seconds into the transient. Initially, the mass flow decreases very rapidly, reaches a minimum, then increases a bit and from about 25s it starts decreasing asymptotically towards the natural circulation flow. The mass flow through the core does not exhibit any fluctuation. As the mass flow and pump head decrease, the free surface levels of the hot and cold leg move towards the same height, as it is shown on Figure 63. When the reactor reaches natural circulation, the hot leg free surface is slightly higher than the cold leg (less than 1cm). The mass flow at natural circulation is about 100 kg/s, which corresponds to about 7% of the forced flow.

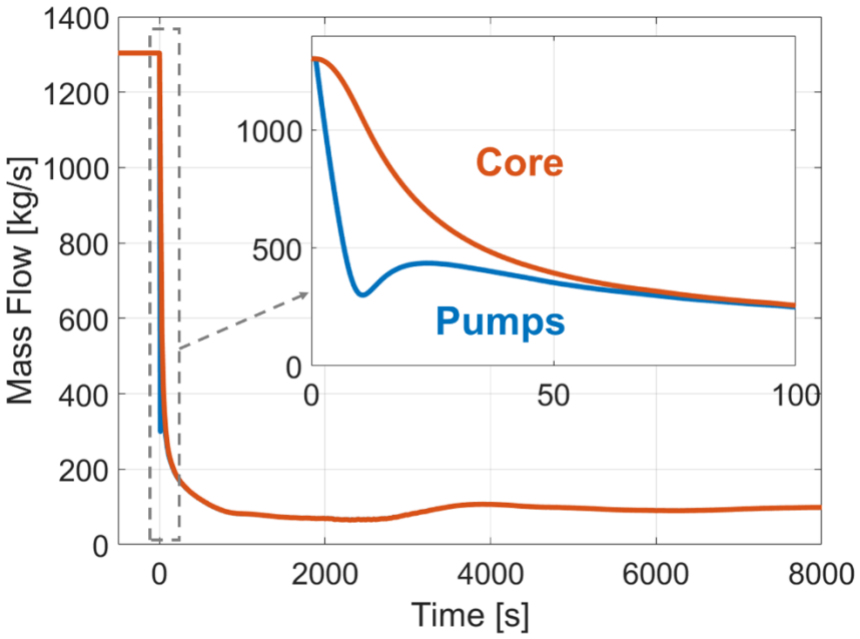

Figure 62 Mass flow through core and pumps during a ULOF transient

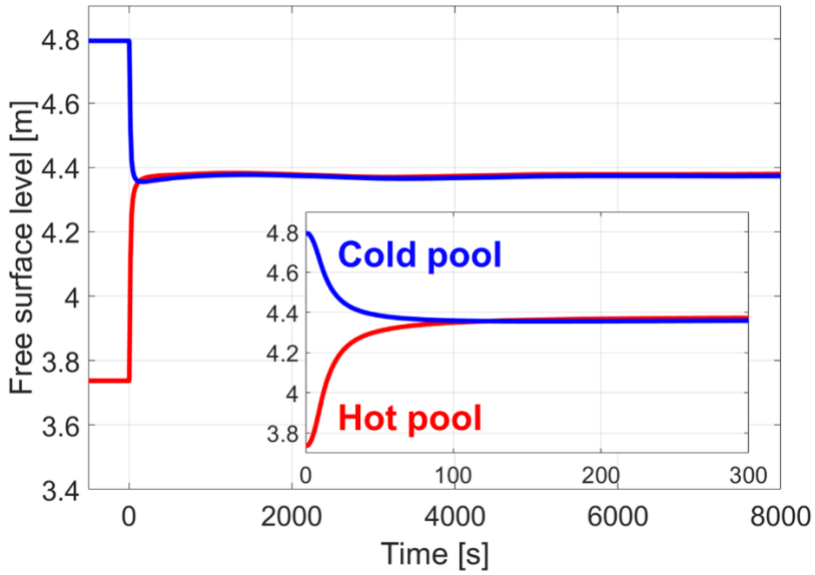

Figure 63 Evolution of the free surface levels during a ULOF transient

Figure 64 shows the evolution of the temperature in the core during the transient. Four curves are displayed: average and maximum temperatures of the coolant and fuel. The maximum temperature reached in the fuel is 933 K, which is only a few degrees above the steady state maximum fuel temperature of 921 K. The maximum coolant temperature is 813 K. For comparison, the steady state maximum coolant temperature is 705 K and the melting point of lead is 2022 K. Although the rapid changes occur in the first 300 sec, the reactor takes more than 8000 sec to fully stabilize.

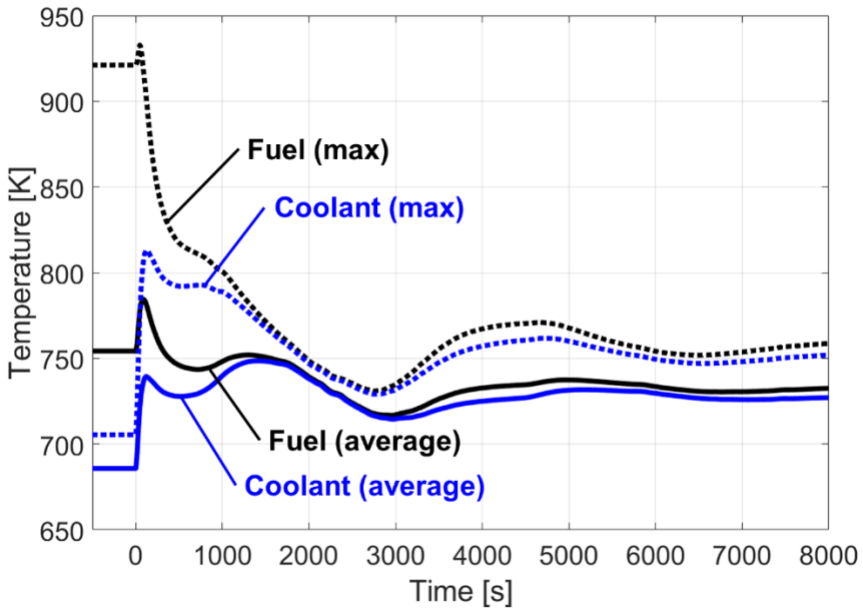

Figure 64 Fuel and coolant temperature inside the core during a ULOF transient

Figure 65 shows the total reactor power (red curve) and reactivity (black curve during the transient. As expected, the reactivity follows the core temperature but in the opposite direction. It varies between -40 pcm and +15 pcm. The power decreases sharply in the beginning of the transient and remains low with small oscillations until reaching its final value of 0.6 MW, which is about 7% of the nominal power. Considering that the temperature drop in the steam generators is constant, this is consistent with the natural circulation mass flow which is also 7%.

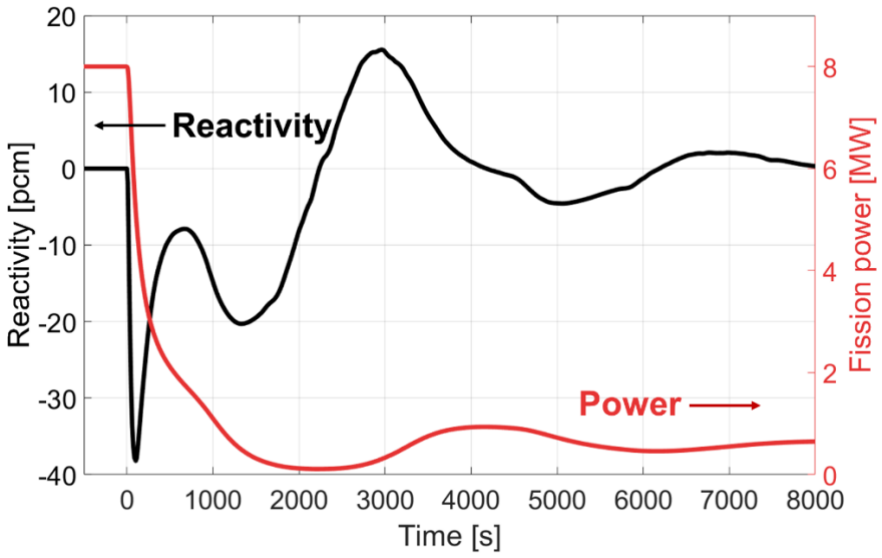

Figure 65 Evolution of the reactivity and power during a ULOF transient

Figure 66 shows the evolution of the temperature distribution throughout the transient. For every time, a cross section with half of the reactor is displayed. The right side corresponds to the centerline of the reactor, the core is located on the right towards the bottom and the pump is on the left towards the top. Refer to figures Figure 55 and Figure 59 for a detailed description of the geometry. Between 0 and 1500 seconds, it is interesting to notice the slow progression of a “hot wave” moving downwards in the cold leg. When that wave reaches the core, around 1500 seconds, the temperature increases again, as can be seen on Figure 64. In fact, the average coolant temperature in the core reaches its maximum at that moment and not at the beginning of the transient.

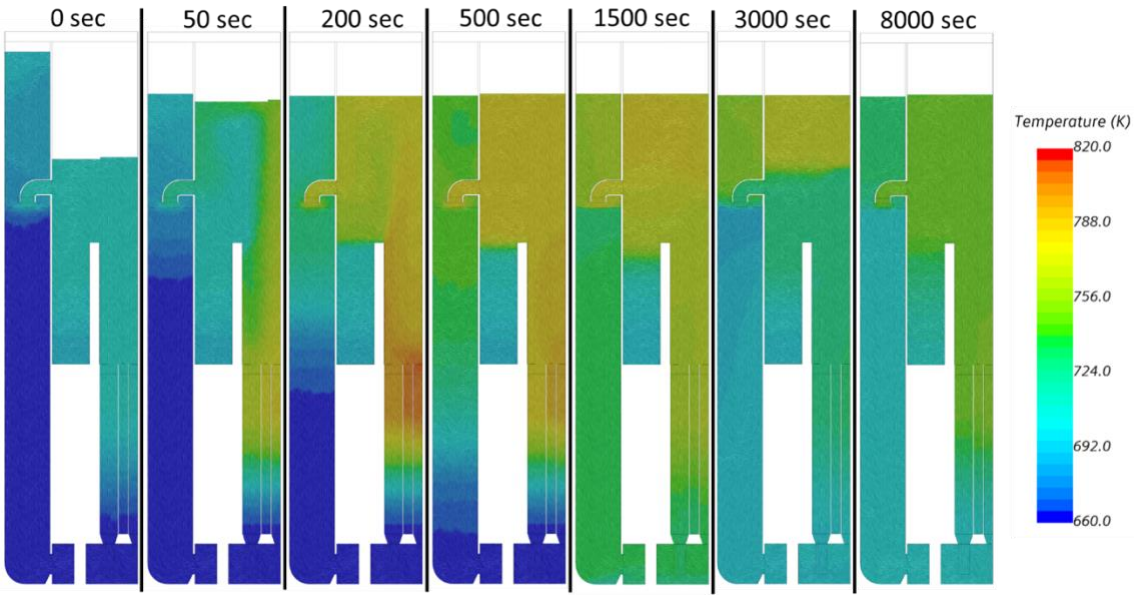

Figure 66 Temperature distribution of the reactor at different times during a ULOF transient

7. Comparison with a lumped parameter model

The results obtained with the CFD-based model were compared against results of the same transient (ULOF) and same reactor calculated with the lumped-parameter code BELLA(Bortot et al., 2015). It should be noted that even though the same reactor design was used in both cases, the geometry is slightly different since simplifications were used in both cases, but at different levels.

Figure 67 shows the mass flow of the first 500 seconds of the transient. The lumped-parameter model uses an exponential decay of the pump head to simulate the loss of flow, whereas the CFD model couples the pump with the kinetic energy of the flywheel. Since there is no equivalent between the pump coastdown time constant used with lumped-parameter and the flywheel moment of inertia used with CFD, two lumped-parameter curves are shown using two different time constants (9s and 20s). As can be seen on the figure, it is not possible to reproduce the CFD results by adjusting the pump time constant of the lumped-parameter. A short time constant (9s) produces the fluctuation at the beginning of transient but reaches natural-convection mush faster, a longer time constant (20s) doesn't show the fluctuation at all and still reaches natural convection faster. This is due to the fact that the lumped-parameter model cannot properly grasp the interaction between the changing free surface levels, pump head and flywheel energy.

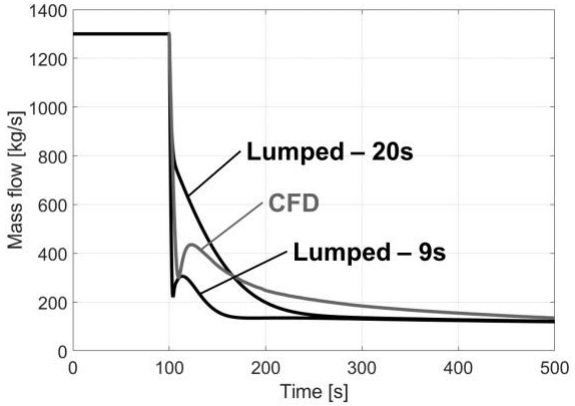

Figure 67 Mass flow of a ULOF transient: comparison between lumped-parameter and CFD

Figure 68 shows the coolant temperature at the inlet and outlet of the core, and Figure 69 shows the inner fuel temperature, where inner is defined as the volume inside a radius that is 1/3 of the fuel radius. The lumped-parameter curves shown here are for a pump time constant of 20s because they are closer to CFD compared to the time constant of 9s. The main difference is that after the initial temperature increase, the CFD model exhibits a second temperature increase between 1000s and 2000s. This is the result of the hot coolant from the initial temperature increase travelling through the whole circuit at a reduced speed, see Figure 66. The lumped-parameter model cannot resolve this behaviour since the entire cold leg is one node. It is clear that the CFD-based model is more accurate both in terms of mass flow and temperatures.

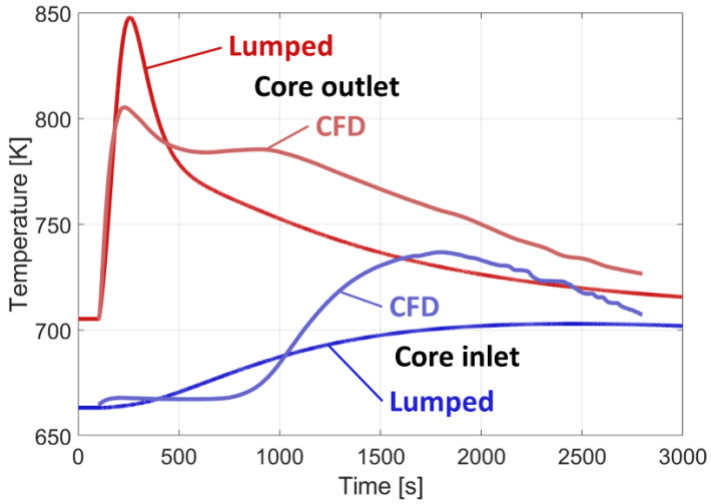

Figure 68 Core inlet and outlet coolant temperature: comparison between lumped-parameter and CFD

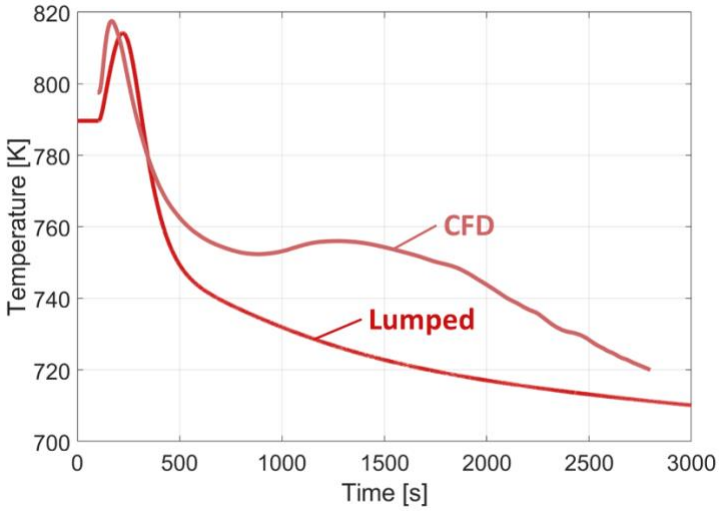

Figure 69 Fuel inner temperature: comparison between lumped-parameter and CFD

8. Influence of the flywheel moment of inertia

The transients presented earlier use a moment of inertia of the flywheel that is small on purpose to obtain the fluctuation at the beginning of the transient. In practice, it would be better to use a flywheel large enough to avoid any type of fluctuation. This section presents the effect of changing the value of the moment of inertia on the evolution of the transient. The reference case is the same as the results presented in the other sections, which corresponds to a disc of stainless steel 1m of diameter and 2cm thick (for each pump). Three other curves are presented where the moment of inertia is modified by +/- 10% and also doubled (+100%).

Figure 70 shows the results for the mass flow. The amplitude of the fluctuation is quite sensitive to the moment of inertia. In the case where the moment of inertia is doubled, the fluctuation disappears completely and there is a gradual and monotonous decrease in the mass flow. Also, it takes significantly more time to attain natural convection.

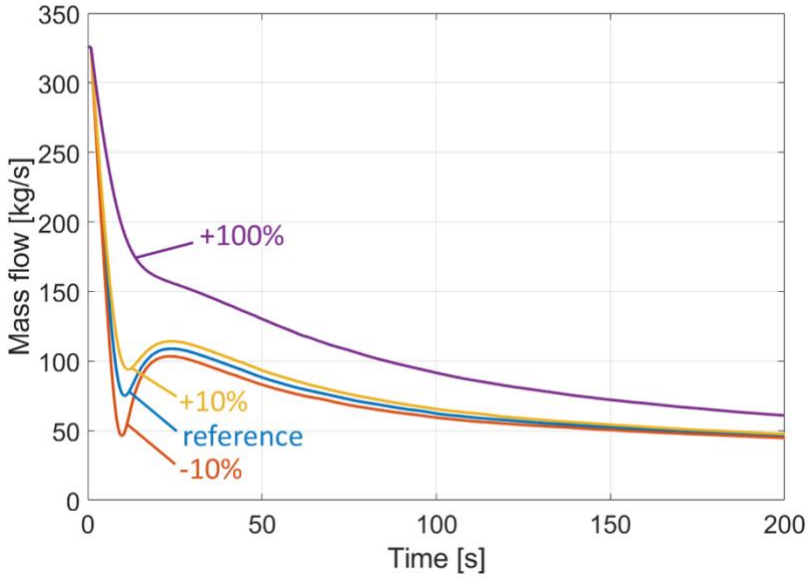

Figure 70 Mass flow during a ULOF transient for different values of flywheel moment of inertia

Figure 71 and Figure 72 show the average fuel and coolant temperature in the core. The reference and the two curves at +/- 10% are almost identical except during the first rapid temperature increase where the peaks have different maximums. As expected, higher moment of inertia results in lower maximum temperature. However, the case where the moment of inertia is doubled (+100%) is considerably different. Since the mass flow is maintained higher than the other cases for the first few hundred seconds, the second "hot wave" arrives earlier and is much less pronounced. Overall, doubling the moment of inertia results in less temperature and mass flow fluctuations during the transient. That is a desired behaviour and the final design of the reactor can and should include a flywheel large enough to produce this type of transients.

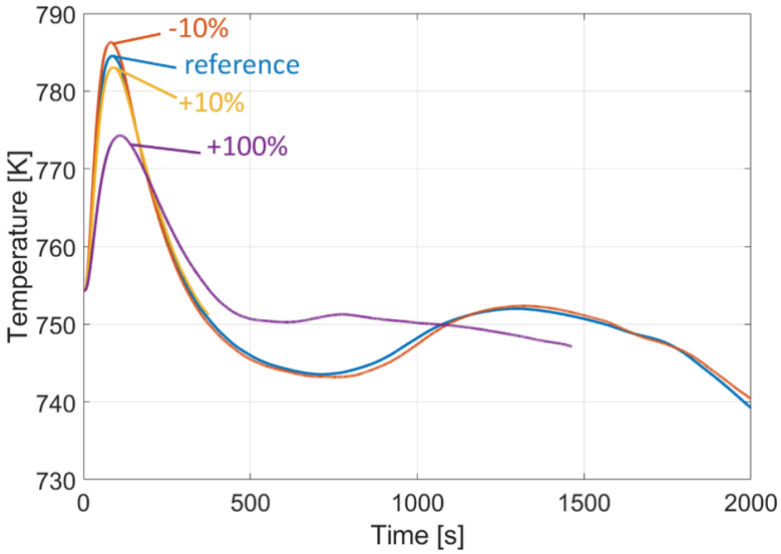

Figure 71 Average fuel temperature during a ULOF transient for different values of flywheel moment of inertia

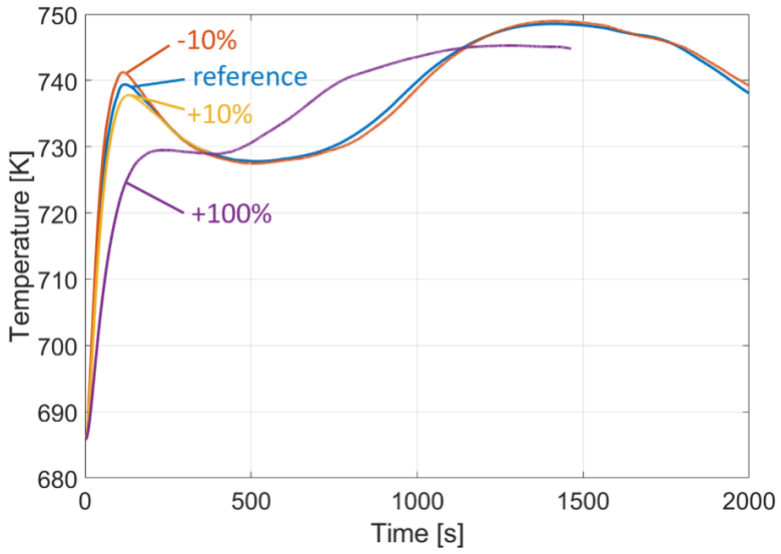

Figure 72 Average coolant temperature in the core during a ULOF transient for different values of flywheel moment of inertia

9. Conclusion

This work presented results of an unprotected loss of flow transient in a small lead cooled reactor. The simulation was performed with a CFD-based model specifically developed for this study. Results show that if a pump flywheel with a small moment of inertia is used, the mass flow at the pumps undergoes a fluctuation at the beginning of the transient. This behaviour was initially identified using a lumped-parameter model and is now confirmed. Additionally, the fuel and coolant temperature during the transient do not increase significantly and remain well below safety limits.

The results from this CFD-based model were compared against results of the same transient calculated with a lumped-parameter model. It is shown that the evolution of the mass flow is significantly different. The lumped-parameter model reaches natural convection much faster even when selecting a long time constant for the pump coastdown. This result is explained by the fact the lumped-parameter model uses an exponential decay for the pump, whereas the CFD-based model couples the kinetic energy of the flywheel with the pump and its characteristic curves. The latter is thus more accurate because it can properly model the interaction between the changing level of the free surface and the pump. The other main difference is that with the CFD-based model, the core undergoes a second increase of temperature a long time after the initial increase. This is due to the coolant in the core that was heated up at the very beginning of the transient travelling the entire circuit a low velocity and re-entering the core. The lumped-parameter model cannot capture this behaviour since the circuit is divided into very few lumps.

Finally, different values for the moment of inertia of the pump flywheel were tested. It was found that a flywheel corresponding to a steel disc 1m of diameter and 4cm thick (for each pump) removes the mass flow disturbance at the beginning of the transient. It also takes much longer to reach natural convection and thus the temperature evolution shows less fluctuations. This is a desired behavior and it can easily be achieved considering that the physical dimensions of that flywheel are relatively small. It’s even conceivable to double or quadruple it to account for friction and other losses.

This study is the first application of this CFD-based model. For further investigations, it could easily be adapted to simulate different types of transients or for other types of reactors. It is particularly well suited for small pool-type reactors where boiling is absent in normal conditions.

10. Acknowledgments

Funding: This work was supported by NSREC-UNENE (Natural Sciences and Engineering Research Council of Canada, and University Network of Excellence in Nuclear Engineering) [grant number IRCPJ309310-14].

11. References

Bortot, S., Suvdantsetseg, E., Wallenius, J., 2015. BELLA: a multi-point dynamics code for safety-informed design of fast reactors. Annals of Nuclear Energy 85, 228–235. https://doi.org/10.1016/j.anucene.2015.05.017

Fiorina, C., Clifford, I., Aufiero, M., Mikityuk, K., 2015. GeN-Foam: a novel OpenFOAM ® based multi-physics solver for 2D/3D transient analysis of nuclear reactors. Nuclear Engineering and Design 294, 24–37. https://doi.org/10.1016/j.nucengdes.2015.05.035

Hernandez, C.R., 2020. Dynamic sensitivity and uncertainty analysis of a small lead cooled reactor. Annals of Nuclear Energy 10.

Moreau, V., Profir, M., Keijers, S., Van Tichelen, K., 2019. An improved CFD model for a MYRRHA based primary coolant loop. Nuclear Engineering and Design 353, 110221. https://doi.org/10.1016/j.nucengdes.2019.110221

Reale Hernandez, C., Grishchenko, D., Kudinov, P., Wallenius, J., Luxat, J., 2022. Development of a CFD-based model to simulate loss of flow transients in a small lead-cooled reactor. Nuclear Engineering and Design 392, 111773. https://doi.org/10.1016/j.nucengdes.2022.111773

Roelofs, F., Zwijsen, K., Uitslag-Doolaard, H., Alcaro, F., Stempniewicz, M., Wallenius, J., 2019. Validation of Thermal Hydraulic Design Support and Safety Methodology and Application to SEALER. Presented at the IAEA BENEFITS AND CHALLENGES OF SMALL MODULAR FAST REACTORS, INTL ATOMIC ENERGY AGENCY, Milan, Italy.

Wallenius, J., Qvist, S., Mickus, I., Bortot, S., Szakalos, P., Ejenstam, J., 2018. Design of SEALER, a very small lead-cooled reactor for commercial power production in off-grid applications. Nuclear Engineering and Design 338, 23–33. https://doi.org/10.1016/j.nucengdes.2018.07.031

Chapter 7 - Conclusion and Future Work

7.1 Summary

The theme of this thesis was on the safety assessment of small modular reactors that could eventually see the light in Canada. One particular reactor was selected for a detailed investigation, the SEALER reactor. It is a small lead cooled reactor developed by Professor Janne Wallenius in KTH (Stockholm) with whom a collaboration has been set up. With an electric power of 3 to 10 MW, it is intended for remote communities in northern Canada and mines. The safety aspect that is considered in this work is related to reactor transients, like loss of flow or overpower. At the time of starting the thesis, the authors of the SEALER design have already performed transient calculations with a lumped-parameter model. One particular issue that they identified was a fluctuation of the mass flow in the pumps at the beginning of a loss of flow transient. Therefore, one of the main objectives of this thesis became to investigate that issue.

The first step in that process was to use the previously mentioned lumped-parameter model to perform an uncertainty and sensitivity analysis. Different types of parameters were tested in that study: geometry, material properties, correlations and neutronics. The effect of those parameters was studied on two transients: an unprotected loss of flow and an unprotected overpower. The uncertainty analysis concluded that all the relevant temperatures remain well within safety limits throughout the transients. However, with respect to the mass flow fluctuation issue, it was found that varying some parameters in a realistic manner could cause reverse flow at the pumps. This was all published in the first article of the thesis.

Following these results, it was decided to develop a more accurate model for simulating the same type of transients. This would allow to confirm the results already obtained and to explore the effect of selected parameters. The development of this model is the second part of the thesis and constitutes its main achievement. The model uses CFD to simulate the flow of lead in the entire primary circuit. The free surfaces are resolved by using multiphase (lead and helium) with the volume of fluid method. Similar to the porous

medium, the complex components are replaced by a simple geometry with momentum and heat sources/sink. The CFD simulation is coupled with a custom-made code for fuel heat transfer and point kinetics for neutronics.

In order to demonstrate the viability of the model, a validation exercise was undertaken to compare experimental results with CFD simulations. The experimental data was taken from the TALL-3D facility which contains a section specifically designed to validate CFD. The main phenomena targeted by this validation are temperature stratification and a jet into a plenum. The CFD case was set up exactly with the same configuration as for the model.

The details of the modelling methods and the validation exercise are all contained in the second article of the thesis. The third and last article presents only a summary of the modelling methods and focuses on the simulation results. The mass flow fluctuation issue that was initially identified with the lumped-parameter model is also present in the simulations with the CFD-based model. However, the shape is different and the overall mass flow evolution is slower, meaning that it takes more time to reach natural circulation. This is the result of coupling the pump with a flywheel in the CFD-based model compared to a simple exponential pump coastdown in the lumped-parameter model. Temperature variations during the transient also tend to be less pronounced with the CFD-based model and always remain far from safety concerns. Most importantly, simulations were performed with different flywheel sizes and it was found that the mass flow disturbance can be completely eliminated with a very reasonable size. Temperature variations with such a flywheel are also smoother.

7.2 Contributions to knowledge

The contribution of this thesis can be divided in two parts. First, the flow fluctuation that occurs in a loss of flow accident of the SEALER reactor was thoroughly investigated with two different models. The mechanism of that behavior, the parameters that have an effect on it, and the extent to which it can be amplified are well documented. It should also be noted that this behavior could potentially occur in any type of pool reactor where the hot

and cold legs have different free surface levels. It is not limited to the SEALER reactor. Understanding this phenomenon is an important step in ensuring the safety of this reactor.

The second part is the development of a new model for simulating transients of the SEALER reactor. The components of the model have all been used in other works (CFD with porous media, point kinetics, heat transfer model based on control volume). The novelty here is the integration of those specific components into one model. Also, it's significantly more precise than a lumped parameter model but still relatively simple to implement since the core is treated like a set of 1D channels with correlations, and neutronics is calculated with point kinetics. Again, this model could be adapted to any small reactor that is single-phase and pool-type. This model could also be the basis for an improved version to study different phenomena.

7.3 Future work

The CFD based model developed in this thesis could serve as the basis for other studies. Another transient of interest in this type of reactor is the introduction of void into the core from, for example, a steam generator rupture. This would involve using CFD's multiphase capabilities, using an appropriate neutronics model, etc. Severe accidents could also be studied, like fission product transport from fuel pin damage. Indeed, CFD is also capable of simulating the transport of particles or bubbles. Finally, coupling this model with thermal mechanics to study the effect and feedback on materials would also be an interesting project.

Without major modifications, this model could also be used for other applications. For example, simulating other type of transients like an unprotected overpower. Asymmetrical transient calculations could be made by modeling the entire reactor instead of only a quarter. For example, modelling the pump seizure of one of the eight pumps. The model can also be adapted to other reactors of the same type, i.e. small pool-type reactors.

Improving the accuracy of the present model would also be useful. One of the main things would be to add heat transfer through the solid parts of the reactor since the current model

only simulates the fluid areas. Another important aspect is the neutronics solver, it should be improved by switching to a transport code. Concerning the fuel pin heat transfer solver, its current version lacks radiative heat transfer across the gap between fuel and clad. That should be added for improved fidelity.

References

List of references outside of the three articles. Note that each article has its own reference list.

Banerjee, A., Raju, S., Divakar, R., Mohandas, E., Panneerselvam, G., Antony, M.P., 2005. Thermal property characterization of a titanium modified austenitic stainless steel (alloy D9). Journal of Nuclear Materials 347, 20–30. https://doi.org/10.1016/j.jnucmat.2005.06.009

Best Practice Guidelines for the Use of CFD in Nuclear Reactor Safety Application - Revision, 2014. 176.

Bonifetto, R., Dulla, S., Ravetto, P., Richard, L.S., Zanino, R., 2013. A full-core coupled neutronic/thermal-hydraulic code for the modeling of lead-cooled nuclear fast reactors. Nuclear Engineering and Design 261, 85–94. https://doi.org/10.1016/j.nucengdes.2013.03.030

Borgonovo, E., 2017. Sensitivity analysis. Springer Berlin Heidelberg, New York, NY.

Bortot, S., Suvdantsetseg, E., Wallenius, J., 2015. BELLA: a multi-point dynamics code for safety-informed design of fast reactors. Annals of Nuclear Energy 85, 228–235. https://doi.org/10.1016/j.anucene.2015.05.017

Bubelis, E., Schikorr, M., 2008. Review and proposal for best fit of wire-wrapped fuel bundle friction factor and pressure drop predictions using various existing correlations. Nuclear Engineering and Design 238, 3299–3320. https://doi.org/10.1016/j.nucengdes.2008.06.024

Carbajo, J.J., Yoder, G.L., Popov, S.G., Ivanov, V.K., 2001. A review of the thermophysical properties of MOX and UO2 fuels. Journal of Nuclear Materials 299, 181–198. https://doi.org/10.1016/S0022-3115(01)00692-4

Chen, S.K., Chen, Y.M., Todreas, N.E., 2018. The upgraded Cheng and Todreas correlation for pressure drop in hexagonal wire-wrapped rod bundles. Nuclear Engineering and Design 335, 356–373. https://doi.org/10.1016/j.nucengdes.2018.05.010

Ejenstam, J., Halvarsson, M., Weidow, J., Jönsson, B., Szakalos, P., 2013. Oxidation studies of Fe10CrAl–RE alloys exposed to Pb at 550°C for 10,000h. Journal of Nuclear Materials 443, 161–170. https://doi.org/10.1016/j.jnucmat.2013.07.023

Fiorina, C., Clifford, I., Aufiero, M., Mikityuk, K., 2015. GeN-Foam: a novel OpenFOAM ® based multi-physics solver for 2D/3D transient analysis of nuclear reactors. Nuclear Engineering and Design 294, 24–37. https://doi.org/10.1016/j.nucengdes.2015.05.035

Gajev, I., Ma, W., Kozlowski, T., 2014. Sensitivity analysis of input uncertain parameters on BWR stability using TRACE/PARCS. Annals of Nuclear Energy 67, 49–58. https://doi.org/10.1016/j.anucene.2013.10.016

Grishchenko, D., Jeltsov, M., Kööp, K., Karbojian, A., Villanueva, W., Kudinov, P., 2015. The TALL-3D facility design and commissioning tests for validation of coupled STH and CFD codes. Nuclear Engineering and Design 290, 144–153. https://doi.org/10.1016/j.nucengdes.2014.11.045

Grishchenko, D., Papukchiev, A., Liu, C., Geffray, C., Polidori, M., Kööp, K., Jeltsov, M., Kudinov, P., 2020. TALL-3D open and blind benchmark on natural circulation instability. Nuclear Engineering and Design 358, 110386. https://doi.org/10.1016/j.nucengdes.2019.110386

Handbook on Lead-bismuth Eutectic Alloy and Lead Properties, Materials Compatibility, Thermal-hydraulics and Technologies, 2015. 950.

Jeltsov, M., Grishchenko, D., Kudinov, P., 2019. Validation of Star-CCM+ for liquid metal thermal-hydraulics using TALL-3D experiment. Nuclear Engineering and Design 341, 306–325. https://doi.org/10.1016/j.nucengdes.2018.11.015

Kennedy, G., Tichelen, K.V., Doolaard, H., 2015. Experimental Investigation of the Pressure Loss Characteristics of the Full-Scale MYRRHA Fuel Bundle in the COMPLOT LBE Facility 13.

Kennedy, G., Van Tichelen, K., Pacio, J., Di Piazza, I., Uitslag-Doolaard, H., 2020. Thermal-Hydraulic Experimental Testing of the MYRRHA Wire-Wrapped Fuel Assembly. Nuclear Technology 206, 179–190. https://doi.org/10.1080/00295450.2019.1620539

Krepel, J., Pelloni, S., Chenu, A., Petkevich, P., Chawla, R., 2010. FAST Code System: Review of Recent Developments and Near-Future Plans. Journal of Engineering for Gas Turbines and Power 7. https://doi.org/10.1115/1.4000336

Leibowitz, L., Blomquist, R.A., 1988. Thermal conductivity and thermal expansion of stainless steels D9 and HT9. International Journal of Thermophysics 9, 873–883. https://doi.org/10.1007/BF00503252

Martinez, P., Galpin, J., 2014. CFD modeling of the EPR primary circuit. Nuclear Engineering and Design 278, 529–541. https://doi.org/10.1016/j.nucengdes.2014.08.013

Moreau, V., Profir, M., Keijers, S., Van Tichelen, K., 2019. An improved CFD model for a MYRRHA based primary coolant loop. Nuclear Engineering and Design 353, 110221. https://doi.org/10.1016/j.nucengdes.2019.110221

Pacio, J., Daubner, M., Wetzel, T., Di Piazza, I., Tarantino, M., Martelli, D., Angelucci, M., 2018. Experimental Nusselt Number in Rod Bundles Cooled by Heavy-Liquid Metals, in: Volume 6B: Thermal-Hydraulics and Safety Analyses. Presented at the 2018 26th International Conference on Nuclear Engineering, American Society of Mechanical Engineers, London, England. https://doi.org/10.1115/ICONE26-82213

Roelofs, F., 2019. Thermal Hydraulics Aspects of Liquid Metal Cooled Nuclear Reactors. Woodhead Publishing.

Roelofs, F., Koloszar, L., Buckingham, S., 2018. Best Practice Guidelines for Liquid Metal Report (No. D6.1). SESAME.

Saltelli, A., Tarantola, S., Campolongo, F., Ratto, M., 2004. Sensitivity Analysis in Practice, A Guide to Assessing Scientific Models. John Wiley & Sonds, Ltd.

Todreas, N.E., Kazimi, M.S., 1990. Nuclear systems II. Hemisphere Pub. Corp, New York.

Wallenius, J., Qvist, S., Mickus, I., Bortot, S., Szakalos, P., Ejenstam, J., 2018. Design of SEALER, a very small lead-cooled reactor for commercial power production in off-grid applications. Nuclear Engineering and Design 338, 23–33. https://doi.org/10.1016/j.nucengdes.2018.07.031

Wang, J., Wang, Q., Ding, M., 2020. Review on neutronic/thermal-hydraulic coupling simulation methods for nuclear reactor analysis. Annals of Nuclear Energy 137, 107165. https://doi.org/10.1016/j.anucene.2019.107165

Zwijsen, K., Dovizio, D., Moreau, V., Roelofs, F., 2019. CFD modelling of the CIRCE facility. Nuclear Engineering and Design 353, 110277. https://doi.org/10.1016/j.nucengdes.2019.110277

Zwijsen, K., Uitslag-Doolaard, H., Roelofs, F., Wallenius, J., 2020. Thermal-Hydraulic Design Support and Safety Analyses of SEALER UK Demo 10.